FLOW-INDUCED VIBRATION OF A WEB FLOATING OVER A PRESSURE-PAD AIR BAR

By

HYUN-KI CHO

Bachelor of Science
Konkuk University
Seoul, Korea
1997

Master of Science
Oklahoma State University
Stillwater, Oklahoma
1999

Submitted to the Faculty of the
Graduate College of the
Oklahoma State University
in partial fulfillment of
the requirements for
the Degree of
DOCTOR OF PHILOSOPHY
July, 2005

FLOW-INDUCED VIBRATION OF A WEB FLOATING

OVER A PRESSURE-PAD AIR BAR

Dissertation Approved:

Dr. Peter M. Moretti

Thesis Adviser

Dr. Andrew S. Arena

Dr. Arland H. Johannes

Dr. John J. Shelton

Dr. A. Gordon Emslie

Dean of the Graduate College

ACKNOWLEDGMENTS

I would like to express my sincere appreciation to my advisor, Dr. Peter. M. Moretti, for his excellent guidance and inspiration throughout this study. My sincere appreciation extends to my other committee members, Dr. John J. Shelton, Dr. Andrew S. Arena, and Dr. Arland H. Johannes, who provided invaluable suggestions, discussions, and assistance.

I would also like to give my special gratitude to my wife, Myungjin for encouraging and praying for me at times of difficulty. Thanks also go to my beloved parents and sisters for their support and encouragement.

This study was supported by the Web Handling Research Center (WHRC) at Oklahoma State University.

TABLE OF CONTENTS

LIST OF FIGURES

Figure Page

NOMENCLATURE

A	Flow area of cross section
b	Nozzle thickness of the pressure-pad air bar
$\overline{b}$	Nondimensional nozzle thickness, b/L
C_d	Discharge coefficient
C_f	Skin-friction coefficient
D	Nondimensional flexural rigidity, $\sqrt{EI/TL^2}$
D_e	Effective diameter
D_h	Hydraulic diameter
E	Young's modulus
EI	Flexural rigidity-per-unit-width
f	Darcy friction factor
G	Gyral operator, $2V\partial/\partial\overline{x}$
G	Green's function
H	Heaviside unit function
h	Flotation height (air gap between the web and air bar)
$\overline{h}$	Nondimensional flotation height, h/L
$\tilde{h}$	Unsteady flotation height

I	Identity operator
I	Identity matrix
i	$\sqrt{-1}$
K	Stiffness operator, $\left(V^2-1\right)\partial^2/\partial\overline{x}^2+D^2\,\partial^4/\partial\overline{x}^4$
k	Friction coefficient
L	Web length
M	Mass operator
m	Mass-per-unit-area
N	Number of displacement mode
n	Order of mode
P	Wetted perimeter of cross section
p	Cushion pressure
$\overline{p}$	Nondimensional pressure, pL/T
$\tilde{p}$	Unsteady pressure
p_j	Effective total pressure
p_0	Supply pressure
$\overline{p}_0$	Nondimensional supply pressure, p_0L/T
Q	Flow-rate-per-unit-depth, hu_{ave}
$\overline{Q}$	Nondimensional flow rate, $Q\sqrt{m/TL^2}$
$\tilde{Q}$	Unsteady flow rate
q	External excitation vector

$\mathbf{q}_0$ Eigenvector

Re Reynolds number, Q/ν

T Tension-per-unit-width

t Time

$\overline{t}$ Nondimensional time, $t\sqrt{T/mL^2}$

U Air velocity at the nozzle

u Air velocity in the x direction

u_{ave} Average air velocity in the x direction

V Nondimensional web velocity, $V_w\sqrt{m/T}$

V_w Web velocity

v Air velocity in the y direction

$\mathbf{w}$ Real state vector

w Width of the air bar

x Coordinate in machine direction

x_C Location of the air bar, $\left(x_R + x_L\right)/2$

x_L Left endpoint of the cushion region

x_R Right endpoint of the cushion region

$\overline{x}$ Nondimensional x, x/L

$\overline{x}_C$ Nondimensional x_C, x_C/L

$\overline{x}_L$ Nondimensional x_L, x_L/L

$\overline{x}_R$ Nondimensional x_R, x_R/L

y Coordinate in the out-of-plane direction

$\bar{y}$ Nondimensional y, y/L

$\tilde{y}$ Unsteady web displacement

Greek Symbols

α Nondimensional parameter, $\sqrt{1-V^2}/D$

δ Vertical distance from the x axis to the head surface of the air bar

$\bar{\delta}$ Nondimensional δ, δ/L

δ_{nm} Kronecker delta

ε Deviation from equilibrium

$\mathbf{\Phi}$ Vector eigenfunction

λ Eigenvalue

μ Air viscosity

ν Kinetic viscosity of air

$\bar{\nu}$ Nondimensional air density, $\nu\sqrt{m/TL^2}$

θ Angle of jet ejection

ρ Air density

$\bar{\rho}$ Nondimensional air density, $\rho L/m$

τ Fluid shear stress

Ω Dimensional circular frequency

$\mathbf{\Omega}$ Diagonal matrix composed of the natural frequencies of the web, $\mathrm{Diag}(\omega_n)$

ω Natural frequency

ξ Generalized coordinate

ψ Scalar eigenfunction

ζ_{in} Pressure loss coefficient at the inlet

ζ_{ex} Pressure loss coefficient at the outlet

Superscripts

$-$ Nondimensional value

$\sim$ Unsteady value

$*$ Equilibrium value

CHAPTER I

INTRODUCTION

1.1 Problem Statement

Continuous, strip-formed, and flexible materials are called webs, and are manufactured through various processes, e.g., coating, printing, and drying. When newly coated webs are transported, good quality requires non-contact suspension; webs are floated on the air, which avoids damage to coatings. Air flotation ovens, which consist of air bars arranged as shown in Figure 1, are widely used for effective drying and suspending the coated webs, using hot air which emerges from two nozzles of each air bar. This type of the air bar is called a pressure-pad air bar because the pressure generated between the air bar and the web plays the role of a cushion supporting the web without contact.

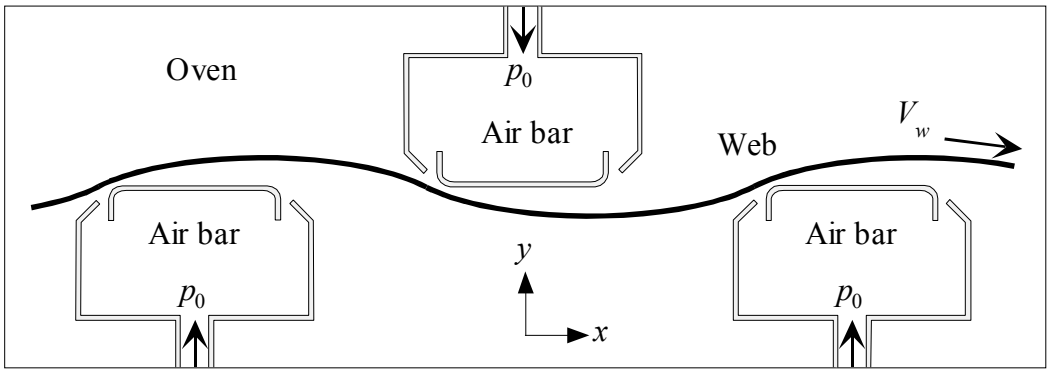

Figure 1 A Sinusoidally Deflected Web and Air Bars in an Air Flotation Oven

In order to study the air-web interaction system in a fundamental and academic approach, the flexible web can be modeled as a traveling Euler-Bernoulli beam under tension which is exposed to high-speed air flows underneath it, and subjected to two pinned supports. When a web travels at the constant speed V_w over a pressure-pad air bar, the cushion pressure p developed in the region $x \in (x_L, x_R)$ suspends the web floating over the air bar as shown in Figure 2. The sinusoidal web path usually tends closer towards one of the two slot nozzles, and away from the other, while the web is running over multiple air bars. The air-jet flow emerging from the nozzle closer to the web follows along the top surface of the air bar, called Coanda effect, and the air jet from the other nozzle flows out into the ambient, along with the flow. By virtue of the Coanda flows, effects of air-jet impingement on webs are negligible, because most of the air-jet flows along the rounded corner right after the nozzle.

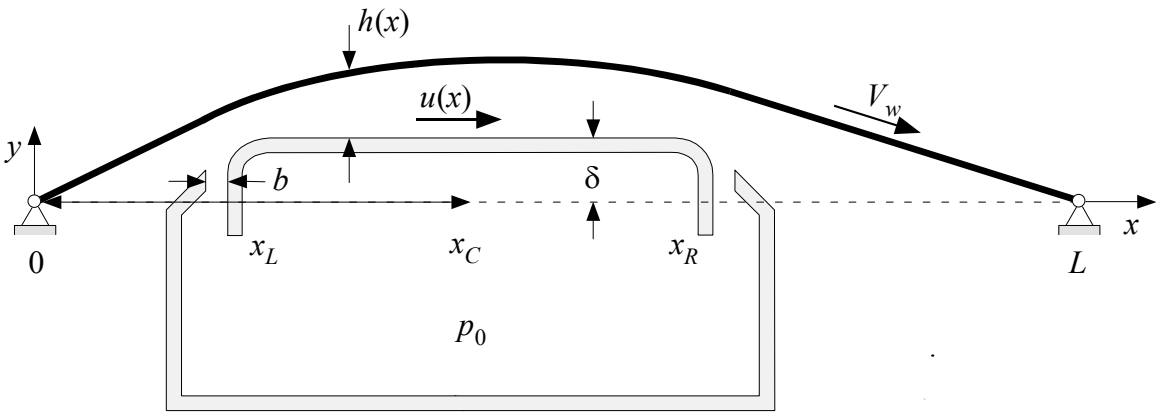

Figure 2 Schematic of a Moving Web over a Pressure-Pad Air Bar

Proper operating conditions for high productivity and stable travel of webs involve many factors such as web speed, pressure supplied to air bars, or web tension.

One of the most serious problems with the air flotation oven is web flutter which leads to poor web quality. It is necessary, therefore, to carry out a fundamental study on the aeroelastically coupled web and air jet to find flutter prediction criteria.

1.2 Objectives of the Study

The primary objectives of the present study are as follows:

(1) To develop the analytical model for air-web interaction over a pressure-pad air bar and predict the string-mode instability.

(2) To verify the analytical model through experiments.

(3) To provide design guides and operating conditions of air-flotation devices that may prevent flutter problems in air flotation ovens.

1.3 Scope and Limitations

The present study is largely divided into two main phases. One is the analytical development of the air-web interaction model and its computational implementation. Theories of elasticity and fluid dynamics are applied to develop the aeroelastic model. As shown in Figure 2, the continuous web running through multiple air bars is reduced to the web traveling over one air bar between two fixed supports. The web can be modeled as a traveling threadline (no variation across the width) if the web is assumed to be wide enough, which allows web instability to be classified into a string-mode flutter. Although simplified, the proposed model is effective for identifying the mechanism of air-web instability over pressure-pad air bars.

The other part of this study is experimentation to verify the analytical model. Air dams are installed along both free edges of the web to block the air from escaping in the cross-machine direction, which keeps air flows two-dimensional. Due to limitation of experimental set-up, experiments are performed for the case of a non-traveling web exposed to air-jet flows. The present study is focused on effects of high-speed air flows on the flexible tensioned web; the velocity of the web is neglected because the velocity of the air jet is much higher than the translational velocity in practical applications. Stability criteria are provided and compared through experiments and computations.

CHAPTER II

LITERATURE REVIEW

2.1 Air-Flotation Devices

Air-flotation systems represent the latest technology for drying coated webs transported without contact. Bezella (1976) summarized applications of air-flotation ovens and various drying methods. Obrzut (1976) explained the unique characteristics of air-flotation ovens. Krizek (1986) discussed some design aspects of various commercial air bars used to aerodynamically support and dry webs.

Several experimental studies of various commercial air bars have been carried out to determine aerodynamic forces on rigid-stationary webs. Pinnamaraju (1992) measured pressure distributions on a flat plate to investigate the effects of flotation height (distance between an air bar and a web) on the aerodynamic forces. Another series of experiments on measuring pressures on a plate was performed by Perdue (1993). He studied the effects of the machine-directional tilt angle of a flat web on out-of-plane instability of webs in air-flotation ovens. Pinnamaraju's experiments were continued and extended by Nisankararao (1994). He examined the effects of the cross-machine-directional tilt angle of a rigid web on the cushion pressure, which might cause lateral instability of webs in air-flotation ovens. In general, their experimental studies show that the cushion pressure acting on flat webs decreases with increase in flotation height and tilt angle of webs, and

the cushion pressure is almost uniform within a small tilt angle, which provides good agreement with ground-effect theories.

Muftu *et al*. (1998) analyzed the cushion pressure on an air reverser, which is a large hollow drum with holes in its surface for changing the direction of a coated web. They pointed out that viscous forces dominate the air pressure generation rather than inertial forces associated with acceleration of the air jet at low operating clearances on the order of microns; the air flow between the web and air-flotation device is commonly represented by the Reynolds equation, and the effects of fluid inertia on the momentum equations are significant at clearances on the order of centimeters; the air flow is governed by Euler's equations.

2.2 Ground-Effect Theories

With the advent of workable air-cushion devices such as hovercrafts in the 1950's, several ground-effect theories were developed and have been applied in industry. They provide aerodynamic characteristics between air-cushion forces acting on the ground and floating heights; aerodynamic forces reduce as a flotation height increases or a jet-nozzle width decreases. These theories are generally divided into two models, by whether the flow profile across air jets is uniform or not. This is largely a function of whether the jet is thick or thin, relative to floating heights.

Thin Jet Model

Mair (1964) studied the peripheral-jet hovercraft that travels at high speed over land or water. Using the momentum balance between the air jet and the cushion pressure, which

acts like a spring, a ground-effect model was developed. He discussed stability, control, and design parameters for the hovercraft with a simple peripheral jet system. Jaumotte and Kiedrzynski (1965) also a presented ground-effect model similar to Mair's and carried out experiments to verify the derived equations. They examined the effects of viscosity of the air jet and the flying speed of a cushion vehicle. The effects of both viscosity and flying speed are a reduction of lift force or cushion pressure. They attempted to compare their ground-effect theories with various other theories that had been presented. The ground-effect theory was applied to the basic aerodynamics of air flotation ovens by Davies and Wood (1983). They pointed out that although the basic theory was originally derived by using extremely crude assumptions, it is accurate and useful for practical engineering purposes, because it can be derived by approximating the full Navier-Stokes equations. Cho (1999) developed the ground-effect model for a flat web tilted in the machine direction to analyze the effects of the tilt angle of a web on the cushion pressure.

When the classical thin jet model is applied to the pressure-pad air bar, the cushion pressure can be expressed as

$$\frac{p}{p_j} = \frac{2\left(1+\cos\theta\right)}{h/b+1+\cos\theta} \tag{2.2.1}$$

where p is the cushion pressure, p_j is the effective total pressure at the nozzle, h is the flotation height, b is the nozzle width, and θ is the angle of jet ejection. However, the thin-jet model is valid only for a large flotation height, $b/h << 1$, because it overpredicts the cushion pressure at small flotation heights; cushion pressure is greater than the total jet pressure at the nozzle, which is physically impossible.

Thick Jet Model

In order to make up for the drawback of the thin-jet model overestimating the cushion pressure at small flotation heights, Crewe and Eggington (1960) derived a thick-jet model for air-cushion vehicles by considering the equilibrium for the pressure difference across the air jet having a pressure gradient within it from the centrifugal force, and performing integration using the Bernoulli equation. The thick-jet model improved by Stanton-Jones was re-examined by Mair (1964), and Jaumotte and Kiedrzynski (1965). This model treated the radius of the jet-flow path as a constant while Crewe and Eggington considered it as a variable. The above thick jet models, however, still have problems at small flotation heights. Chang and Moretti (2000) presented comprehensive summaries and comparison of various ground-effect theories, and investigated the aerodynamic forces of air bars with vent holes. They pointed out that the thick-jet model derived by Stanton-Jones is the best choice for all ranges of flotation height;

$$\frac{p}{p_j} = 1 - e^{-\frac{2(1+\cos\theta)}{h/b}} . \qquad (2.2.2)$$

Figure 3 shows a typical trend of the ground-effect model. The thin jet model (2.2.1) predicts a higher cushion pressure than the thick jet model (2.2.2) as the flotation height decreases. It is shown that the ground-effect theories can be useful for analysis of the aerodynamic characteristics of pressure-pad air bars.

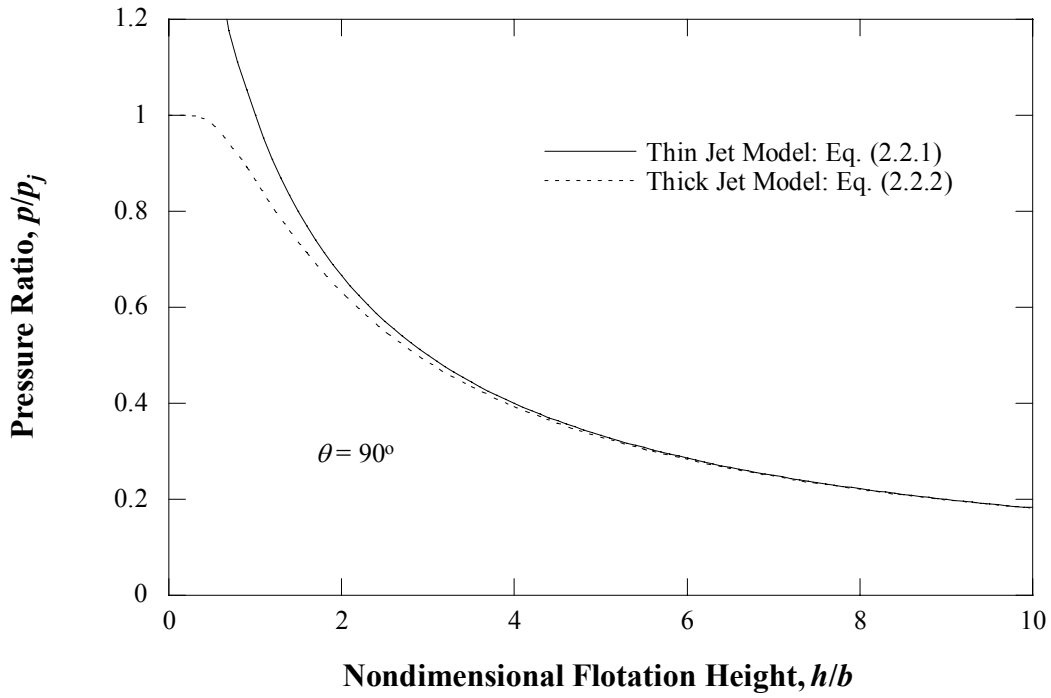

Figure 3 Comparison of Thin Jet Model and Thick Jet Model

2.3 Dynamics of Traveling Continua

Due to technological importance, many researchers have given considerable attention to the dynamics of axially traveling continua such as threadlines, strings, magnetic tapes, belts, band-saw blades, beams, and pipes conveying fluids.

The vast literature on vibrations of axially moving materials is reviewed by Ulsoy *et al*. (1978), and Wickert and Mote (1988). Basic characteristics of axially moving continua show that they lose stability due to high speed of continua and surrounding fluid flows.

Pramila (1986) considered the effects of surrounding air-flows on instability of a web traveling between two rollers. His results show that the critical velocities and the eigenfrequencies are only 15-30% of the values of earlier predictions that neglected the

interaction between a web and surrounding air. A more extended model was presented by Chang (1990). His threadline model of a running web shows that each of the aerodynamic terms (transverse, Coriolis, and centripetal acceleration) in a traveling threadline model is affected differently by the surrounding air. Stability criteria for edge flutter induced by lateral air flows were also presented. Some simple experiments on stability of a flexible web with an air bar were performed by Moretti and Chang (1998). The results demonstrate that when a web is forced to be tilted in the machine direction, it starts to flutter violently with increases in web tension and supply pressure. The main reason for onset of flutter is that the tilted web can destabilize itself. When the tension of an air-floated web running in ovens fluctuates, it causes the flotation height to change. This tension fluctuation can affect the longitudinal dynamics of the air-floated web so that it may touch air bars or begin to flutter. Chang *et al*. (1999) presented an analytical model for prediction of both out-of-plane and longitudinal stiffness (inverse of resiliency) of an air-floated web. The results show that at low tension the longitudinal stiffness is small (i.e., the effect of the air cushion is dominant) while at high tension the effect of material deformation becomes more significant than that of the air cushion.

Wickert and Mote (1990) examined transverse vibrations of traveling strings and beams with the aid of a novel modal analysis proposed by Meirovitch (1974; 1975) who studied the matrix eigenvalue problem for discrete gyroscopic systems. Using traveling string eigenfunctions and a convenient orthogonal basis suitable for discretization, they cast the equations of motion for axially moving materials in a canonical first-order form that is amenable to the formal solution, and established a modal analysis and a Green's function representation of the response to arbitrary excitation and initial conditions.

Wickert (1993) studied free linear vibration of coupled traveling string and air bearing systems. Through the Green's function for the moving string, its deformation is embedded directly in the lubrication equation, and the resulting integro-differential equation governs the equilibrium pressure distribution. The string's equation of motion and the fluid film lubrication equation are linearized about equilibrium and then discretized using the Galerkin's method. The free vibration analysis directly provides natural frequencies, damping ratios, and vibration modes.

Some researches have been conducted on theoretical instability analysis of continua axially moving in a fluid-filled narrow passage with axial leakage flows or shear fluid flows. In most of these studies, governing equations of motion of continua coupled with the shear fluid flow in the narrow channel are derived from the Bernoulli-Euler's beam equation and the Navier-Stokes equations, and the characteristic equation of the system whose roots are used to examine stabilities is presented as a function of the axial speed of the continua. Nagakura and Kaneko (1991) studied instabilities of a flexible cantilever beam subjected to one-dimensional leakage flows while Inada and Hayama (1990) examined the case of an elastically supported rigid plat subjected to the leakage flow. For a rigid body supported by a damper-spring system in a narrow passage, Fujita *et al*. (2000) investigated effects on stability of gap width, body length, and pressure loss coefficients at the inlet and outlet of the passage. Watanabe and Kobayashi (2001) studied vibrations of an axially moving web subjected to two rollers and exposed to shear fluid flows in a narrow passage. The analytical results showed that both divergence-type instability and flutter-type instability occur in the traveling web due to shear fluid flows,

clarifying the effects of the added mass, tensile force, and viscous damping on the instability region.

CHAPTER III

THEORIES

3.1 Equations of Motion

Assuming that a web vibrates in the direction perpendicular to the flow direction, its motion with velocity V_w, mass-per-unit-area m, tension-per-unit-width T, and flexural rigidity-per-unit-width EI is given over $0 \le x \le L$ by

$$\begin{aligned} & m\left(\frac{\partial^2 y}{\partial t^2}+2V_w\frac{\partial^2 y}{\partial t\partial x}+V_w^2\frac{\partial^2 y}{\partial x^2}\right)-T\frac{\partial^2 y}{\partial x^2}+EI\frac{\partial^4 y}{\partial x^4} \\ & = p\left(\mathrm{H}\left(x-x_L\right)-\mathrm{H}\left(x-x_R\right)\right) \end{aligned} \tag{3.1.1}$$

where p is the cushion-pressure which develops within $\left(x_L, x_R\right)$, and deflects the web from its initial configuration. H is the Heaviside unit function defined as

$$\mathrm{H}\left(x\right)=\begin{cases} 1\ , & x>0 \\ 0\ , & x<0 \end{cases}.$$

The web is subjected to the pinned boundary conditons such that

$$\begin{aligned} & y\left(0\right)=y''\left(0\right)=0 \\ & y\left(L\right)=y''\left(L\right)=0 \end{aligned}. \tag{3.1.2}$$

With introduction of the independent variables

$$\begin{aligned} & \overline{x}=\frac{x}{L} \\ & \overline{t}=t\sqrt{\frac{T}{mL^2}} \end{aligned}, \tag{3.1.3}$$

the dependent variables

$$\begin{aligned} \overline{y} &= \frac{y}{L} \\ \overline{p} &= \frac{pL}{T} \end{aligned}, \tag{3.1.4}$$

and the parameters

$$\begin{aligned} \overline{x}_L &= \frac{x_L}{L} \\ \overline{x}_R &= \frac{x_R}{L} \\ D &= \sqrt{\frac{EI}{TL^2}} \\ V &= V_w\sqrt{\frac{m}{T}} \end{aligned}, \tag{3.1.5}$$

the governing equation for the axially-moving web over $0 \le x \le 1$ is written in the dimensionless form

$$\frac{\partial^2 \overline{y}}{\partial \overline{t}^{\,2}} + 2V\frac{\partial^2 \overline{y}}{\partial \overline{t}\,\partial \overline{x}} + \left(V^2 - 1\right)\frac{\partial^2 \overline{y}}{\partial \overline{x}^2} + D^2\frac{\partial^4 \overline{y}}{\partial \overline{x}^4} = \overline{p}\left(\mathrm{H}\left(\overline{x} - \overline{x}_L\right) - \mathrm{H}\left(\overline{x} - \overline{x}_R\right)\right). \tag{3.1.6}$$

The boundary conditons also are given in the dimensionless form by

$$\begin{aligned} \overline{y}(0) &= \overline{y}''(0) = 0 \\ \overline{y}(1) &= \overline{y}''(1) = 0 \end{aligned}. \tag{3.1.7}$$

The motion of air flows between the web and air bar in $x_L \le x \le x_R$ are described by the continuity and Navier-Stokes equations

$$\frac{\partial u}{\partial x} + \frac{\partial v}{\partial y} = 0 \tag{3.1.8}$$

$$\frac{\partial u}{\partial t} + u\frac{\partial u}{\partial x} + v\frac{\partial u}{\partial y} = -\frac{1}{\rho}\frac{\partial p}{\partial x} + \nu\left(\frac{\partial^2 u}{\partial x^2} + \frac{\partial^2 u}{\partial y^2}\right) \tag{3.1.9}$$

$$\frac{\partial v}{\partial t}+u\frac{\partial v}{\partial x}+v\frac{\partial v}{\partial y}=-\frac{1}{\rho}\frac{\partial p}{\partial y}+\nu\left(\frac{\partial^2 v}{\partial x^2}+\frac{\partial^2 v}{\partial y^2}\right) \tag{3.1.10}$$

where u and v are the velocities of the air flow in the x and y directions, respectively, p is the air pressure, ρ is the density of air, and ν is the kinetic viscosity of air. The air flow is incompressible, viscous, and Newtonian.

The air flow is assumed to be almost parallel to the axial direction x, which allows the velocity v and its derivatives to be neglected in Eq. (3.1.10). The transverse pressure gradient is negligible; $\partial p/\partial y \approx 0$, so that the air pressure is the function of only axial displacment; $p = p(x)$.

Integrating the continuity (3.1.8) over y from 0 to h yields

$$\int_0^h \frac{\partial u}{\partial x}dy+\int_0^h \frac{\partial v}{\partial y}dy=0 \tag{3.1.11}$$

where h is the air gap between the web and air bar defined as

$$h = y-\delta\,, \tag{3.1.12}$$

and δ denotes the vertical distance from the x axis to the head surface of the air bar. In view of the fact that we can always write

$$\frac{\partial}{\partial x}\int_{f(x)}^{g(x)} F(x,y)\,dy=\int_{f(x)}^{g(x)}\frac{\partial}{\partial x}F(x,y)\,dy+F\left(x,g(x)\right)\frac{\partial g}{\partial x}-F\left(x,f(x)\right)\frac{\partial f}{\partial x} \tag{3.1.13}$$

which is the Leibnitz integral rule, i.e., a formula for differentiation of a definite integral whose limits are functions of the differential variable, and Eq. (3.1.11) becomes

$$\frac{\partial}{\partial x}\int_0^h u dy-u\big|_{y=h}\frac{\partial h}{\partial x}+v\big|_{y=0}^{y=h}=0\,. \tag{3.1.14}$$

By virtue of the kinematic condition at the upper surface (flexible web) and the zero vertical velocity at the lower surface (air-bar head)

$$v\big|_{y=h} = \frac{\partial h}{\partial t} + u\big|_{y=h}\frac{\partial h}{\partial x} \quad \text{and} \quad v\big|_{y=0} = 0, \tag{3.1.15}$$

Eq. (3.1.14) is rewritten as

$$\frac{\partial h}{\partial t} + \frac{\partial Q}{\partial x} = 0 \tag{3.1.16}$$

where Q is the flow-rate-per-unit-depth defined as

$$Q = \int_0^h u dy. \tag{3.1.17}$$

On the other hand, in order to integrate Eq. (3.1.9), multiplying the continuity (3.1.8) by u, and adding the resultant equation and Navier-Stokes equation (3.1.9), we have

$$\frac{\partial u}{\partial t} + \frac{\partial u^2}{\partial x} + \frac{\partial uv}{\partial y} = -\frac{1}{\rho}\frac{\partial p}{\partial x} + \nu\left(\frac{\partial^2 u}{\partial x^2} + \frac{\partial^2 u}{\partial y^2}\right). \tag{3.1.18}$$

To investigate the relation between pressure and gap height, integrating both sides of Eq. (3.1.18) over y from 0 to h gives

$$\int_0^h \frac{\partial u}{\partial t} dy + \int_0^h \frac{\partial u^2}{\partial x} dy + \int_0^h \frac{\partial uv}{\partial y} dy = -\frac{1}{\rho}\int_0^h \frac{\partial p}{\partial x} dy + \nu\int_0^h \frac{\partial^2 u}{\partial x^2} dy + \nu\int_0^h \frac{\partial^2 u}{\partial y^2} dy. \tag{3.1.19}$$

Applying the formula (3.1.13) yields

$$\begin{aligned} &\frac{\partial}{\partial t}\int_0^h u dy + \frac{\partial}{\partial x}\int_0^h u^2 dy - u\big|_{y=h}\left(\frac{\partial h}{\partial t} + u\big|_{y=h}\frac{\partial h}{\partial x}\right) + uv\Big|_{y=0}^{y=h} \\ &= -\frac{1}{\rho}\int_0^h \frac{\partial p}{\partial x} dy + \nu\int_0^h \frac{\partial^2 u}{\partial x^2} dy + \nu\frac{\partial u}{\partial y}\Big|_{y=0}^{y=h} \end{aligned}, \tag{3.1.20}$$

and using the given conditions (3.1.15) gives

$$\frac{\partial}{\partial t}\int_0^h u dy + \frac{\partial}{\partial x}\int_0^h u^2 dy = -\frac{1}{\rho}\int_0^h \frac{\partial p}{\partial x} dy + \nu\int_0^h \frac{\partial^2 u}{\partial x^2} dy + \nu\frac{\partial u}{\partial y}\Big|_{y=0}^{y=h}. \tag{3.1.21}$$

When Eq. (3.1.8) is differentiated with respect to x, we have

$$\frac{\partial^2 u}{\partial x^2} = -\frac{\partial^2 v}{\partial x \partial y} \tag{3.1.22}$$

so that, in view of the assumption that the velocity v is negligible, it is concluded that $\partial^2 u / \partial x^2 \approx 0$. Furthermore, by virtue of the assumption that h and p are independent of y and the replacement of u by Q, Eq. (3.1.21) becomes in the simpler form

$$\frac{\partial Q}{\partial t} + \frac{\partial}{\partial x}\left(\frac{Q^2}{h}\right) = -\frac{h}{\rho}\frac{\partial p}{\partial x} + \nu \left.\frac{\partial u}{\partial y}\right|_{y=0}^{y=h} \tag{3.1.23}$$

where the second term on the left hand side is approximated (Cancelli and Pedley, 1985; Inada and Hayama, 1990; Hayashi *et al*., 1999; Samin, 1999) as

$$\int_0^h u^2 dy \approx \frac{1}{h}\left(\int_0^h u dy\right)^2 = \frac{Q^2}{h}. \tag{3.1.24}$$

The second term on the right hand side represents the difference between the viscous stresses on the two surfaces defined by

$$\frac{\tau}{\rho} = \nu \frac{\partial u}{\partial y}. \tag{3.1.25}$$

In view of the classical relation that the fluid shear stress τ imposed on the wall by the fluid friction is proportional to the friction factor, it is expressed by

$$\tau = \frac{\rho u_{ave}^2}{2} C_f = \frac{\rho u_{ave}^2}{2}\frac{f}{4} \tag{3.1.26}$$

where C_f is the skin-friction coefficient, f is the Darcy friction factor, and u_{ave} is the average flow velocity over the cross section such that

$$u_{ave} = \frac{1}{h}\int_0^h u dy = \frac{Q}{h}. \tag{3.1.27}$$

Therefore, the last term becomes

$$\nu \left. \frac{\partial u}{\partial y} \right|_{y=0}^{y=h} = -\frac{2\tau}{\rho} = -\frac{u_{ave}^2 f}{4} = -\frac{Q^2 f}{4h^2} \tag{3.1.28}$$

so that the integral of Navier-Stokes equation (3.1.9) over y is cast into the form

$$\frac{\partial Q}{\partial t} + \frac{\partial}{\partial x}\left(\frac{Q^2}{h}\right) = -\frac{h}{\rho}\frac{\partial p}{\partial x} - \frac{Q^2 f}{4h^2}. \tag{3.1.29}$$

There is, however, the friction factor f which needs to be expressed in terms of the flow rate Q. It is given in Appendix A such that

$$f = \frac{48}{\mathrm{Re}} \qquad \text{for laminar flow} \tag{3.1.30}$$

and

$$f = \frac{0.280}{\mathrm{Re}^{0.25}} \quad \text{for turbulent flow} \tag{3.1.31}$$

where

$$\mathrm{Re} = \frac{hu_{ave}}{\nu} = \frac{Q}{\nu}. \tag{3.1.32}$$

To examine the flow rate Q, applying the Bernoulli's equation to the air jet at the nozzle provides the velocity of the air jet through the nozzle

$$p_0 = \frac{p}{2} + \frac{\rho U^2}{2} \tag{3.1.33}$$

where p_0 is the supply pressure. Since the air jet emerging through the nozzle faces both the ambient pressure and the cushion pressure, it is reasonable to assume that the static pressure can be taken as the average of these two pressures. Introducing the discharge coefficient C_d, the velocity is expressed by

$$U = C_d \sqrt{\frac{2\left(p_0 - 0.5p\right)}{\rho}} \tag{3.1.34}$$

where the empirical constant C_d accounts for the losses due to turbulence and contraction of the effective flow rate area near the nozzle. The flow rate Q in the entire flow field can be assumed as the same as the total flow rate through the nozzle with its width b

$$Q = bU = bC_d \sqrt{\frac{2\left(p_0 - 0.5p\right)}{\rho}} \,. \tag{3.1.35}$$

Introducing the independent variables

$$\begin{aligned} \overline{x} &= \frac{x}{L} \\ \overline{t} &= t\sqrt{\frac{T}{mL^2}} \end{aligned}, \tag{3.1.3}$$

the dependent variables

$$\begin{aligned} \overline{h} &= \frac{h}{L} \\ \overline{y} &= \frac{y}{L} \\ \overline{p} &= \frac{pL}{T} \\ \overline{U} &= U\sqrt{\frac{m}{T}} \\ \overline{Q} &= Q\sqrt{\frac{m}{TL^2}} \end{aligned} \quad , \tag{3.1.36}$$

and the parameters

$$\begin{aligned}\bar{b} &= \frac{b}{L} \\ \bar{\delta} &= \frac{\delta}{L} \\ \bar{\rho} &= \rho\frac{L}{m} \\ \bar{v} &= v\sqrt{\frac{m}{TL^2}}\end{aligned} \tag{3.1.37}$$

into the integrated continuity (3.1.16) and Navier-Stokes equation (3.1.29) over y, and the air gap (3.1.12), the governing equations over $\bar{x}_L \le \bar{x} \le \bar{x}_R$ with the coupling condition

$$\bar{h} = \bar{y} - \bar{\delta} \tag{3.1.38}$$

are given in the nondimensional forms

$$\frac{\partial \bar{h}}{\partial \bar{t}} + \frac{\partial \bar{Q}}{\partial \bar{x}} = 0 \tag{3.1.39}$$

and

$$\frac{\partial \bar{Q}}{\partial \bar{t}} + \frac{\partial}{\partial \bar{x}}\left(\frac{\bar{Q}^2}{\bar{h}}\right) = -\frac{\bar{h}}{\bar{\rho}}\frac{\partial \bar{p}}{\partial \bar{x}} - \frac{\bar{Q}^2 f}{4\bar{h}^2} \tag{3.1.40}$$

where

$$\bar{Q} = \bar{b}C_d\sqrt{\frac{2\left(\bar{p}_0 - 0.5\bar{p}\right)}{\bar{\rho}}}\,. \tag{3.1.41}$$

3.2 Equilibrium Solution

The equilibrium web displacement $\bar{y}^*(x)$ and air pressure $\bar{p}^*(x)$ satisfy the time-independent form of Eqs. (3.1.6), (3.1.38), (3.1.39), and (3.1.40) such that, respectively,

$$D^2\frac{\partial^4 \bar{y}^*}{\partial \bar{x}^4} + \left(V^2 - 1\right)\frac{\partial^2 \bar{y}^*}{\partial \bar{x}^2} = \bar{p}^*\left(\mathrm{H}\left(\bar{x} - \bar{x}_L\right) - \mathrm{H}\left(\bar{x} - \bar{x}_R\right)\right), \tag{3.2.1}$$

$$\bar{h}^* = \bar{y}^* - \bar{\delta}\,, \tag{3.2.2}$$

$$\frac{\partial \bar{Q}^*}{\partial \bar{x}} = 0\,, \tag{3.2.3}$$

and

$$\frac{\partial}{\partial \bar{x}}\left(\frac{\bar{Q}^{*2}}{\bar{h}^*}\right) = -\frac{\bar{h}^*}{\bar{\rho}}\frac{\partial \bar{p}^*}{\partial \bar{x}} - \frac{\bar{Q}^{*2} f^*}{4\bar{h}^{*2}}\,, \tag{3.2.4}$$

where the equilibrium flow rate $\bar{Q}^*$ is the same as the total flow rate through the nozzle with its width $\bar{b} = b/L$ in view of Eq. (3.1.41)

$$\bar{Q}^* = \bar{b} C_d \sqrt{\frac{2\left(\bar{p}_0 - 0.5\bar{p}^*\right)}{\bar{\rho}}}\,. \tag{3.2.5}$$

Eq. (3.2.4) can be rewritten to solve the equilibrium pressure

$$\frac{\partial \bar{p}^*}{\partial \bar{x}} = \frac{\bar{\rho}\bar{Q}^{*2}}{\bar{h}^{*3}}\left(\frac{\partial \bar{h}^*}{\partial \bar{x}} - \frac{2\bar{h}^*}{\bar{Q}^*}\frac{\partial \bar{Q}^*}{\partial \bar{x}} - \frac{f^*}{4}\right). \tag{3.2.6}$$

Using using Eqs. (3.2.2), (3.2.3), and (3.2.5), the equilibrium air pressure can be expressed by

$$\frac{\partial \bar{p}^*}{\partial \bar{x}} = \frac{2\bar{b}^2 C_d^2\left(\bar{p}_0 - 0.5\bar{p}^*\right)}{\left(\bar{y}^* - \bar{\delta}\right)^3}\left(\frac{\partial \bar{y}^*}{\partial \bar{x}} - \frac{f^*}{4}\right) \tag{3.2.7}$$

where, for laminar and turbulent flows, respectively,

$$f^* = \frac{48}{\mathrm{Re}^*} = \frac{48}{\bar{Q}^*/\bar{\nu}} \tag{3.2.8}$$

and

$$f^* = \frac{0.280}{\mathrm{Re}^{*0.25}} = \frac{0.280}{\left(\bar{Q}^*/\bar{\nu}\right)^{0.25}}\,. \tag{3.2.9}$$

Because Eq. (3.2.7) is the first-order differential equation, one boundary condition is necessary to solve it. The condition can be given from ground-effect theories. Applying the Stanton-Jones' thick jet model to the air jet coming through the right-hand nozzle as shown in Figure 1 provides (Chang and Moretti, 2000)

$$\frac{\overline{p}^*}{\overline{p}_0} = 1 - e^{-\frac{2C_d^2\overline{b}}{\overline{y}^* - \overline{\delta}}}. \tag{3.2.10}$$

The aero-elastic equations to describe the air-web system are presented. A Green's function is one of useful methods to solve an inhomogeneous differential equation with boundary conditions. The Green's function is introduced to the coupled system in order to obtain equilibrium solution to the problem. It enables us to avoid simultaneous solution of, and iteration between, the elastic and pressure equations. Through the Green's function for static deflection of a traveling web, the elastic equation (3.2.1) is inverted in closed form for $\overline{y}^*$ so that its diplacement is represented explicitly in terms of the pressure by convolution. Substitution of that solution into the pressure equation (3.2.7) provides a single integro-differential equation for $\overline{p}^*$. Furthermore, only $\overline{p}^*$ is discretized in the present approach so that fewer degrees of freedom are required for numerical solution.

In order to construct the Green's function for the elastic equation (3.2.1), it can be rewritten by

$$\frac{\partial^4 G}{\partial \overline{x}^4} - \alpha^2 \frac{\partial^2 G}{\partial \overline{x}^2} = \frac{1}{D^2}\delta\left(\overline{x} - \xi\right), \tag{3.2.11}$$

which has the concentrated load at $\overline{x}_L \le \overline{x} = \xi \le \overline{x}_R$, and α denotes $\sqrt{1-V^2}/D$. Because of the Dirac delta function, we have two solutions to this equation as follows:

$$G_1(\bar{x}) = A_1 + B_1\bar{x} + C_1 e^{\alpha\bar{x}} + D_1 e^{-\alpha\bar{x}}, \quad (\bar{x} < \xi) \tag{3.2.12}$$

$$G_2(\bar{x}) = A_2 + B_2\bar{x} + C_2 e^{\alpha\bar{x}} + D_2 e^{-\alpha\bar{x}}, \quad (\bar{x} > \xi) \tag{3.2.13}$$

which are subject to the boundary conditions

$$\begin{aligned} G_1(0) &= G_1''(0) = 0 \\ G_2(1) &= G_2''(1) = 0 \end{aligned} . \tag{3.2.14}$$

The two boundary conditions at $\bar{x} = 0$ can enable two of the constants of the set A_1, B_1, C_1, D_1 to be eliminated, while the two boundary conditions at $\bar{x} = 1$ can allow the set A_2, B_2, C_2, D_2 to be reduced to two.

Four conditions are required at $\bar{x} = \xi$ to determine the others. Continuity conditions on the deflection, slope, and curvature provide three of them

$$\begin{aligned} G_1(\xi - \varepsilon) &= G_2(\xi + \varepsilon) \\ G_1'(\xi - \varepsilon) &= G_2'(\xi + \varepsilon) \\ G_1''(\xi - \varepsilon) &= G_2''(\xi + \varepsilon) \end{aligned} \tag{3.2.15}$$

where ε is an arbitrarily small quantity.

The fourth is a jump condition on the shear, and may be established by integration across the load discontinuity $\bar{x} = \xi$. Thus,

$$\int_{\xi-\varepsilon}^{\xi+\varepsilon} G^{IV} d\bar{x} - \alpha^2 \int_{\xi-\varepsilon}^{\xi+\varepsilon} G'' d\bar{x} = \frac{1}{D^2} \int_{\xi-\varepsilon}^{\xi+\varepsilon} \delta(\bar{x} - \zeta) d\bar{x} \tag{3.2.16}$$

or

$$G'''(\bar{x})\Big|_{\xi-\varepsilon}^{\xi+\varepsilon} - \alpha^2 G'(\bar{x})\Big|_{\xi-\varepsilon}^{\xi+\varepsilon} = \frac{1}{D^2}. \tag{3.2.17}$$

In view of $G_1'(\xi - \varepsilon) = G_2'(\xi + \varepsilon)$, that is, the slope is continuous across $\bar{x} = \xi$, the second term on the left hand side vanishes so that the fourth condition can be found as

$$G_2'''(\xi) - G_1'''(\xi) = \frac{1}{D^2}. \tag{3.2.18}$$

The Green's function associated with Eq. (3.2.1) can be constructed through the application of the eight conditions (3.2.14), (3.2.15), and (3.2.18) into Eqs. (3.2.12) and (3.2.13) (See Appendix B)

$$\begin{aligned} G(\bar{x},\xi) = {} & \frac{1}{1-V^2}\left((1-\xi)\bar{x} - \frac{\sinh\alpha(1-\xi)\sinh\alpha\bar{x}}{\alpha\sinh\alpha}\right)\mathrm{H}(\xi-\bar{x}) \\ & + \frac{1}{1-V^2}\left((1-\bar{x})\xi - \frac{\sinh\alpha\xi\sinh\alpha(1-\bar{x})}{\alpha\sinh\alpha}\right)\mathrm{H}(\bar{x}-\xi) \end{aligned}. \tag{3.2.19}$$

A Green's function is called a structural influence function because it is possible to interpret the Green's function as the transverse deflection of a web at $\bar{x}$ when the only load is a unit concentrated force at ξ, and its ends are kept fixed. It is notable that the Green's function is itself symmetric in its arguments such that

$$G(\bar{x},\xi) = G(\xi,\bar{x}). \tag{3.2.20}$$

The displacement can be expressed explicitly in terms of the pressure by convolution

$$\bar{y}^*(x) = \int_{\bar{x}_L}^{\bar{x}_R} G(\bar{x},\xi)\,\bar{p}^*(\xi)\,d\xi. \tag{3.2.21}$$

Substitution of the equilibrium displacement (3.2.21) into the pressure equation (3.2.7) yields an integro-differential equation for p^*

$$\frac{\partial\bar{p}^*}{\partial\bar{x}} = 2\bar{b}^2 C_d^2\left(\bar{p}_0 - 0.5\bar{p}^*\right)\frac{\int_{\bar{x}_L}^{\bar{x}_R}\frac{\partial G(\bar{x},\xi)}{\partial\bar{x}}\bar{p}^*(\xi)\,d\xi - \frac{f^*}{4}}{\left(\int_{\bar{x}_L}^{\bar{x}_R} G(\bar{x},\xi)\,\bar{p}^*(\xi)\,d\xi - \bar{\delta}\right)^3} \tag{3.2.22}$$

where

$$\frac{\partial G(\bar{x},\xi)}{\partial \bar{x}} = \frac{1}{1-V^2}\left(1-\xi-\frac{\sinh\alpha(1-\xi)\cosh\alpha\bar{x}}{\sinh\alpha}\right)\mathrm{H}(\xi-\bar{x}) + \frac{1}{1-V^2}\left(-\xi+\frac{\sinh\alpha\xi\cosh\alpha(1-\bar{x})}{\sinh\alpha}\right)\mathrm{H}(\bar{x}-\xi) \quad . \tag{3.2.23}$$

Also, substitution into the boundary condition (3.2.10) gives

$$\frac{\bar{p}^*}{\bar{p}_0} = 1-e^{-2C_d^2\bar{b}\left(\int_{\bar{x}_L}^{\bar{x}_R} G(\bar{x},\xi)\bar{p}^*(\xi)d\xi-\bar{\delta}\right)^{-1}} \quad . \tag{3.2.24}$$

For numerical solutions, the displacement is expressed in terms of the nodal pressures

$$\bar{y}_n^* = \sum_{m=1}^{N-1}\frac{\bar{x}_{m+1}-\bar{x}_m}{2}\left(G(\bar{x}_n,\bar{x}_{m+1})\,\bar{p}_{m+1}^* + G(\bar{x}_n,\bar{x}_m)\,\bar{p}_m^*\right) \tag{3.2.25}$$

at the spatial nodes, for $n = 1, 2, \ldots, N$,

$$\bar{x}_n = \bar{x}_L + \frac{\bar{x}_R-\bar{x}_L}{N-1}(n-1). \tag{3.2.26}$$

The equilibrium pressures (3.2.22) and (3.2.24) are discretized by a finite difference method to obtain the set $\mathbf{f}(\bar{\mathbf{p}}^*)=0$ of nonlinear algebraic equations in terms of the vector $\bar{\mathbf{p}}^*$ of nodal pressure $\bar{p}_n^*$ at N stations within $(\bar{x}_L,\bar{x}_R)$. When the multi-dimensional Newton-Raphson method is used to find roots, estimates of the solution at each stage of iteration are updated as

$$\bar{\mathbf{p}}_{\text{new}}^* = \bar{\mathbf{p}}_{\text{old}}^* - \left(\nabla\mathbf{f}\left(\bar{\mathbf{p}}_{\text{old}}^*\right)\right)^{-1}\mathbf{f}\left(\bar{\mathbf{p}}_{\text{old}}^*\right). \tag{3.2.27}$$

where ∇ is the Jacobian operator. The numerical procedure for equilibrium solution is presented in Appendix C. Both the equilibrium pressure distribution and deflection profile are obtained for the web and air-bar system through the numerical implementation. Calculated results show good agreement with ground-effect theories.

The effect of supply pressure on the cushion pressure and web deflection is plotted in Figures 4 and 5, respectively. Higher pressure supplied to the air bar makes the static cushion pressure larger so that the web deflection also increases with the corresponding air pressure.

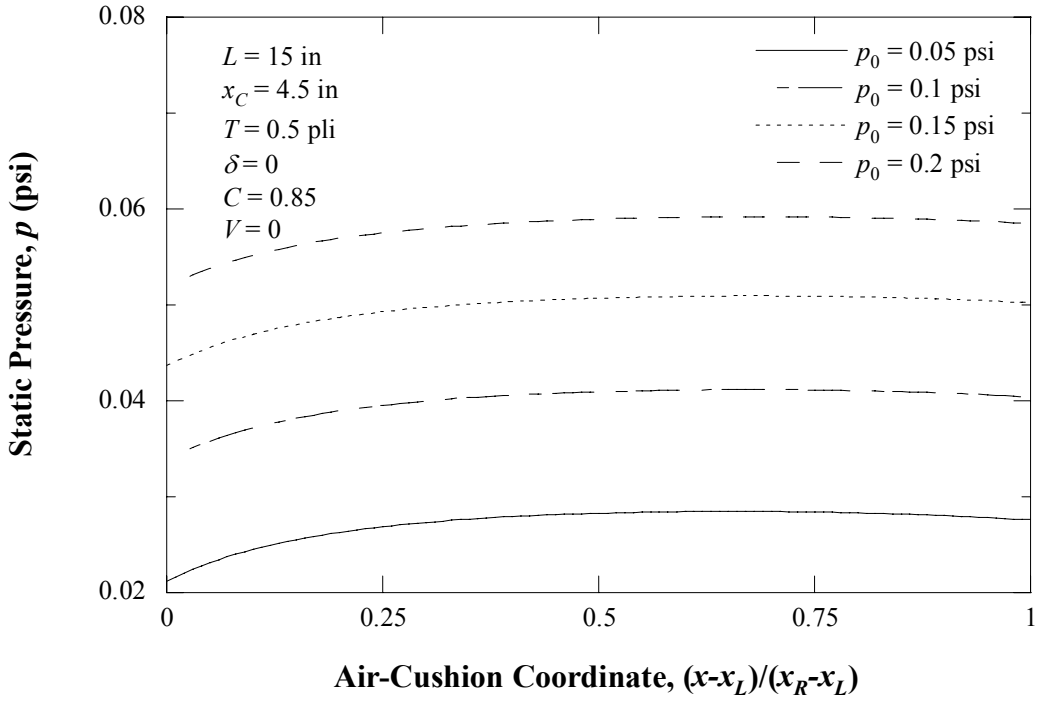

Figure 4 Effect of Supply Pressure on Cushion Pressure

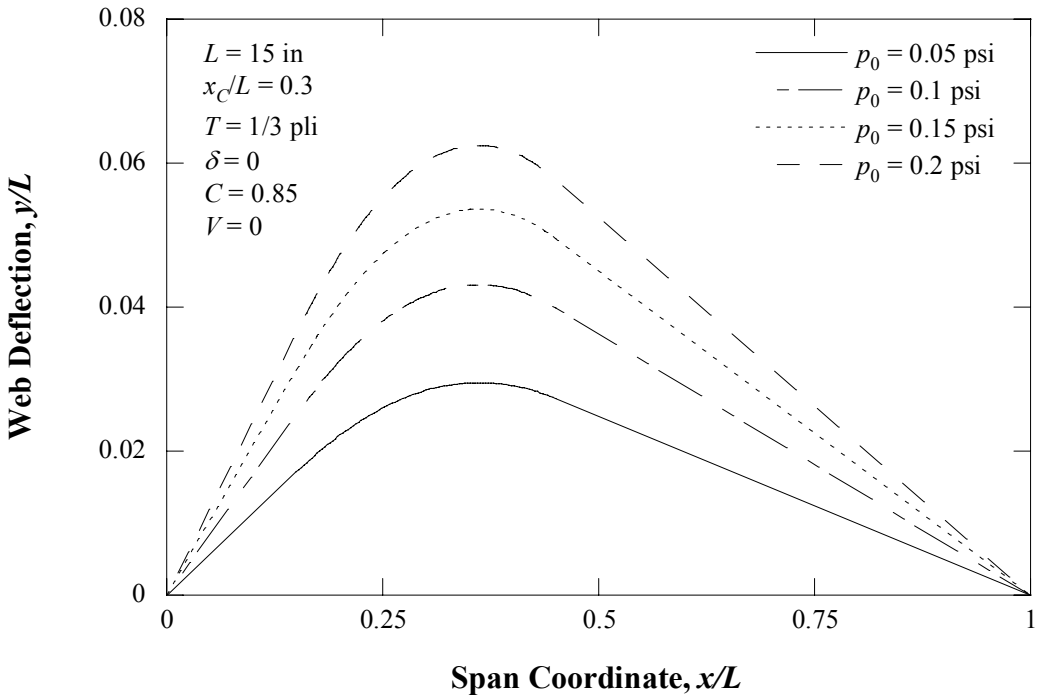

Figure 5 Effect of Supply Pressure on Web Deflection

Figure 6 shows the effect of tension on the air pressure. When the web tension increases with keeping a certain supply pressure, the static pressure also increases but drops significantly in the entrance region of the air-bar head while it becomes almost uniform in the other region. As presented in Figure 7, since the higher tension results in the smaller gap at the entrance, the air velocity increases so that the air pressure should be reduced.

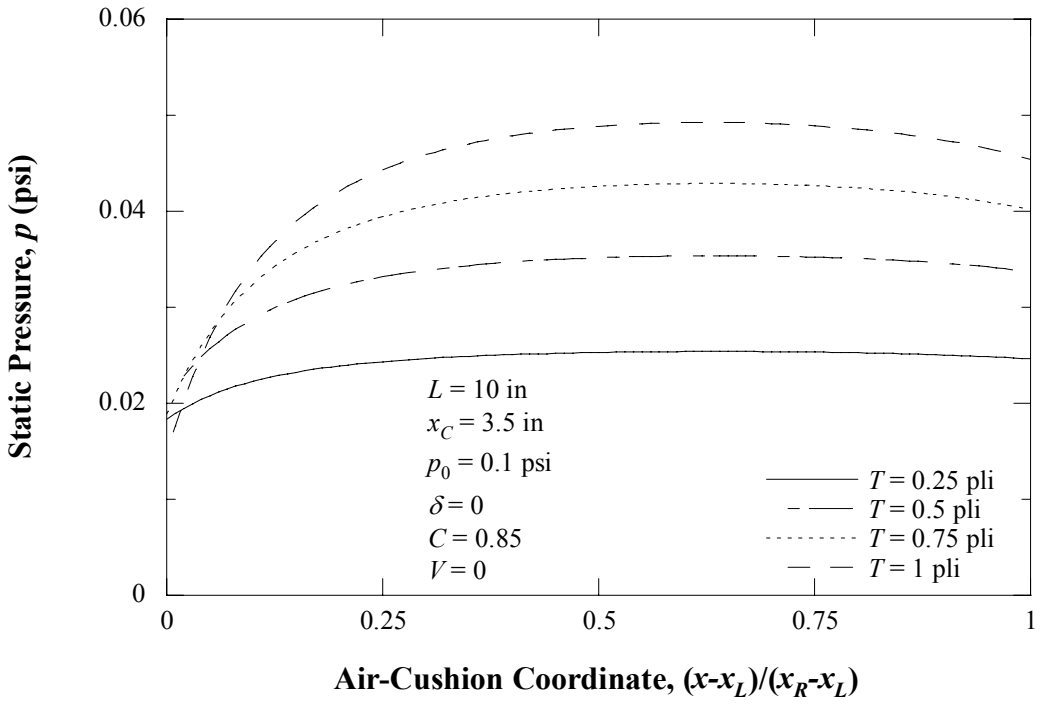

Figure 6 Effect of Tension on Cushion Pressure

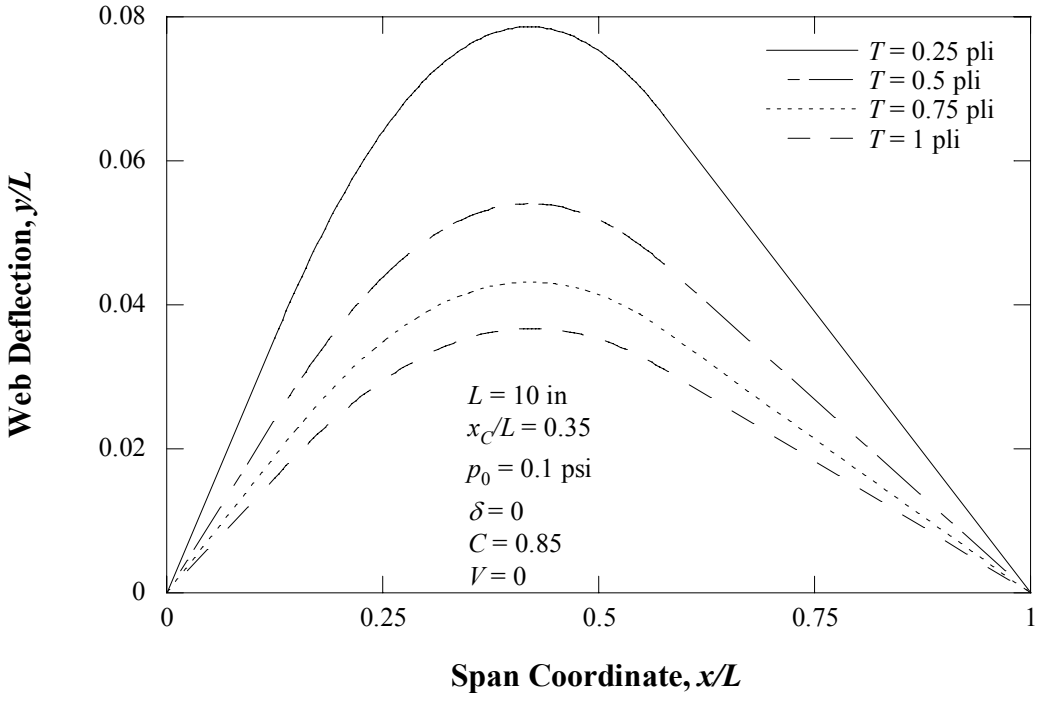

Figure 7 Effect of Tension on Web Deflection

The horizontal location of the air bar has a remarkable effect on the cushion pressure as shown in Figure 8. With the supply pressure and tension being constant, as the air bar moves from the middle of the web span to the left-end support, and vice versa, the cushion pressure decreases, and loses its uniformity; a significant pressure drop occurs in the entrance region. Also, the web deflection decreases, and shifts to the origin as plotted in Figure 9.

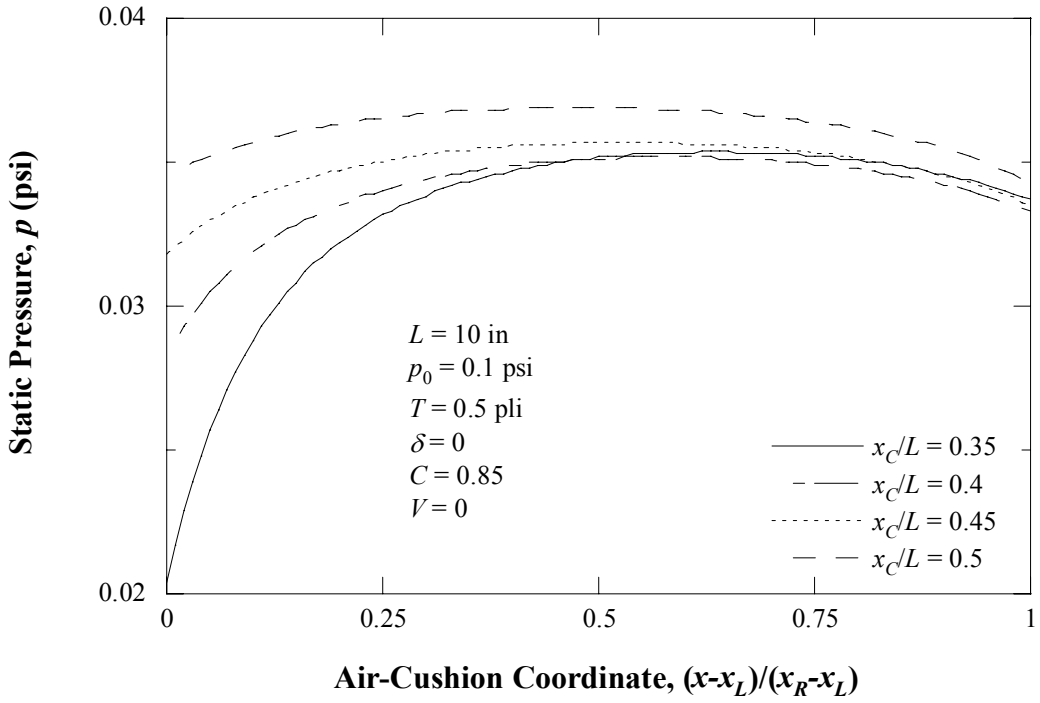

Figure 8 Effect of Horizontal Location of Air-Bar Center on Cushion Pressure

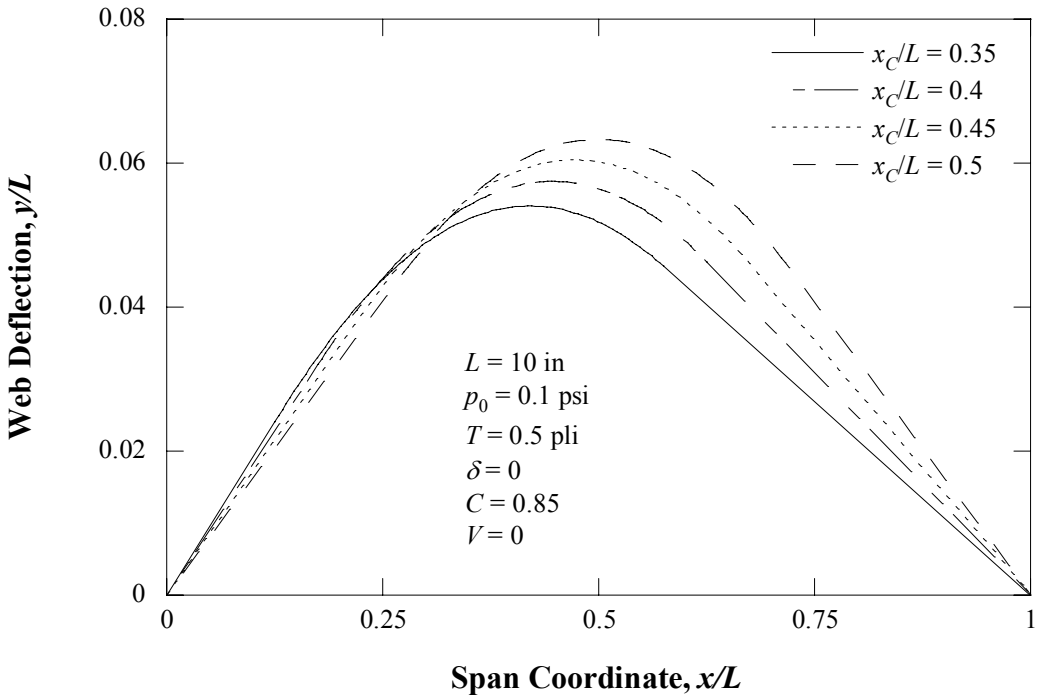

Figure 9 Effect of Horizontal Location of Air-Bar Center on Web Deflection

The effect of web length on the cushion pressure and web deflection is presented in Figures 10 and 11, respectively. When the supply pressure and tension are kept constant, and the air bar is positioned at the center half of the web span, the longer web length results in the lower static pressure and higher deflection; the longer web is deformed more easily than the shorter at the same air pressure.

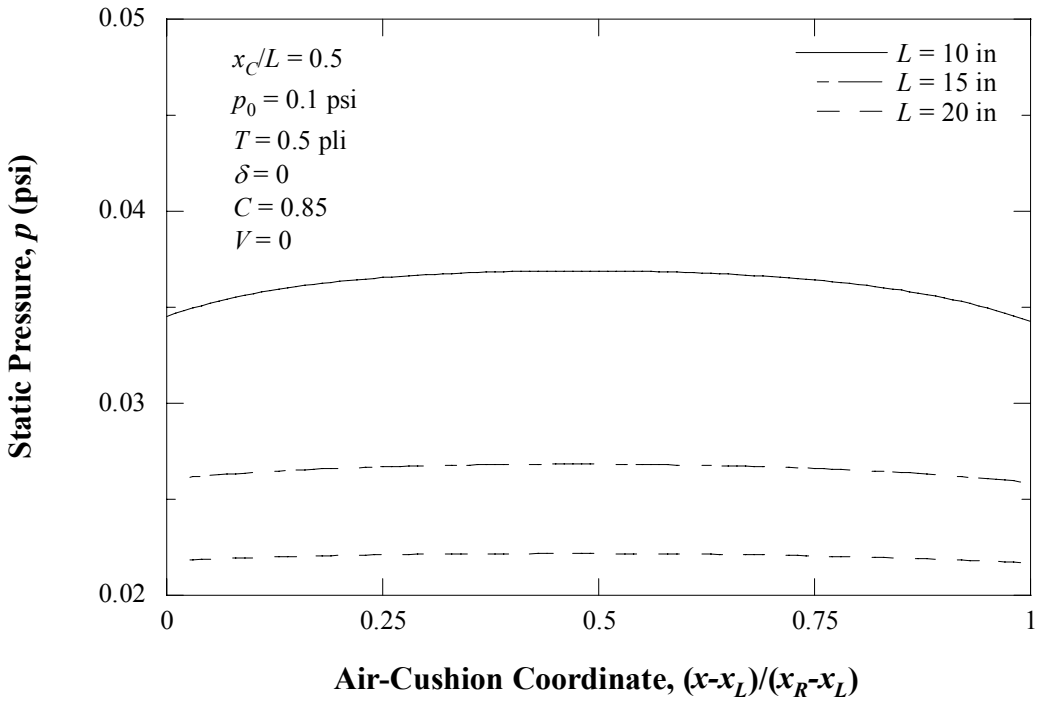

Figure 10 Effect of Web Length on Cushion Pressure

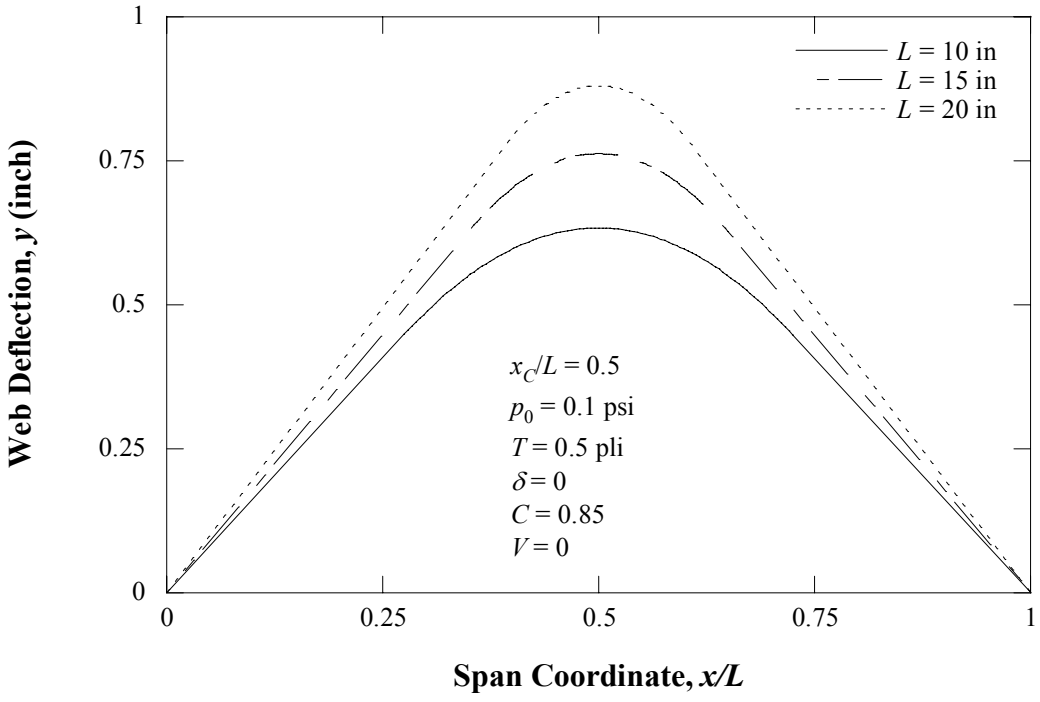

Figure 11 Effect of Web Length on Web Deflection

Figures 12 and 13 show the effect of vertical distance from the air-bar head on the cushion pressure and web deflection, respectively. With the supply pressure, tension, and air-bar position being fixed, as the vertical distance from the air-bar head to the x axis increases, the cushion pressure increases but loses its uniformity. It is shown in Figure 13 that an increase in δ leads to an increase in web deflection. It is notable that, however, the actual air gap becomes smaller as δ becomes larger.

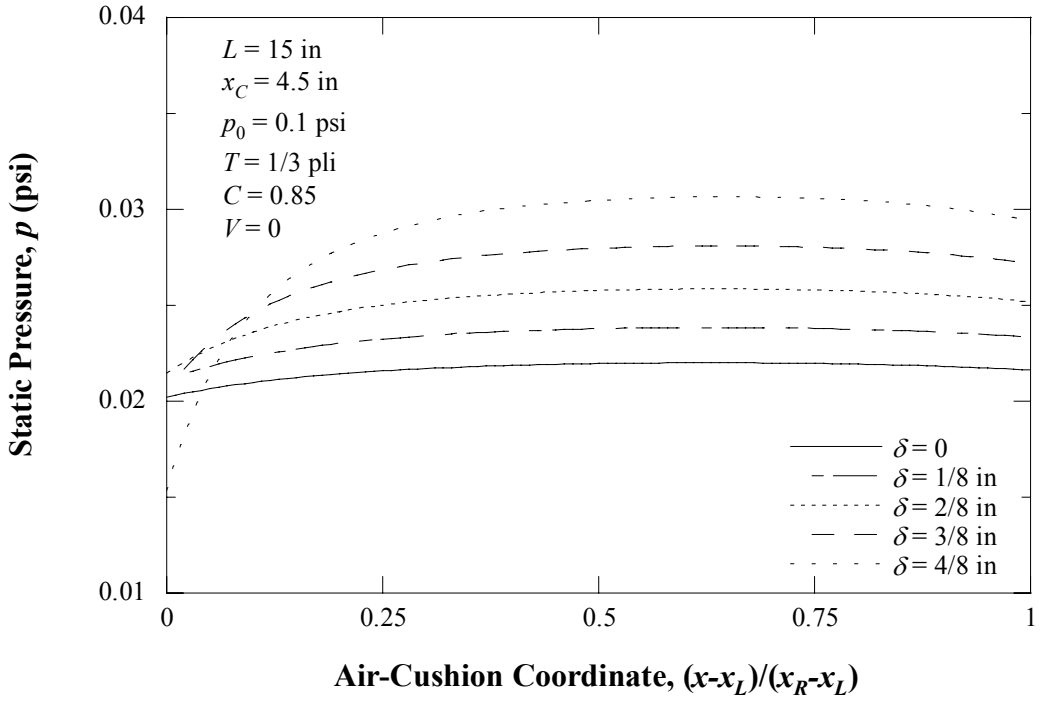

Figure 12 Effect of Vertical Location of Air-Bar Head on Cushion Pressure

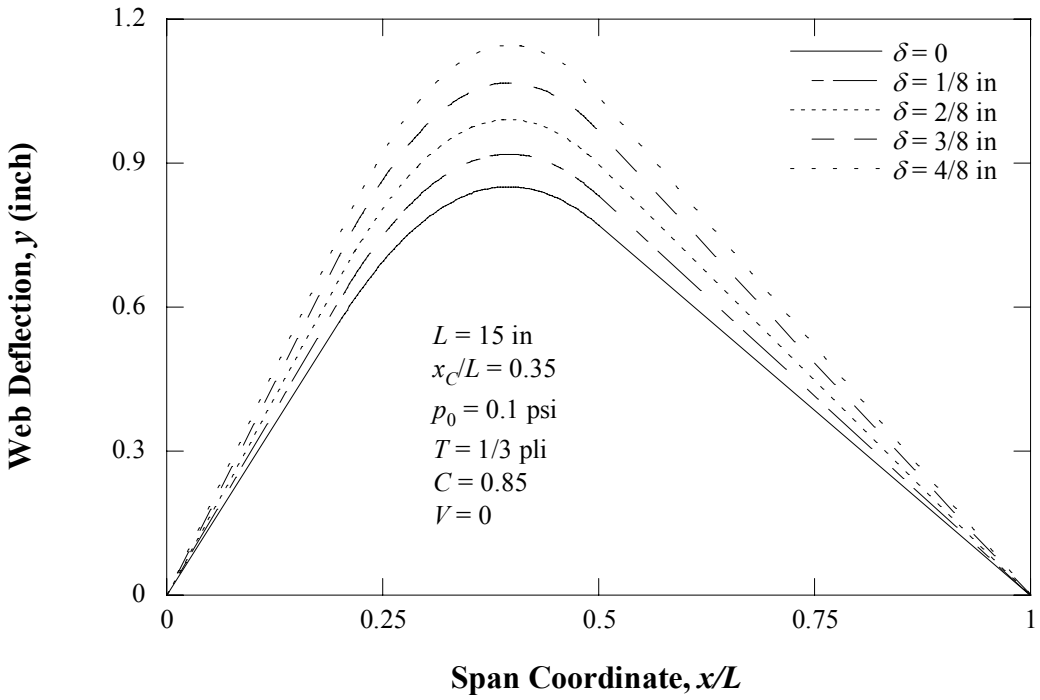

Figure 13 Effect of Vertical Location of Air-Bar Head on Web Deflection

With the supply pressure, tension, and air-bar position being fixed, as the web transports at high speed, the web becomes bulging so that the cushion pressure decreses as plotted in Figures 14 and 15. It is concluded that the effect of web speed (centrifugal effect) on the pressure and deformation is opposite to that of web tension (centripetal effect).

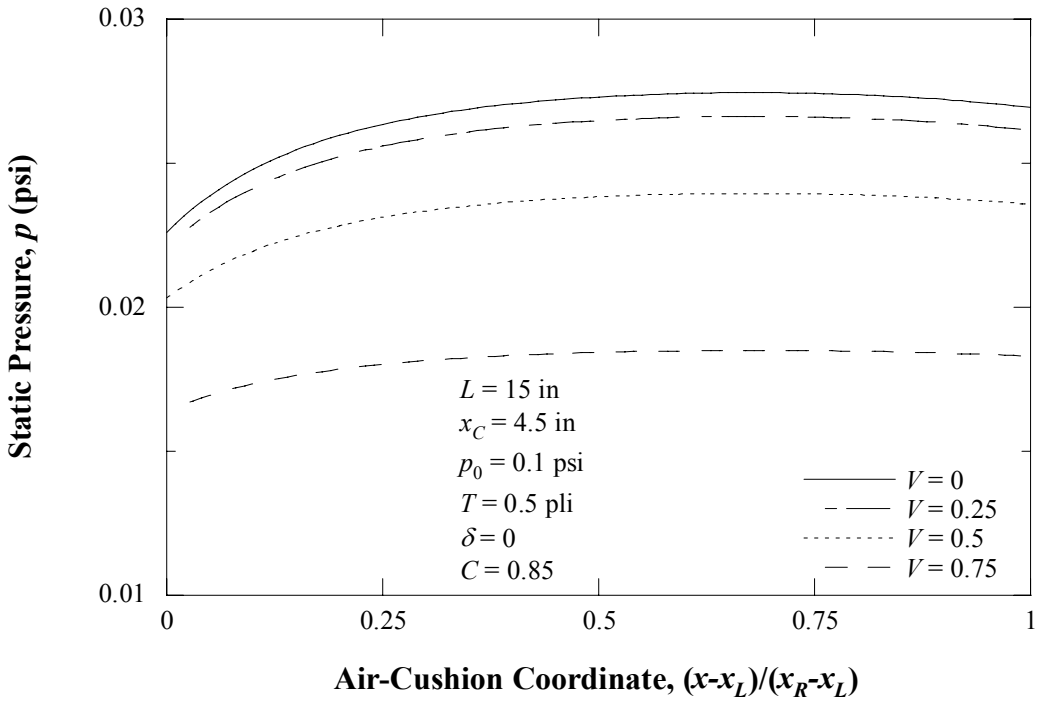

Figure 14 Effect of Web Speed on Cushion Pressure

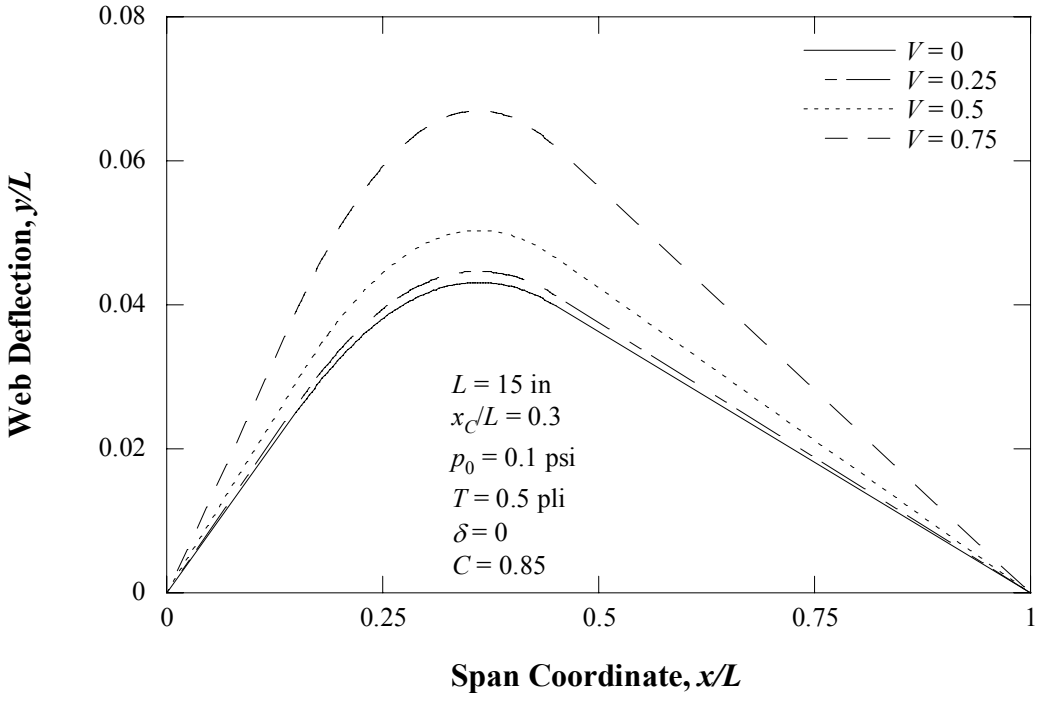

Figure 15 Effect of Web Speed on Web Deflection

3.3 Linearization

The elastic equation (3.1.6) can be linearized about equilibrium by the following substitutions

$$\begin{aligned} \bar{y} &\to \bar{y}^* + \varepsilon \tilde{y} \\ \bar{p} &\to \bar{p}^* + \varepsilon \tilde{p} \end{aligned}, \tag{3.3.1}$$

where the small parameter ε scales the deviation from equilibrium, such that

$$\begin{aligned} &\frac{\partial^2}{\partial \bar{t}^2}\left(\bar{y}^* + \varepsilon \tilde{y}\right) + 2V \frac{\partial^2}{\partial \bar{t}\,\partial \bar{x}}\left(\bar{y}^* + \varepsilon \tilde{y}\right) + \left(V^2 - 1\right)\frac{\partial^2}{\partial \bar{x}^2}\left(\bar{y}^* + \varepsilon \tilde{y}\right) \\ &+ D^2 \frac{\partial^4}{\partial \bar{x}^4}\left(\bar{y}^* + \varepsilon \tilde{y}\right) = \left(\bar{p}^* + \varepsilon \tilde{p}\right)\left(\mathrm{H}\left(\bar{x} - \bar{x}_L\right) - \mathrm{H}\left(\bar{x} - \bar{x}_R\right)\right) \end{aligned} \tag{3.3.2}$$

or

$$\begin{aligned} &\frac{\partial^2 \bar{y}^*}{\partial \bar{t}^2} + 2V \frac{\partial^2 \bar{y}^*}{\partial \bar{t}\,\partial \bar{x}} + \left(V^2 - 1\right)\frac{\partial^2 \bar{y}^*}{\partial \bar{x}^2} + D^2 \frac{\partial^4 \bar{y}^*}{\partial \bar{x}^4} \\ &+ \varepsilon\left[\frac{\partial^2 \tilde{y}}{\partial \bar{t}^2} + 2V \frac{\partial^2 \tilde{y}}{\partial \bar{t}\,\partial \bar{x}} + \left(V^2 - 1\right)\frac{\partial^2 \tilde{y}}{\partial \bar{x}^2} + D^2 \frac{\partial^4 \tilde{y}}{\partial \bar{x}^4}\right] \\ &= \bar{p}^*\left(\mathrm{H}\left(\bar{x} - \bar{x}_L\right) - \mathrm{H}\left(\bar{x} - \bar{x}_R\right)\right) + \varepsilon \tilde{p}\left(\mathrm{H}\left(\bar{x} - \bar{x}_L\right) - \mathrm{H}\left(\bar{x} - \bar{x}_R\right)\right) \end{aligned} \quad . \tag{3.3.3}$$

The terms in ε^0 imply the elastic equation in equilibrium which is presented in Eq. (3.2.1). Retaining only the first order terms in ε, we have the linearized elastic equation

$$\frac{\partial^2 \tilde{y}}{\partial \bar{t}^2} + 2V \frac{\partial^2 \tilde{y}}{\partial \bar{t}\,\partial \bar{x}} + \left(V^2 - 1\right)\frac{\partial^2 \tilde{y}}{\partial \bar{x}^2} + D^2 \frac{\partial^4 \tilde{y}}{\partial \bar{x}^4} = \tilde{p}\left(\mathrm{H}\left(\bar{x} - \bar{x}_L\right) - \mathrm{H}\left(\bar{x} - \bar{x}_R\right)\right). \tag{3.3.4}$$

In a similar way, the fluid equations (3.1.39) and (3.1.40) are linearized about equilibrium. Following the substitutions

$$\begin{aligned} \bar{h} &\to \bar{h}^* + \varepsilon \tilde{h} \\ \bar{p} &\to \bar{p}^* + \varepsilon \tilde{p} \\ \bar{Q} &\to \bar{Q}^* + \varepsilon \tilde{Q} \\ f &\to f^* + \varepsilon \frac{\partial f^*}{\partial \bar{Q}^*} \tilde{Q} \end{aligned} \quad , \tag{3.3.5}$$

we have, respectively,

$$\frac{\partial}{\partial \bar{t}}\left(\bar{h}^* + \varepsilon\tilde{h}\right) + \frac{\partial}{\partial \bar{x}}\left(\bar{Q}^* + \varepsilon\tilde{Q}\right) = 0 \tag{3.3.6}$$

and

$$\begin{aligned} &\frac{\partial}{\partial \bar{t}}\left(\bar{Q}^* + \varepsilon\tilde{Q}\right) + \frac{\partial}{\partial \bar{x}}\left(\frac{\left(\bar{Q}^* + \varepsilon\tilde{Q}\right)^2}{\bar{h}^* + \varepsilon\tilde{h}}\right) \\ &= -\frac{\bar{h}^* + \varepsilon\tilde{h}}{\bar{\rho}}\frac{\partial}{\partial \bar{x}}\left(\bar{p}^* + \varepsilon\tilde{p}\right) - \frac{\left(\bar{Q}^* + \varepsilon\tilde{Q}\right)^2}{4\left(\bar{h}^* + \varepsilon\tilde{h}\right)^2}\left(f^* + \varepsilon\frac{\partial f^*}{\partial \bar{Q}^*}\tilde{Q}\right) \end{aligned} . \tag{3.3.7}$$

Retaining only the first order terms of the unsteady components and using the following

$$\frac{\partial \bar{Q}^*}{\partial \bar{t}} = \frac{\partial \bar{Q}^*}{\partial \bar{x}} = 0\,, \tag{3.3.8}$$

the linearized fluid equations with respect to the unsteady components are obtained

$$\frac{\partial \tilde{h}}{\partial \bar{t}} + \frac{\partial \tilde{Q}}{\partial \bar{x}} = 0 \tag{3.3.9}$$

and

$$\begin{aligned} -\frac{\bar{h}^*}{\bar{\rho}}\frac{\partial \tilde{p}}{\partial \bar{x}} = \frac{\partial \tilde{Q}}{\partial \bar{t}} + \left(\frac{f^*\bar{Q}^*}{4\bar{h}^{*2}}\left(2 + \frac{\bar{Q}^*}{f^*}\frac{\partial f^*}{\partial \bar{Q}^*}\right) - \frac{2\bar{Q}^*}{\bar{h}^{*2}}\frac{\partial \bar{h}^*}{\partial \bar{x}}\right)\tilde{Q} \\ + \frac{2\bar{Q}^*}{\bar{h}^*}\frac{\partial \tilde{Q}}{\partial \bar{x}} + \frac{3}{\bar{\rho}}\frac{\partial \bar{p}^*}{\partial \bar{x}}\tilde{h} - \frac{\bar{Q}^{*2}}{\bar{h}^{*2}}\frac{\partial \tilde{h}}{\partial \bar{x}} \end{aligned} \tag{3.3.10}$$

where

$$\frac{\partial \bar{p}^*}{\partial \bar{x}} = \frac{\bar{\rho}\bar{Q}^{*2}}{\bar{h}^{*3}}\left(\frac{\partial \bar{h}^*}{\partial \bar{x}} - \frac{f^*}{4}\right). \tag{3.3.11}$$

Substituting Eqs. (3.3.9) and (3.3.11) into Eq. (3.3.10) yields

$$\frac{\partial \tilde{Q}}{\partial \bar{t}}+\left(\frac{f^{*}\bar{Q}^{*}}{4\bar{h}^{*2}}\left(2+\frac{\bar{Q}^{*}}{f^{*}}\frac{\partial f^{*}}{\partial \bar{Q}^{*}}\right)-\frac{2\bar{Q}^{*}}{\bar{h}^{*2}}\frac{\partial \bar{h}^{*}}{\partial \bar{x}}\right)\tilde{Q}$$
$$-\frac{2\bar{Q}^{*}}{\bar{h}^{*}}\frac{\partial \tilde{h}}{\partial \bar{t}}+\frac{3\bar{Q}^{*2}}{\bar{h}^{*3}}\left(\frac{\partial \bar{h}^{*}}{\partial \bar{x}}-\frac{f^{*}}{4}\right)\tilde{h}-\frac{\bar{Q}^{*2}}{\bar{h}^{*2}}\frac{\partial \tilde{h}}{\partial \bar{x}}+\frac{\bar{h}^{*}}{\bar{\rho}}\frac{\partial \tilde{p}}{\partial \bar{x}}=0 \quad . \tag{3.3.12}$$

Moreover, the substitutions

$$\begin{aligned}\bar{h} &\to \bar{h}^{*}+\varepsilon\tilde{h}\\ \bar{y} &\to \bar{y}^{*}+\varepsilon\tilde{y}\end{aligned} \tag{3.3.13}$$

into Eq. (3.1.38) gives

$$\tilde{h}=\tilde{y}\,. \tag{3.3.14}$$

Using Eqs. (3.3.9) and (3.3.14), the unsteady flow rate $\tilde{Q}$ can be expressed as

$$\begin{aligned}\tilde{Q} &= \int \frac{\partial \tilde{Q}}{\partial \bar{x}}d\bar{x}+\tilde{Q}\left(\bar{x}_{L},\bar{t}\right)\\ &= -\int \frac{\partial \tilde{y}}{\partial \bar{t}}d\bar{x}+\tilde{Q}\left(\bar{x}_{L},\bar{t}\right)\end{aligned} \quad . \tag{3.3.15}$$

In order to find $\tilde{Q}\left(\bar{x}_{L},\bar{t}\right)$, following the substitutions

$$\begin{aligned}\bar{p} &\to \bar{p}^{*}+\varepsilon\tilde{p}\\ \bar{Q} &\to \bar{Q}^{*}+\varepsilon\tilde{Q}\end{aligned} \tag{3.3.16}$$

into Eq. (3.1.41)

$$\bar{Q}\left(\bar{x}_{L},\bar{t}\right)=\bar{b}C_{d}\sqrt{\frac{2\left(\bar{p}_{0}-0.5\bar{p}\left(\bar{x}_{L},\bar{t}\right)\right)}{\bar{\rho}}}\,,$$

we have its linearized form

$$\tilde{Q}\left(\bar{x}_{L},\bar{t}\right)=-\frac{\bar{b}^{2}C_{d}^{2}}{2\bar{\rho}\bar{Q}^{*}}\tilde{p}\left(\bar{x}_{L},\bar{t}\right). \tag{3.3.17}$$

And following the substitutions

$$\begin{aligned}\overline{h} &\to \overline{h}^{*} + \varepsilon\tilde{h} \\ \overline{p} &\to \overline{p}^{*} + \varepsilon\tilde{p} \\ \overline{Q} &\to \overline{Q}^{*} + \varepsilon\tilde{Q}\end{aligned}, \tag{3.3.18}$$

into the boundary conditions at the inlet and the oulet,

$$\begin{aligned}p\left(\overline{x}_L,\overline{t}\right) &= \overline{p}_{in} - \zeta_{in}\frac{\overline{\rho}\overline{Q}^2\left(\overline{x}_L,\overline{t}\right)}{2\overline{h}^2\left(\overline{x}_L,\overline{t}\right)} \\ p\left(\overline{x}_R,\overline{t}\right) &= \overline{p}_{ex} + \zeta_{ex}\frac{\overline{\rho}\overline{Q}^2\left(\overline{x}_R,\overline{t}\right)}{2\overline{h}^2\left(\overline{x}_R,\overline{t}\right)}\end{aligned}, \tag{3.3.19}$$

we have the linearized boundary conditions

$$\begin{aligned}\tilde{p}\left(\overline{x}_L,\overline{t}\right) &= \zeta_{in}\frac{\overline{\rho}\overline{Q}^{*2}\left(\overline{x}_L,\overline{t}\right)}{\overline{h}^{*2}\left(\overline{x}_L,\overline{t}\right)}\left(\frac{\tilde{h}\left(\overline{x}_L,\overline{t}\right)}{\overline{h}^{*}\left(\overline{x}_L,\overline{t}\right)} - \frac{\tilde{Q}\left(\overline{x}_L,\overline{t}\right)}{\overline{Q}^{*}\left(\overline{x}_L,\overline{t}\right)}\right) \\ \tilde{p}\left(\overline{x}_R,\overline{t}\right) &= -\zeta_{ex}\frac{\overline{\rho}\overline{Q}^{*2}\left(\overline{x}_R,\overline{t}\right)}{\overline{h}^{*2}\left(\overline{x}_R,\overline{t}\right)}\left(\frac{\tilde{h}\left(\overline{x}_R,\overline{t}\right)}{\overline{h}^{*}\left(\overline{x}_R,\overline{t}\right)} - \frac{\tilde{Q}\left(\overline{x}_R,\overline{t}\right)}{\overline{Q}^{*}\left(\overline{x}_R,\overline{t}\right)}\right)\end{aligned} \tag{3.3.20}$$

where $\overline{p}_{in}$ and $\overline{p}_{ex}$ are constant air pressures, and ζ_{in} and ζ_{ex} are pressure loss coefficients at the inlet and oulet, respectively. Assuming that the variation of flow rate is smaller that the variation of gap,

$$\frac{\tilde{Q}\left(\overline{x}_L,\overline{t}\right)}{\overline{Q}^{*}\left(\overline{x}_L,\overline{t}\right)} << \frac{\tilde{h}\left(\overline{x}_L,\overline{t}\right)}{\overline{h}^{*}\left(\overline{x}_L,\overline{t}\right)} \tag{3.3.21}$$

then, using Eq. (3.3.14), we have

$$\tilde{p}\left(\overline{x}_L,\overline{t}\right) = \zeta_{in}\overline{\rho}\overline{Q}^{*2}\frac{\tilde{y}\left(\overline{x}_L,\overline{t}\right)}{\overline{h}^{*3}\left(\overline{x}_L,\overline{t}\right)} \tag{3.3.22}$$

Using Eqs. (3.3.17) and (3.3.22), $\tilde{Q}$ is given by

$$\tilde{Q} = -\int\frac{\partial\tilde{y}}{\partial\overline{t}}d\overline{x} - \frac{\zeta_{in}\overline{b}^2C_d^2\overline{Q}^{*}}{2}\frac{\tilde{y}\left(\overline{x}_L,\overline{t}\right)}{\overline{h}^{*3}\left(\overline{x}_L,\overline{t}\right)}. \tag{3.3.23}$$

Introducing Eqs. (3.3.14) and (3.3.23) into the linearized Navier-Stokes equation (3.3.12), it can be expressed in terms of the unsteady components $\tilde{y}$ and $\tilde{p}$

$$\begin{aligned}\frac{\partial \tilde{p}}{\partial \bar{x}} = {} & \frac{\bar{\rho}}{\bar{h}^*}\frac{\partial}{\partial \bar{t}}\left(\int \frac{\partial \tilde{y}}{\partial \bar{t}}\,d\bar{x} + \frac{\zeta_{in}\bar{b}^2 C_d^2 \bar{Q}^*}{2}\frac{\tilde{y}\left(\bar{x}_L,\bar{t}\right)}{\bar{h}^{*3}\left(\bar{x}_L,\bar{t}\right)}\right) \\ & -\frac{2\bar{\rho}\bar{Q}^*}{\bar{h}^{*3}}\left(\frac{\partial \bar{h}^*}{\partial \bar{x}} - \frac{f^*}{8}\left(2 + \frac{\bar{Q}^*}{f^*}\frac{\partial f^*}{\partial \bar{Q}^*}\right)\right)\left(\int \frac{\partial \tilde{y}}{\partial \bar{t}}\,d\bar{x} + \frac{\zeta_{in}\bar{b}^2 C_d^2 \bar{Q}^*}{2}\frac{\tilde{y}\left(\bar{x}_L,\bar{t}\right)}{\bar{h}^{*3}\left(\bar{x}_L,\bar{t}\right)}\right) \\ & +\frac{2\bar{\rho}\bar{Q}^*}{\bar{h}^{*2}}\frac{\partial \tilde{y}}{\partial \bar{t}} - \frac{3\bar{\rho}\bar{Q}^{*2}}{\bar{h}^{*4}}\left(\frac{\partial \bar{h}^*}{\partial \bar{x}} - \frac{f^*}{4}\right)\tilde{y} + \frac{\bar{\rho}\bar{Q}^{*2}}{\bar{h}^{*3}}\frac{\partial \tilde{y}}{\partial \bar{x}}\end{aligned} \tag{3.3.24}$$

where

$$\frac{\bar{Q}^*}{f^*}\frac{\partial f^*}{\partial \bar{Q}^*} = \begin{cases} -1 & \text{for laminar flow} \\ -0.25 & \text{for turbulent flow} \end{cases}. \tag{3.3.25}$$

3.4 Eigenvalue Problem

In order to obtain a discrete model of the linearized system presented in Sec. 3.3, it is necessary to review the eigenvalue problem for linear gyroscopic systems. The equation of motion cast in a first order form defined by one symmetric and one skew symmetric matrix represents a general linear gyroscopic system, and arises in connection with its small oscillation about steady motion. It is notable that the character of the eigenvalue problem for linear gyroscopic systems is different from that for natural systems. Meirovitch (1974) developed a new method of eigensolutions to the matrix eigenvalue problem for discrete gyroscopic systems, and Meirovitch (1975) subsequently presented a closed-form modal analysis for the response of linear gyroscopic systems.

Let us consider a system described by a set of ordinary differential equations in the first order form

$$\mathbf{A}\dot{\mathbf{w}} + \mathbf{B}\mathbf{w} = \mathbf{q} \tag{3.4.1}$$

where $\mathbf{A}$ and $\mathbf{B}$ are real nonsingular matrices, the first symmetric and the second skew symmetric, $\mathbf{w}$ is a real state vector, and $\mathbf{q}$ is an external excitation vector.

The general solution to Eq. (3.4.1) can be represented as

$$\mathbf{w}(x,t) = \mathrm{Re}\left\{\mathbf{\Phi}(x)e^{\lambda t}\right\}. \tag{3.4.2}$$

where $\mathbf{\Phi}(x)$ is a two-dimensional vector eigenfunction with complex components, λ is a complex eigenvalue. Substitution of the separable solution (3.4.2) into the first order homogeneous differential equation of Eq. (3.4.1) in which the external excitation is zero, leads to the eigenvalue problem for the linear gyroscopic system

$$\lambda\mathbf{A}\mathbf{\Phi} + \mathbf{B}\mathbf{\Phi} = \mathbf{0}, \tag{3.4.3}$$

where $\mathbf{0}$ is the two-dimensional null vector. The solution to the eigenvalue problem consists of a pair of eigenvalues λ_n and associated eigenfunctions $\mathbf{\Phi}_n$.

By virtue of the fact that $\mathbf{A}$ is symmetric and $\mathbf{B}$ is skew symmetric, i.e.,

$$\mathbf{A}^T = \mathbf{A} \quad \text{and} \quad \mathbf{B}^T = -\mathbf{B}, \tag{3.4.4}$$

and the determinant of a matrix is equal to that of its transposed matrix, we have characteristic equations

$$\begin{aligned} \det\left(\lambda\mathbf{A} + \mathbf{B}\right) &= \det\left(\lambda\mathbf{A} + \mathbf{B}\right)^T \\ &= \det\left(\lambda\mathbf{A}^T + \mathbf{B}^T\right) \\ &= \det\left(\lambda\mathbf{A} - \mathbf{B}\right) \\ &= \det\left(-\lambda\mathbf{A} + \mathbf{B}\right) \\ &= 0 \end{aligned} \tag{3.4.5}$$

so that, if λ is an eigenvalue, then $-\lambda$ is also an eigenvalue.

For given eigensolutions λ_n and $\boldsymbol{\Phi}_n$, multiplying the eigenvalue problem (3.4.3) on the left by the complex conjugates $\bar{\boldsymbol{\Phi}}_n^T$ gives

$$\lambda_n \bar{\boldsymbol{\Phi}}_n^T \mathbf{A} \boldsymbol{\Phi}_n + \bar{\boldsymbol{\Phi}}_n^T \mathbf{B} \boldsymbol{\Phi}_n = 0 . \tag{3.4.6}$$

Let the complex vectors have the structure

$$\boldsymbol{\Phi}_n = \boldsymbol{\Phi}_n^R + i\boldsymbol{\Phi}_n^I , \tag{3.4.7}$$

where $\boldsymbol{\Phi}_n^R$ and $\boldsymbol{\Phi}_n^I$ are their real and imaginary parts, respectively. Substitution Eq. (3.4.7) into Eq. (3.4.6) gives

$$\lambda_n \left(\boldsymbol{\Phi}_n^R - i\boldsymbol{\Phi}_n^I \right)^T \mathbf{A} \left(\boldsymbol{\Phi}_n^R + i\boldsymbol{\Phi}_n^I \right) + \left(\boldsymbol{\Phi}_n^R - i\boldsymbol{\Phi}_n^I \right)^T \mathbf{B} \left(\boldsymbol{\Phi}_n^R + i\boldsymbol{\Phi}_n^I \right) = 0 \tag{3.4.8}$$

or

$$\begin{aligned} &\lambda_n \left(\boldsymbol{\Phi}_n^{R^T} \mathbf{A} \boldsymbol{\Phi}_n^R + \boldsymbol{\Phi}_n^{I^T} \mathbf{A} \boldsymbol{\Phi}_n^I \right) + i\lambda_n \left(\boldsymbol{\Phi}_n^{R^T} \mathbf{A} \boldsymbol{\Phi}_n^I - \boldsymbol{\Phi}_n^{I^T} \mathbf{A} \boldsymbol{\Phi}_n^R \right) \\ &+ \boldsymbol{\Phi}_n^{R^T} \mathbf{B} \boldsymbol{\Phi}_n^R + \boldsymbol{\Phi}_n^{I^T} \mathbf{B} \boldsymbol{\Phi}_n^I + i \left(\boldsymbol{\Phi}_n^{R^T} \mathbf{B} \boldsymbol{\Phi}_n^I - \boldsymbol{\Phi}_n^{I^T} \mathbf{B} \boldsymbol{\Phi}_n^R \right) = 0 \end{aligned} . \tag{3.4.9}$$

By virtue of Eq. (3.4.4), we have the following

$$\begin{aligned} \boldsymbol{\Phi}_n^{I^T} \mathbf{A} \boldsymbol{\Phi}_n^R &= \left(\boldsymbol{\Phi}_n^{R^T} \mathbf{A} \boldsymbol{\Phi}_n^I \right)^T \\ \boldsymbol{\Phi}_n^{R^T} \mathbf{B} \boldsymbol{\Phi}_n^R &= -\left(\boldsymbol{\Phi}_n^{R^T} \mathbf{B} \boldsymbol{\Phi}_n^R \right)^T \\ \boldsymbol{\Phi}_n^{I^T} \mathbf{B} \boldsymbol{\Phi}_n^I &= -\left(\boldsymbol{\Phi}_n^{I^T} \mathbf{B} \boldsymbol{\Phi}_n^I \right)^T \\ \boldsymbol{\Phi}_n^{I^T} \mathbf{B} \boldsymbol{\Phi}_n^R &= -\left(\boldsymbol{\Phi}_n^{R^T} \mathbf{B} \boldsymbol{\Phi}_n^I \right)^T \end{aligned} . \tag{3.4.10}$$

Because each triple matrix product represents a real scalar function, its transpose is equal to itself. Eq. (3.4.9) can be rewritten as

$$\lambda_n \left(\boldsymbol{\Phi}_n^{R^T} \mathbf{A} \boldsymbol{\Phi}_n^R + \boldsymbol{\Phi}_n^{I^T} \mathbf{A} \boldsymbol{\Phi}_n^I \right) + i2\boldsymbol{\Phi}_n^{R^T} \mathbf{B} \boldsymbol{\Phi}_n^I = 0 , \tag{3.4.11}$$

which implies that λ_n should be pure imaginary. Since $-\lambda_n$ are also an eigenvalue, the solution to the eigenvalue problem consists of a pair of pure imaginary complex conjugate eigenvalues λ_n and $\overline{\lambda}_n = -\lambda_n$, and a pair of complex conjugate eigenfunctions $\mathbf{\Phi}_n$ and $\overline{\mathbf{\Phi}}_n$. When eigenvalues are denoted by $\lambda_n = \pm i\omega_n$ where ω_n are the real oscillation frequencies, it is concluded that if $i\omega_n$ and $\mathbf{\Phi}_n$ constitute a solution of the eigenvalue problem, then $-i\omega_n$ and $\overline{\mathbf{\Phi}}_n$ also do its solution.

Next, a simple standard form of the eigenvalue problem is examined. Substituting $\lambda_n = i\omega_n$ and $\mathbf{\Phi}_n = \mathbf{\Phi}_n^R + i\mathbf{\Phi}_n^I$ into the eigenvalue problem (3.4.3), and separating the real and imaginary parts of the resultant equation, we obtain two equations in terms of real quantities

$$-\omega_n \mathbf{A}\mathbf{\Phi}_n^I + \mathbf{B}\mathbf{\Phi}_n^R = 0 \tag{3.4.12}$$

and

$$\omega_n \mathbf{A}\mathbf{\Phi}_n^R + \mathbf{B}\mathbf{\Phi}_n^I = 0\,. \tag{3.4.13}$$

Solving Eq. (3.4.12) for $\mathbf{\Phi}_n^I$ gives

$$\mathbf{\Phi}_n^I = \frac{\mathbf{A}^{-1}\mathbf{B}\mathbf{\Phi}_n^R}{\omega_n} \tag{3.4.14}$$

so that substitution into Eq. (3.4.13) gives

$$\omega_n^2 \mathbf{A}\mathbf{\Phi}_n^R = \mathbf{K}\mathbf{\Phi}_n^R \tag{3.4.15}$$

where

$$\mathbf{K} = -\mathbf{B}\mathbf{A}^{-1}\mathbf{B} = \mathbf{B}^T\mathbf{A}^{-1}\mathbf{B} \tag{3.4.16}$$

is a real symmetric matrix, $\mathbf{K} = \mathbf{K}^T$, because $\mathbf{A}$ is a real symmetric matrix, and $\mathbf{B}$ is a real skew symmetric matrix. In a similar way, solving Eq. (3.4.13) for $\mathbf{\Phi}_n^R$ yields

$$\boldsymbol{\Phi}_n^R = -\frac{\mathbf{A}^{-1}\mathbf{B}\boldsymbol{\Phi}_n^I}{\omega_n} \tag{3.4.17}$$

so that, inserting into Eq. (3.4.12), we obtain

$$\omega_n^2 \mathbf{A}\boldsymbol{\Phi}_n^I = \mathbf{K}\boldsymbol{\Phi}_n^I . \tag{3.4.18}$$

As shown by working with real quantities instead of complex quantities, the complex solution of the eigenvalue problem defined by $\mathbf{A}$ and $\mathbf{B}$ is transformed to the real solution of the eigenvalue problems (3.4.15) and (3.4.18) defined by two real symmetric matrices $\mathbf{A}$ and $\mathbf{K}$ which consists of a pair of repeated eigenvalues ω_n^2 and a pair of associated eigenfunctions $\boldsymbol{\Phi}_n^R$ and $\boldsymbol{\Phi}_n^I$.

To obtain a more convenient standard form of the eigenvalue problem, i.e., one defined by only one symmetric matrix instead of two, we rewrite Eq. (3.4.15) as

$$\omega_n^2 \mathbf{A}^{1/2}\mathbf{A}^{1/2}\boldsymbol{\Phi}_n^R = \mathbf{K}\mathbf{A}^{-1/2}\mathbf{A}^{1/2}\boldsymbol{\Phi}_n^R . \tag{3.4.19}$$

Introducing the linear transformation

$$\boldsymbol{\Phi}_n^{R\prime} = \mathbf{A}^{1/2}\boldsymbol{\Phi}_n^R , \tag{3.4.20}$$

and multipling Eq. (3.4.19) on the left by $\mathbf{A}^{-1/2}$ provide

$$\omega_n^2 \boldsymbol{\Phi}_n^{R\prime} = \mathbf{K}'\boldsymbol{\Phi}_n^{R\prime} \tag{3.4.21}$$

where

$$\mathbf{K}' = \mathbf{A}^{-1/2}\mathbf{K}\mathbf{A}^{-1/2} \tag{3.4.22}$$

is a real symmetric matrix because both $\mathbf{A}$ and $\mathbf{K}$ are real symmetric matrices. Similarly, rewritng Eq. (3.4.18) as

$$\omega_n^2 \mathbf{A}^{1/2}\mathbf{A}^{1/2}\boldsymbol{\Phi}_n^I = \mathbf{K}\mathbf{A}^{-1/2}\mathbf{A}^{1/2}\boldsymbol{\Phi}_n^I , \tag{3.4.23}$$

introducing the linear transformation

$$\boldsymbol{\Phi}_n^{I\prime} = \mathbf{A}^{1/2}\boldsymbol{\Phi}_n^{I}, \tag{3.4.24}$$

and multipling Eq. (3.4.23) on the left by $\mathbf{A}^{-1/2}$, we have

$$\omega_n^2\boldsymbol{\Phi}_n^{I\prime} = \mathbf{K}'\boldsymbol{\Phi}_n^{I\prime}. \tag{3.4.25}$$

The standard form through the linear transformations is possible only if $\mathbf{A}^{1/2}$ and $\mathbf{A}^{-1/2}$ exist. According to Theorem 6.12 of Murdoch (1970), if $\mathbf{A}$ is a real symmetric matrix, a nonsingular transformation matrix $\mathbf{P}$ exists such that

$$\mathbf{P}^{-1}\mathbf{A}\mathbf{P} = \mathbf{R} \tag{3.4.26}$$

where $\mathbf{R}$ is a diagonal matrix, and diagonalizes $\mathbf{A}$. Then, $\mathbf{A}$ is said to be similar to $\mathbf{R}$ so that diagonal elements of $\mathbf{R}$ are eigenvalues of $\mathbf{A}$ (Theorem 6.4 of Murdoch). Eq. (3.4.26) can be written as

$$\left(\mathbf{P}^{-1}\mathbf{A}^{1/2}\mathbf{P}\right)\left(\mathbf{P}^{-1}\mathbf{A}^{1/2}\mathbf{P}\right) = \mathbf{R} \tag{3.4.27}$$

so that

$$\mathbf{R}^{1/2} = \mathbf{P}^{-1}\mathbf{A}^{1/2}\mathbf{P} \tag{3.4.28}$$

where $\mathbf{R}^{1/2}$ is also a diagonal matrix whose elements are equal to the square root of diagonal elements of $\mathbf{R}$. Therefore, the necessary condition for $\mathbf{A}^{1/2}$ to exist is that all the eigenvalues of $\mathbf{A}$ are positive because the diagonal elements of $\mathbf{R}^{1/2}$ cannot be complex. To meet the condition, $\mathbf{A}$ must be positive definite (Theorem 6.15 of Murdoch), and then $\mathbf{A}^{1/2}$ exists. Similarly, because $\mathbf{R}^{-1/2}$ is the inverse of $\mathbf{R}^{1/2}$ such that

$$\mathbf{R}^{-1/2} = \mathbf{P}^{-1}\mathbf{A}^{-1/2}\mathbf{P}, \tag{3.4.29}$$

$\mathbf{A}^{-1/2}$ exists if $\mathbf{A}$ is positive definite. Moreover, in view of Eq. (3.4.22), $\mathbf{K}'$ also exists if $\mathbf{A}$ is positive definite. Inserting Eq. (3.4.16) into (3.4.22) yields

$$\begin{aligned}\mathbf{K}' &= \mathbf{A}^{-1/2}\mathbf{B}^T\mathbf{A}^{-1}\mathbf{B}\mathbf{A}^{-1/2} \\ &= \left(\mathbf{A}^{-1/2}\mathbf{B}^T\mathbf{A}^{-1/2}\right)\left(\mathbf{A}^{-1/2}\mathbf{B}\mathbf{A}^{-1/2}\right) \\ &= \mathbf{C}^T\mathbf{C}\end{aligned} \tag{3.4.30}$$

where

$$\mathbf{C} = \mathbf{A}^{-1/2}\mathbf{B}\mathbf{A}^{-1/2} \tag{3.4.31}$$

is a nonsingular matrix because $\mathbf{A}^{-1/2}$ and $\mathbf{B}$ are nonsingular. It follows that if $\mathbf{A}$ is positive definite, then $\mathbf{K}'$ is positive definite (Theorem 6.16 of Murdoch) so that $\mathbf{K}'$ has only positive eigenvalues, namely, no ω_n can be zero.

Orthonormality properties of eigenfunctions $\mathbf{\Phi}_n$ with respect to the matrices $\mathbf{A}$ and $\mathbf{B}$ are investigated through the developed standard form of the eigenvalue problem defined by a real symmetric matrix. In view of the fact that two eigenfunctions $\mathbf{\Phi}_n^{R'}$ and $\mathbf{\Phi}_n^{I'}$ of the real symmetric matrix $\mathbf{K}'$ corresponding to two different eigenvalues are orthogonal (Theorem 6.13 of Murdoch), we have the orthogonality relations for $\omega_n^2 \neq \omega_m^2$

$$\begin{aligned}&\mathbf{\Phi}_n^{R'T}\mathbf{\Phi}_m^{R'} = 0 \\ &\mathbf{\Phi}_n^{R'T}\mathbf{\Phi}_m^{I'} = 0 \\ &\mathbf{\Phi}_n^{I'T}\mathbf{\Phi}_m^{R'} = 0 \\ &\mathbf{\Phi}_n^{I'T}\mathbf{\Phi}_m^{I'} = 0\end{aligned} \quad . \tag{3.4.32}$$

Because ω_n^2 is a double root with corresponding eigenfunctions $\mathbf{\Phi}_n^{R'}$ and $\mathbf{\Phi}_n^{I'}$, the second and third of the preceding orthogonality relations (3.4.32) are valid also for repeated roots. Recalling transformations (3.4.20) and (3.4.24), the orthogonality relations (3.4.32) can be rewritten as

$$\mathbf{\Phi}_n^{RT}\mathbf{A}\mathbf{\Phi}_m^{R} = 0 \quad \text{and} \quad \mathbf{\Phi}_n^{RT}\mathbf{A}\mathbf{\Phi}_m^{R} = 0 \quad \text{for } \omega_n^2 \neq \omega_m^2 \tag{3.4.33}$$

and

$$\boldsymbol{\Phi}_n^{R\,T}\mathbf{A}\boldsymbol{\Phi}_m^I = 0 \quad \text{and} \quad \boldsymbol{\Phi}_n^{I\,T}\mathbf{A}\boldsymbol{\Phi}_m^R = 0\,, \tag{3.4.34}$$

which represents that the eigenfunctions $\boldsymbol{\Phi}_n^R$ and $\boldsymbol{\Phi}_n^I$ are orthogonal with respect to the matrix $\mathbf{A}$, and the two eigenfunctions $\boldsymbol{\Phi}_n^R$ and $\boldsymbol{\Phi}_n^I$ corresponding to the same eigenvalue ω_n^2 are independent, so that any linear combination of $\boldsymbol{\Phi}_n^R$ and $\boldsymbol{\Phi}_n^I$ is also eigenfunctions. For convenience, when the eigenfunctions are normalized as

$$\boldsymbol{\Phi}_n^{R\,T}\mathbf{A}\boldsymbol{\Phi}_n^R = \boldsymbol{\Phi}_n^{I\,T}\mathbf{A}\boldsymbol{\Phi}_n^I = 1 \tag{3.4.35}$$

where $\boldsymbol{\Phi}_n^R$ and $\boldsymbol{\Phi}_n^I$ are orthonormal, then the orthogonality relations are rewritten as

$$\begin{aligned} \boldsymbol{\Phi}_n^{R\,T}\mathbf{A}\boldsymbol{\Phi}_m^R &= \boldsymbol{\Phi}_n^{I\,T}\mathbf{A}\boldsymbol{\Phi}_m^I = \delta_{nm} \\ \boldsymbol{\Phi}_n^{R\,T}\mathbf{A}\boldsymbol{\Phi}_m^I &= \boldsymbol{\Phi}_n^{I\,T}\mathbf{A}\boldsymbol{\Phi}_m^R = 0 \end{aligned} \tag{3.4.36}$$

where δ_{nm} is the Kronecker delta. Because of the symmetric matrix $\mathbf{A}$, of course, Eq. (3.4.36) are valid also when the positions of each eigenfunction are interchanged.

On the other hand, to examine the orthogonality relations with respect to the matrix $\mathbf{B}$, multiplying Eq. (3.4.12) on the left by $\boldsymbol{\Phi}_m^{I\,T}$ and Eq. (3.4.13) on the left by $\boldsymbol{\Phi}_m^{R\,T}$, and applying the first two properties (3.4.36) provide

$$\boldsymbol{\Phi}_m^{I\,T}\mathbf{B}\boldsymbol{\Phi}_n^R = -\boldsymbol{\Phi}_m^{R\,T}\mathbf{B}\boldsymbol{\Phi}_n^I = \omega_n\delta_{nm}\,. \tag{3.4.37}$$

Similarly, multiplying Eq. (3.4.12) on the left by $\boldsymbol{\Phi}_m^{R\,T}$ and Eq. (3.4.13) on the left by $\boldsymbol{\Phi}_m^{I\,T}$, and applying the last two properties (3.4.36), we have

$$\boldsymbol{\Phi}_m^{R\,T}\mathbf{B}\boldsymbol{\Phi}_n^R = \boldsymbol{\Phi}_m^{I\,T}\mathbf{B}\boldsymbol{\Phi}_n^I = 0\,. \tag{3.4.38}$$

Because the vector functions $\mathbf{\Phi}_n^R$ and $\mathbf{\Phi}_n^I$ are orthogonal (with respect to the matrix **A**), namely, independent, they form a basis in a two-dimensional vector space. Any arbitrary two-dimensional vector can be expanded as a linear combination of the eigenfunctions $\mathbf{\Phi}_n^R$ and $\mathbf{\Phi}_n^I$ so that the solution can be taken as their linear combination. A modal analysis for gyroscopic systems is based on the expansion theorem and the orthogonality relations.

3.5 Discrete Model

With the introduction of the mass, gyral, and stiffness operators

$$\begin{aligned} \mathrm{M} &= \mathrm{I} \\ \mathrm{G} &= 2V\frac{\partial}{\partial \bar{x}} \\ \mathrm{K} &= \left(V^2-1\right)\frac{\partial^2}{\partial \bar{x}^2}+D^2\frac{\partial^4}{\partial \bar{x}^4} \end{aligned} \tag{3.5.1}$$

where I is the identity operator, the linearized nondimensional structure equation (3.3.4) is presented in the dimensionless symbolic form

$$\mathrm{M}\frac{\partial^2 \tilde{y}}{\partial \bar{t}^2}+\mathrm{G}\frac{\partial \tilde{y}}{\partial \bar{t}}+\mathrm{K}\tilde{y}=\tilde{p} \tag{3.5.2}$$

where

$$\tilde{p}=\tilde{p}\left(\mathrm{H}\left(\bar{x}-\bar{x}_L\right)-\mathrm{H}\left(\bar{x}-\bar{x}_R\right)\right). \tag{3.5.3}$$

Following a state space representation with the real state and external excitation vectors

$$\mathbf{w}\left(\bar{x},\bar{t}\right)=\begin{Bmatrix}\dot{\tilde{y}}\\ \tilde{y}\end{Bmatrix} \tag{3.5.4}$$

and

$$\mathbf{q}\left(\bar{x},\bar{t}\right)=\begin{Bmatrix}\tilde{p}\\0\end{Bmatrix}, \tag{3.5.5}$$

Eq. (3.5.2) can be cast in first order form as shown in Eq. (3.4.1)

$$\mathbf{A}\dot{\mathbf{w}}+\mathbf{B}\mathbf{w}=\mathbf{q} \tag{3.5.6}$$

where the matrix differential operators $\mathbf{A}$ and $\mathbf{B}$ are real nonsingular matrices, the first symmetric and the second skew symmetric such that

$$\mathbf{A}=\begin{bmatrix}\mathrm{M} & 0\\0 & \mathrm{K}\end{bmatrix} \tag{3.5.7}$$

and

$$\mathbf{B}=\begin{bmatrix}\mathrm{G} & \mathrm{K}\\-\mathrm{K} & 0\end{bmatrix}. \tag{3.5.8}$$

The general solution to Eq. (3.5.6) can be represented as

$$\mathbf{w}\left(\bar{x},\bar{t}\right)=\mathrm{Re}\left\{\mathbf{\Phi}\left(\bar{x}\right)e^{\lambda\bar{t}}\right\} \tag{3.5.9}$$

where $\mathbf{\Phi}\left(\bar{x}\right)$ is a two-dimensional vector eigenfunction with complex components, λ is a complex eigenvalue. The vector eigenfunction $\mathbf{\Phi}\left(\bar{x}\right)$ associated with $\mathbf{w}\left(\bar{x},\bar{t}\right)$ can be expressed in terms of the scalar eigenfunction $\psi\left(\bar{x}\right)$ associated with $\tilde{y}\left(\bar{x},\bar{t}\right)$. Assuming the solution of web displacement as

$$\tilde{y}\left(\bar{x},\bar{t}\right)=\mathrm{Re}\left\{\psi\left(\bar{x}\right)e^{\lambda\bar{t}}\right\} \tag{3.5.10}$$

where $\psi\left(\bar{x}\right)$ is the normalized scalar eigenfunction associated with $\tilde{y}$, and recalling Eqs. (3.5.4) and (3.5.9), the eigenfunctions can be selected as

$$\mathbf{\Phi}_n\left(\bar{x}\right)=\begin{Bmatrix}\lambda_n\psi_n\left(\bar{x}\right)\\\psi_n\left(\bar{x}\right)\end{Bmatrix} \tag{3.5.11}$$

where

$$\psi_n(\bar{x}) = \psi_n^R(\bar{x}) + i\psi_n^I(\bar{x}). \tag{3.5.12}$$

Inserting $\lambda_n = i\omega_n$ provides

$$\mathbf{\Phi}_n(\bar{x}) = \begin{Bmatrix} -\omega_n \psi_n^I(\bar{x}) \\ \psi_n^R(\bar{x}) \end{Bmatrix} + i \begin{Bmatrix} \omega_n \psi_n^R(\bar{x}) \\ \psi_n^I(\bar{x}) \end{Bmatrix} \tag{3.5.13}$$

so that we have

$$\mathbf{\Phi}_n^R(\bar{x}) = \begin{Bmatrix} -\omega_n \psi_n^I(\bar{x}) \\ \psi_n^R(\bar{x}) \end{Bmatrix} \tag{3.5.14}$$

and

$$\mathbf{\Phi}_n^I(\bar{x}) = \begin{Bmatrix} \omega_n \psi_n^R(\bar{x}) \\ \psi_n^I(\bar{x}) \end{Bmatrix}. \tag{3.5.15}$$

The eigenfunctions for the traveling web can be found in a closed form for the case of vanishing flexural stiffness, which is admissible because mode shapes of a traveling string model with fixed end conditions is a useful analog for those of a moving beam model with the pinned end conditions. Substituting the assumed solution (3.5.10) into the homogeneous version of Eq. (3.3.4) in the limit of vanishing flexible stiffness yields the differential equation

$$\left(V^2 - 1\right)\frac{\partial^2 \psi}{\partial \bar{x}^2} + 2V\lambda\frac{\partial \psi}{\partial \bar{x}} + \lambda^2 \psi = 0. \tag{3.5.16}$$

over the domain $0 \le \bar{x} \le 1$, which is subject to the boundary conditions

$$\begin{aligned} \psi(0) &= 0 \\ \psi(1) &= 0 \end{aligned}. \tag{3.5.17}$$

The solution can be written in the form

$$\psi\left(\bar{x}\right) = C_1 e^{-\frac{\lambda\bar{x}}{1+V}} + C_2 e^{\frac{\lambda\bar{x}}{1-V}}. \tag{3.5.18}$$

Inserting the first boundary condition into Eq. (3.5.17), we have that $C_2 = -C_1$, so that the solution reduces to

$$\psi\left(\bar{x}\right) = C_1\left(e^{-\frac{\lambda\bar{x}}{1+V}} - e^{\frac{\lambda\bar{x}}{1-V}}\right). \tag{3.5.19}$$

On the other hand, introducing the second boundary condition into Eq. (3.5.17), and avoiding a nontrivial solution, we have the characteristic equation

$$e^{-\frac{\lambda}{1+V}} - e^{\frac{\lambda}{1-V}} = -2e^{\frac{\lambda V}{1-V^2}}\sinh\left(\frac{\lambda}{1-V^2}\right) = 0 \tag{3.5.20}$$

or

$$\sinh\left(\frac{\lambda}{1-V^2}\right) = 0 \tag{3.5.21}$$

so that the infinite set of eigenvalues becomes

$$\lambda_n = in\pi\left(1-V^2\right), \tag{3.5.22}$$

and then the natural frequencies become

$$\omega_n = n\pi\left(1-V^2\right) \tag{3.5.23}$$

where $\lambda_n = i\omega_n$. The corresponding eigenfunctions are given by

$$\psi_n\left(\bar{x}\right) = C_n e^{in\pi V\bar{x}}\sin\left(n\pi\bar{x}\right) \tag{3.5.24}$$

where the constants C_n are found by normalizing the eigenfunctions with respect to $\mathbf{A}$ such that $\mathbf{\Phi}_n^{R\,T}\mathbf{A}\mathbf{\Phi}_m^R = \delta_{nm}$ or

$$\left\{-\omega_n\psi_n^I \quad \psi_n^R\right\}\begin{bmatrix} M & 0 \\ 0 & K \end{bmatrix}\begin{Bmatrix} -\omega_n\psi_n^I \\ \psi_n^R \end{Bmatrix} = 1. \tag{3.5.25}$$

Integrating Eq. (3.5.25) over $0 \le \bar{x} \le 1$ yields

$$\int_0^1 \left(\left(\omega_n \psi_n^I\right)^2 + \left(V^2 - 1\right) \psi_n^R \frac{\partial^2 \psi_n^R}{\partial \bar{x}^2} d\bar{x} \right) = 1 \tag{3.5.26}$$

where

$$\psi_n^R\left(\bar{x}\right) = C_n \cos\left(n\pi V \bar{x}\right) \sin\left(n\pi \bar{x}\right) \tag{3.5.27}$$

and

$$\psi_n^I\left(\bar{x}\right) = C_n \sin\left(n\pi V \bar{x}\right) \sin\left(n\pi \bar{x}\right). \tag{3.5.28}$$

After evaluating the integral, the constants C_n are given by

$$C_n = \frac{1}{n\pi} \sqrt{\frac{2}{1 - V^2}} \tag{3.5.29}$$

so that the normalized eigenfunctions become

$$\psi_n\left(\bar{x}\right) = \frac{1}{n\pi} \sqrt{\frac{2}{1 - V^2}} e^{in\pi V \bar{x}} \sin\left(n\pi \bar{x}\right). \tag{3.5.30}$$

By virtue of the expansion theorem, the solution of Eq. (3.5.6) can be assumed as an eigenfunction expansion

$$\mathbf{w} = \sum_{n=1}^{N} \xi_n^R\left(\bar{t}\right) \mathbf{\Phi}_n^R\left(\bar{x}\right) + \xi_n^I\left(\bar{t}\right) \mathbf{\Phi}_n^I\left(\bar{x}\right) \tag{3.5.31}$$

where $\xi_n^R\left(\bar{t}\right)$ and $\xi_n^I\left(\bar{t}\right)$ are real and generalized coordinates associated with the eigenfunctions $\mathbf{\Phi}_n^R$ and $\mathbf{\Phi}_n^I$, respectively. Also, following Eqs. (3.5.4), (3.5.14), (3.5.15), and (3.5.31), the time history of the elastic displacement in terms of mode shapes and its derivative are expressed by

$$\tilde{y} = \sum_{n=1}^{N} \xi_n^R\left(\bar{t}\right) \psi_n^R\left(\bar{x}\right) + \xi_n^I\left(\bar{t}\right) \psi_n^I\left(\bar{x}\right) \tag{3.5.32}$$

and

$$\dot{\tilde{y}} = \sum_{n=1}^{N} -\xi_n^R\left(\bar{t}\right)\omega_n\psi_n^I\left(\bar{x}\right) + \xi_n^I\left(\bar{t}\right)\omega_n\psi_n^R\left(\bar{x}\right) \tag{3.5.33}$$

Inserting the expansion (3.5.31) into the first order formed governing equation (3.5.6) yields

$$\mathbf{A}\left[\sum_{n=1}^{N}\dot{\xi}_n^R\mathbf{\Phi}_n^R + \dot{\xi}_n^I\mathbf{\Phi}_n^I\right] + \mathbf{B}\left[\sum_{n=1}^{N}\xi_n^R\mathbf{\Phi}_n^R + \xi_n^I\mathbf{\Phi}_n^I\right] = \mathbf{q}\,. \tag{3.5.34}$$

Multiplying Eq. (3.5.34) on the left by $\mathbf{\Phi}_m^{R\,T}$, and taking integrals with respect to x on both sides over the web span provide

$$\begin{aligned}&\sum_{n=1}^{N}\int_0^1\left(\dot{\xi}_n^R\mathbf{\Phi}_m^{R\,T}\mathbf{A}\mathbf{\Phi}_n^R + \dot{\xi}_n^I\mathbf{\Phi}_m^{R\,T}\mathbf{A}\mathbf{\Phi}_n^I + \xi_n^R\mathbf{\Phi}_m^{R\,T}\mathbf{B}\mathbf{\Phi}_n^R + \xi_n^I\mathbf{\Phi}_m^{R\,T}\mathbf{B}\mathbf{\Phi}_n^I\right)d\bar{x}\\ &= \int_0^1\mathbf{\Phi}_m^{R\,T}\mathbf{q}\,d\bar{x}\end{aligned}\,. \tag{3.5.35}$$

Considering the orthogonality properties (3.4.36) to (3.4.38), we have

$$\sum_{n=1}^{N}\left(\dot{\xi}_n^R\delta_{nm} - \omega_n\xi_n^I\delta_{nm}\right) = \int_0^1\mathbf{\Phi}_m^{R\,T}\mathbf{q}\,d\bar{x} \tag{3.5.36}$$

or, using Eqs. (3.5.5) and (3.5.14)

$$\dot{\xi}_m^R - \omega_m\xi_m^I = -\int_{\bar{x}_L}^{\bar{x}_R}\omega_m\psi_m^I\tilde{p}\,d\bar{x} \qquad m = 1,\,2,\,\ldots,\,N\,. \tag{3.5.37}$$

By virtue of integral by parts, we have

$$\dot{\xi}_m^R - \omega_m\xi_m^I = \int_{\bar{x}_L}^{\bar{x}_R}\omega_m\int\psi_m^I d\bar{x}\,\frac{\partial\tilde{p}}{\partial\bar{x}}\,d\bar{x} - \left[\omega_m\int\psi_m^I d\bar{x}\,\tilde{p}\right]_{\bar{x}_L}^{\bar{x}_R}, \tag{3.5.38}$$

and, using Eqs. (3.3.20), (3.3.23), and (3.3.24), it is rewritten as

$$\dot{\xi}_m^R - \omega_m \xi_m^I =$$

$$\omega_m \left(\begin{array}{l} \int_{\bar{x}_L}^{\bar{x}_R} \int \psi_m^I \left(\begin{array}{l} \dfrac{\bar{\rho}}{\bar{h}^*} \left(\int \ddot{\tilde{y}} d\bar{x} + \dfrac{\zeta_{in} \bar{b}^2 C_d^2 \bar{Q}^*}{2} \left[\dfrac{\dot{\tilde{y}}}{\bar{h}^{*3}} \right]_{\bar{x}_L} \right) \\ - \dfrac{2\bar{\rho}\bar{Q}^*}{\bar{h}^{*3}} \left(\dfrac{\partial \bar{h}^*}{\partial \bar{x}} - \dfrac{f^*}{8} \left(2 + \dfrac{\bar{Q}^*}{f^*} \dfrac{\partial f^*}{\partial \bar{Q}^*} \right) \right) \left(\int \dot{\tilde{y}} d\bar{x} + \dfrac{\zeta_{in} \bar{b}^2 C_d^2 \bar{Q}^*}{2} \left[\dfrac{\tilde{y}}{\bar{h}^{*3}} \right]_{\bar{x}_L} \right) \\ + \dfrac{2\bar{\rho}\bar{Q}^*}{\bar{h}^{*2}} \dot{\tilde{y}} - \dfrac{3\bar{\rho}\bar{Q}^{*2}}{\bar{h}^{*4}} \left(\dfrac{\partial \bar{h}^*}{\partial \bar{x}} - \dfrac{f^*}{4} \right) \tilde{y} + \dfrac{\bar{\rho}\bar{Q}^{*2}}{\bar{h}^{*3}} \dfrac{\partial \tilde{y}}{\partial \bar{x}} \end{array} \right) d\bar{x} \\ + \left[\int \psi_m^I \right]_{\bar{x}_L} \zeta_{in} \bar{\rho} \bar{Q}^* \left(\bar{Q}^* \left[\dfrac{\tilde{y}}{\bar{h}^{*3}} \right]_{\bar{x}_L} + \left[\dfrac{\int \dot{\tilde{y}} d\bar{x}}{\bar{h}^{*2}} + \dfrac{\zeta_{in} \bar{b}^2 C_d^2 \bar{Q}^*}{2} \dfrac{\tilde{y}}{\bar{h}^{*5}} \right]_{\bar{x}_L} \right) \\ + \left[\int \psi_m^I \right]_{\bar{x}_R} \zeta_{ex} \bar{\rho} \bar{Q}^* \left(\bar{Q}^* \left[\dfrac{\tilde{y}}{\bar{h}^{*3}} \right]_{\bar{x}_R} + \left[\dfrac{\int \dot{\tilde{y}} d\bar{x}}{\bar{h}^{*2}} + \dfrac{\zeta_{in} \bar{b}^2 C_d^2 \bar{Q}^*}{2\bar{h}^{*2}} \left[\dfrac{\tilde{y}}{\bar{h}^{*3}} \right]_{\bar{x}_L} \right]_{\bar{x}_R} \right) \end{array} \right). \tag{3.5.39}$$

Substituting Eqs. (3.5.32) and (3.5.33) into Eq. (3.5.39) yields

$$\dot{\xi}_m^R + \sum_{n=1}^{NY} \dot{\xi}_n^R \omega_m \omega_n \int_{\bar{x}_L}^{\bar{x}_R} \frac{\bar{\rho}}{\bar{h}^*} \int \psi_m^I \int \psi_n^I d\bar{x} - \sum_{n=1}^{NY} \dot{\xi}_n^I \omega_m \omega_n \int_{\bar{x}_L}^{\bar{x}_R} \frac{\bar{\rho}}{\bar{h}^*} \int \psi_m^I \int \psi_n^R d\bar{x} =$$

$$\sum_{n=1}^{NY} \xi_n^R \omega_m \left(\int_{\bar{x}_L}^{\bar{x}_R} \int \psi_m^I \left(\begin{array}{l} -\omega_n \dfrac{\varsigma_L \bar{\rho} \bar{b}^2 C_d^2 \bar{Q}^*}{2\bar{h}^*} \left[\dfrac{\psi_n^I}{\bar{h}^{*3}} \right]_{\bar{x}_L} \\ -\dfrac{2\bar{\rho}\bar{Q}^*}{\bar{h}^{*3}} \left(\dfrac{\partial \bar{h}^*}{\partial \bar{x}} - \dfrac{f^*}{8} \left(2 + \dfrac{\bar{Q}^*}{f^*} \dfrac{\partial f^*}{\partial \bar{Q}^*} \right) \right) \left(-\omega_n \int \psi_n^I + \dfrac{\varsigma_L \bar{b}^2 C_d^2 \bar{Q}^*}{2} \left[\dfrac{\psi_n^R}{\bar{h}^{*3}} \right]_{\bar{x}_L} \right) \\ -\dfrac{2\bar{\rho}\bar{Q}^*}{\bar{h}^{*2}} \omega_n \psi_n^I - \dfrac{3\bar{\rho}\bar{Q}^{*2}}{\bar{h}^{*4}} \left(\dfrac{\partial \bar{h}^*}{\partial \bar{x}} - \dfrac{f^*}{4} \right) \psi_n^R + \dfrac{\bar{\rho}\bar{Q}^{*2}}{\bar{h}^{*3}} \dfrac{\partial \psi_n^R}{\partial \bar{x}} \end{array} \right) d\bar{x} \right.$$

$$+ \left[\int \psi_m^I \right]_{\bar{x}_L} \zeta_{in} \bar{\rho} \bar{Q}^* \left(\bar{Q}^* \left[\frac{\psi_n^R}{\bar{h}^{*3}} \right]_{\bar{x}_L} - \omega_n \left[\frac{\int \psi_n^I}{\bar{h}^{*2}} \right]_{\bar{x}_L} + \frac{\zeta_{in} \bar{b}^2 C_d^2 \bar{Q}^*}{2} \left[\frac{\psi_n^R}{\bar{h}^{*5}} \right]_{\bar{x}_L} \right)$$

$$\left. + \left[\int \psi_m^I \right]_{\bar{x}_R} \zeta_{ex} \bar{\rho} \bar{Q}^* \left(\bar{Q}^* \left[\frac{\psi_n^R}{\bar{h}^{*3}} \right]_{\bar{x}_R} - \omega_n \left[\frac{\int \psi_n^I}{\bar{h}^{*2}} \right]_{\bar{x}_R} + \frac{\zeta_{in} \bar{b}^2 C_d^2 \bar{Q}^*}{2 \left[\bar{h}^{*2} \right]_{\bar{x}_R}} \left[\frac{\psi_n^R}{\bar{h}^{*3}} \right]_{\bar{x}_L} \right) \right)$$

$$+ \sum_{n=1}^{NY} \xi_n^I \omega_m \left(\int_{\bar{x}_L}^{\bar{x}_R} \int \psi_m^I \left(\begin{array}{l} \omega_n \dfrac{\varsigma_L \bar{\rho} \bar{b}^2 C_d^2 \bar{Q}^*}{2\bar{h}^*} \left[\dfrac{\psi_n^R}{\bar{h}^{*3}} \right]_{\bar{x}_L} \\ -\dfrac{2\bar{\rho}\bar{Q}^*}{\bar{h}^{*3}} \left(\dfrac{\partial \bar{h}^*}{\partial \bar{x}} - \dfrac{f^*}{8} \left(2 + \dfrac{\bar{Q}^*}{f^*} \dfrac{\partial f^*}{\partial \bar{Q}^*} \right) \right) \left(\omega_n \int \psi_n^R + \dfrac{\varsigma_L \bar{b}^2 C_d^2 \bar{Q}^*}{2} \left[\dfrac{\psi_n^I}{\bar{h}^{*3}} \right]_{\bar{x}_L} \right) \\ +\dfrac{2\bar{\rho}\bar{Q}^*}{\bar{h}^{*2}} \omega_n \psi_n^R - \dfrac{3\bar{\rho}\bar{Q}^{*2}}{\bar{h}^{*4}} \left(\dfrac{\partial \bar{h}^*}{\partial \bar{x}} - \dfrac{f^*}{4} \right) \psi_n^I + \dfrac{\bar{\rho}\bar{Q}^{*2}}{\bar{h}^{*3}} \dfrac{\partial \psi_n^I}{\partial \bar{x}} \end{array} \right) d\bar{x} \right.$$

$$+ \left[\int \psi_m^I \right]_{\bar{x}_L} \zeta_{in} \bar{\rho} \bar{Q}^* \left(\bar{Q}^* \left[\frac{\psi_n^I}{\bar{h}^{*3}} \right]_{\bar{x}_L} + \omega_n \left[\frac{\int \psi_n^R}{\bar{h}^{*2}} \right]_{\bar{x}_L} + \frac{\zeta_{in} \bar{b}^2 C_d^2 \bar{Q}^*}{2} \left[\frac{\psi_n^I}{\bar{h}^{*5}} \right]_{\bar{x}_L} \right)$$

$$\left. + \left[\int \psi_m^I \right]_{\bar{x}_R} \zeta_{ex} \bar{\rho} \bar{Q}^* \left(\bar{Q}^* \left[\frac{\psi_n^I}{\bar{h}^{*3}} \right]_{\bar{x}_R} + \omega_n \left[\frac{\int \psi_n^R}{\bar{h}^{*2}} \right]_{\bar{x}_R} + \frac{\zeta_{in} \bar{b}^2 C_d^2 \bar{Q}^*}{2 \left[\bar{h}^{*2} \right]_{\bar{x}_R}} \left[\frac{\psi_n^I}{\bar{h}^{*3}} \right]_{\bar{x}_L} \right) \right)$$

$$+ \omega_m \xi_m^I$$

.

(3.5.40)

In a similar manner, multiplying by $\mathbf{\Phi}_m^{I\,T}$, and taking integrals over both sides provide

$$\sum_{n=1}^{N}\int_0^1\left(\dot{\xi}_n^R{\boldsymbol{\Phi}_m^I}^T\mathbf{A}\boldsymbol{\Phi}_n^R+\dot{\xi}_n^I{\boldsymbol{\Phi}_m^I}^T\mathbf{A}\boldsymbol{\Phi}_n^I+\xi_n^R{\boldsymbol{\Phi}_m^I}^T\mathbf{B}\boldsymbol{\Phi}_n^R+\xi_n^I{\boldsymbol{\Phi}_m^I}^T\mathbf{B}\boldsymbol{\Phi}_n^I\right)d\bar{x} = \int_0^1{\boldsymbol{\Phi}_m^I}^T\mathbf{q}\,d\bar{x} \tag{3.5.41}$$

and considering the orthogonality properties (3.4.36) to (3.4.38) gives

$$\sum_{n=1}^{N}\left(\dot{\xi}_n^I\delta_{nm}+\omega_n\xi_n^R\delta_{nm}\right)=\int_0^1{\boldsymbol{\Phi}_m^I}^T\mathbf{q}\,d\bar{x} \tag{3.5.42}$$

or, using Eqs. (3.5.5) and (3.5.15),

$$\dot{\xi}_m^I+\omega_m\xi_m^R=\int_{\bar{x}_L}^{\bar{x}_R}\omega_m\psi_m^R\tilde{p}\,d\bar{x}\quad m=1,2,\ldots,N. \tag{3.5.43}$$

By virtue of integral by parts, we have

$$\dot{\xi}_m^I+\omega_m\xi_m^R=-\int_{\bar{x}_L}^{\bar{x}_R}\omega_m\int\psi_m^R\frac{\partial\tilde{p}}{\partial\bar{x}}d\bar{x}+\left[\omega_m\int\psi_m^R\tilde{p}\right]_{\bar{x}_L}^{\bar{x}_R}, \tag{3.5.44}$$

and, using Eqs. (3.3.20), (3.3.23), and (3.3.24), it is rewritten as

$$\begin{aligned}&\dot{\xi}_m^I+\omega_m\xi_m^R=\\&-\omega_m\left(\begin{array}{l}\displaystyle\int_{\bar{x}_L}^{\bar{x}_R}\int\psi_m^R\left(\begin{array}{l}\displaystyle\frac{\bar{\rho}}{\bar{h}^*}\left(\int\ddot{\tilde{y}}d\bar{x}+\frac{\zeta_{in}\bar{b}^2C_d^2\bar{Q}^*}{2}\left[\frac{\dot{\tilde{y}}}{\bar{h}^{*3}}\right]_{\bar{x}_L}\right)\\\displaystyle-\frac{2\bar{\rho}\bar{Q}^*}{\bar{h}^{*3}}\left(\frac{\partial\bar{h}^*}{\partial\bar{x}}-\frac{f^*}{8}\left(2+\frac{\bar{Q}^*}{f^*}\frac{\partial f^*}{\partial\bar{Q}^*}\right)\right)\left(\int\dot{\tilde{y}}d\bar{x}+\frac{\zeta_{in}\bar{b}^2C_d^2\bar{Q}^*}{2}\left[\frac{\tilde{y}}{\bar{h}^{*3}}\right]_{\bar{x}_L}\right)\\\displaystyle+\frac{2\bar{\rho}\bar{Q}^*}{\bar{h}^{*2}}\dot{\tilde{y}}-\frac{3\bar{\rho}\bar{Q}^{*2}}{\bar{h}^{*4}}\left(\frac{\partial\bar{h}^*}{\partial\bar{x}}-\frac{f^*}{4}\right)\tilde{y}+\frac{\bar{\rho}\bar{Q}^{*2}}{\bar{h}^{*3}}\frac{\partial\tilde{y}}{\partial\bar{x}}\end{array}\right)d\bar{x}\\+\left[\int\psi_m^R\right]_{\bar{x}_L}\zeta_{in}\bar{\rho}\bar{Q}^*\left(\bar{Q}^*\left[\frac{\tilde{y}}{\bar{h}^{*3}}\right]_{\bar{x}_L}+\left[\frac{\int\dot{\tilde{y}}d\bar{x}}{\bar{h}^{*2}}+\frac{\zeta_{in}\bar{b}^2C_d^2\bar{Q}^*}{2}\frac{\tilde{y}}{\bar{h}^{*5}}\right]_{\bar{x}_L}\right)\\+\left[\int\psi_m^R\right]_{\bar{x}_R}\zeta_{ex}\bar{\rho}\bar{Q}^*\left(\bar{Q}^*\left[\frac{\tilde{y}}{\bar{h}^{*3}}\right]_{\bar{x}_R}+\left[\frac{\int\dot{\tilde{y}}d\bar{x}}{\bar{h}^{*2}}+\frac{\zeta_{in}\bar{b}^2C_d^2\bar{Q}^*}{2\bar{h}^{*2}}\left[\frac{\tilde{y}}{\bar{h}^{*3}}\right]_{\bar{x}_L}\right]_{\bar{x}_R}\right)\end{array}\right).\end{aligned} \tag{3.5.45}$$

Substituting Eqs. (3.5.32) and (3.5.33) into Eq. (3.5.45) yields

$$\dot{\xi}_m^I - \sum_{n=1}^{N} \dot{\xi}_n^R \omega_m \omega_n \int_{\bar{x}_L}^{\bar{x}_R} \frac{\bar{\rho}}{\bar{h}^*} \int \psi_m^R \int \psi_n^I d\bar{x} + \sum_{n=1}^{N} \dot{\xi}_n^I \omega_m \omega_n \int_{\bar{x}_L}^{\bar{x}_R} \frac{\bar{\rho}}{\bar{h}^*} \int \psi_m^R \int \psi_n^R d\bar{x} =$$

$$-\sum_{n=1}^{NY} \xi_n^R \omega_m \left(\int_{\bar{x}_L}^{\bar{x}_R} \int \psi_m^R \left(\begin{array}{l} -\omega_n \dfrac{\zeta_{in} \bar{\rho} \bar{b}^2 C_d^2 \bar{Q}^*}{2\bar{h}^*} \left[\dfrac{\psi_n^I}{\bar{h}^{*3}} \right]_{\bar{x}_L} \\ -\dfrac{2\bar{\rho}\bar{Q}^*}{\bar{h}^{*3}} \left(\dfrac{\partial \bar{h}^*}{\partial \bar{x}} - \dfrac{f^*}{8} \left(2 + \dfrac{\bar{Q}^*}{f^*} \dfrac{\partial f^*}{\partial \bar{Q}^*} \right) \right) \left(-\omega_n \int \psi_n^I + \dfrac{\varsigma_L \bar{b}^2 C_d^2 \bar{Q}^*}{2} \left[\dfrac{\psi_n^R}{\bar{h}^{*3}} \right]_{\bar{x}_L} \right) \\ -\dfrac{2\bar{\rho}\bar{Q}^*}{\bar{h}^{*2}} \omega_n \psi_n^I - \dfrac{3\bar{\rho}\bar{Q}^{*2}}{\bar{h}^{*4}} \left(\dfrac{\partial \bar{h}^*}{\partial \bar{x}} - \dfrac{f^*}{4} \right) \psi_n^R + \dfrac{\bar{\rho}\bar{Q}^{*2}}{\bar{h}^{*3}} \dfrac{\partial \psi_n^R}{\partial \bar{x}} \end{array} \right) d\bar{x} \right.$$

$$+ \left[\int \psi_m^R \right]_{\bar{x}_L} \zeta_{in} \bar{\rho} \bar{Q}^* \left(\bar{Q}^* \left[\frac{\psi_n^R}{\bar{h}^{*3}} \right]_{\bar{x}_L} - \omega_n \left[\frac{\int \psi_n^I}{\bar{h}^{*2}} \right]_{\bar{x}_L} + \frac{\zeta_{in} \bar{b}^2 C_d^2 \bar{Q}^*}{2} \left[\frac{\psi_n^R}{\bar{h}^{*5}} \right]_{\bar{x}_L} \right)$$

$$\left. + \left[\int \psi_m^R \right]_{\bar{x}_R} \zeta_{ex} \bar{\rho} \bar{Q}^* \left(\bar{Q}^* \left[\frac{\psi_n^R}{\bar{h}^{*3}} \right]_{\bar{x}_R} - \omega_n \left[\frac{\int \psi_n^I}{\bar{h}^{*2}} \right]_{\bar{x}_R} + \frac{\zeta_{in} \bar{b}^2 C_d^2 \bar{Q}^*}{2 \left[\bar{h}^{*2} \right]_{\bar{x}_R}} \left[\frac{\psi_n^R}{\bar{h}^{*3}} \right]_{\bar{x}_L} \right) \right)$$

$$-\sum_{n=1}^{NY} \xi_n^I \omega_m \left(\int_{\bar{x}_L}^{\bar{x}_R} \int \psi_m^R \left(\begin{array}{l} \omega_n \dfrac{\zeta_{in} \bar{\rho} \bar{b}^2 C_d^2 \bar{Q}^*}{2\bar{h}^*} \left[\dfrac{\psi_n^R}{\bar{h}^{*3}} \right]_{\bar{x}_L} \\ -\dfrac{2\bar{\rho}\bar{Q}^*}{\bar{h}^{*3}} \left(\dfrac{\partial \bar{h}^*}{\partial \bar{x}} - \dfrac{f^*}{8} \left(2 + \dfrac{\bar{Q}^*}{f^*} \dfrac{\partial f^*}{\partial \bar{Q}^*} \right) \right) \left(\omega_n \int \psi_n^R + \dfrac{\varsigma_L \bar{b}^2 C_d^2 \bar{Q}^*}{2} \left[\dfrac{\psi_n^I}{\bar{h}^{*3}} \right]_{\bar{x}_L} \right) \\ +\dfrac{2\bar{\rho}\bar{Q}^*}{\bar{h}^{*2}} \omega_n \psi_n^R - \dfrac{3\bar{\rho}\bar{Q}^{*2}}{\bar{h}^{*4}} \left(\dfrac{\partial \bar{h}^*}{\partial \bar{x}} - \dfrac{f^*}{4} \right) \psi_n^I + \dfrac{\bar{\rho}\bar{Q}^{*2}}{\bar{h}^{*3}} \dfrac{\partial \psi_n^I}{\partial \bar{x}} \end{array} \right) d\bar{x} \right.$$

$$+ \left[\int \psi_m^R \right]_{\bar{x}_L} \zeta_{in} \bar{\rho} \bar{Q}^* \left(\bar{Q}^* \left[\frac{\psi_n^I}{\bar{h}^{*3}} \right]_{\bar{x}_L} + \omega_n \left[\frac{\int \psi_n^R}{\bar{h}^{*2}} \right]_{\bar{x}_L} + \frac{\zeta_{in} \bar{b}^2 C_d^2 \bar{Q}^*}{2} \left[\frac{\psi_n^I}{\bar{h}^{*5}} \right]_{\bar{x}_L} \right)$$

$$\left. + \left[\int \psi_m^R \right]_{\bar{x}_R} \zeta_{ex} \bar{\rho} \bar{Q}^* \left(\bar{Q}^* \left[\frac{\psi_n^I}{\bar{h}^{*3}} \right]_{\bar{x}_R} + \omega_n \left[\frac{\int \psi_n^R}{\bar{h}^{*2}} \right]_{\bar{x}_R} + \frac{\zeta_{in} \bar{b}^2 C_d^2 \bar{Q}^*}{2 \left[\bar{h}^{*2} \right]_{\bar{x}_R}} \left[\frac{\psi_n^I}{\bar{h}^{*3}} \right]_{\bar{x}_L} \right) \right)$$

$$-\omega_m \xi_m^R \qquad .$$

(3.5.46)

Therefore, the discrete model of the fluid-structure linear system obtained through the Galerkin's method can be expressed in the simple form

$$\mathbf{C}\dot{\mathbf{q}} = \mathbf{D}\mathbf{q} \tag{3.5.47}$$

with $2N$ degrees of freedom for the air-web linear system about equilibrium. The vector $\mathbf{q}$ is the generalized coordinate such that

$$\mathbf{q} = \begin{Bmatrix} \boldsymbol{\xi}^R \\ \boldsymbol{\xi}^I \end{Bmatrix} \tag{3.5.48}$$

where

$$\boldsymbol{\xi}^R = \begin{Bmatrix} \xi_1^R \\ \xi_2^R \\ \vdots \\ \xi_{NY}^R \end{Bmatrix} \quad \text{and} \quad \boldsymbol{\xi}^I = \begin{Bmatrix} \xi_1^I \\ \xi_2^I \\ \vdots \\ \xi_{NY}^I \end{Bmatrix}, \tag{3.5.49}$$

and the matrices $\mathbf{C}$ and $\mathbf{D}$ are such that, respectively,

$$\mathbf{C} = \begin{bmatrix} \mathbf{I} + \mathbf{C}^{RR} & \mathbf{C}^{RI} \\ \mathbf{C}^{IR} & \mathbf{I} + \mathbf{C}^{II} \end{bmatrix} \tag{3.5.50}$$

and

$$\mathbf{D} = \begin{bmatrix} \mathbf{D}^{RR} & \mathbf{D}^{RI} + \boldsymbol{\Omega} \\ \mathbf{D}^{IR} - \boldsymbol{\Omega} & \mathbf{D}^{II} \end{bmatrix} \tag{3.5.51}$$

where

$\mathbf{I}$ is the identity matrix,

$\boldsymbol{\Omega} = \mathrm{Diag}(\omega_n)$ is the diagonal matrix composed of the natural frequencies of the web,

$$\mathbf{C}_{mn}^{RR} = \omega_m \omega_n \int_{\bar{x}_L}^{\bar{x}_R} \frac{\bar{\rho}}{\bar{h}^*} \int \psi_m^I \int \psi_n^I d\bar{x} \,,$$

$$\mathbf{C}_{mn}^{RI} = -\omega_m \omega_n \int_{\bar{x}_L}^{\bar{x}_R} \frac{\bar{\rho}}{\bar{h}^*} \int \psi_m^I \int \psi_n^R d\bar{x} \,,$$

$$\mathbf{C}_{mn}^{IR} = -\omega_m \omega_n \int_{\bar{x}_L}^{\bar{x}_R} \frac{\bar{\rho}}{\bar{h}^*} \int \psi_m^R \int \psi_n^I d\bar{x} \,,$$

$$\mathbf{C}_{mn}^{II} = \omega_m \omega_n \int_{\bar{x}_L}^{\bar{x}_R} \frac{\bar{\rho}}{\bar{h}^*} \int \psi_m^R \int \psi_n^R d\bar{x} \,,$$

$$\mathbf{D}_{mn}^{RR} =$$

$$\omega_m \int_{\bar{x}_L}^{\bar{x}_R} \int \psi_m^I \left(\begin{array}{l} -\omega_n \dfrac{\varsigma_L \bar{\rho} \bar{b}^2 C_d^2 \bar{Q}^*}{2\bar{h}^*} \left[\dfrac{\psi_n^I}{\bar{h}^{*3}} \right]_{\bar{x}_L} \\ -\dfrac{2\bar{\rho}\bar{Q}^*}{\bar{h}^{*3}} \left(\dfrac{\partial \bar{h}^*}{\partial \bar{x}} - \dfrac{f^*}{8} \left(2 + \dfrac{\bar{Q}^*}{f^*} \dfrac{\partial f^*}{\partial \bar{Q}^*} \right) \right) \left(-\omega_n \int \psi_n^I + \dfrac{\varsigma_L \bar{b}^2 C_d^2 \bar{Q}^*}{2} \left[\dfrac{\psi_n^R}{\bar{h}^{*3}} \right]_{\bar{x}_L} \right) \\ -\dfrac{2\bar{\rho}\bar{Q}^*}{\bar{h}^{*2}} \omega_n \psi_n^I - \dfrac{3\bar{\rho}\bar{Q}^{*2}}{\bar{h}^{*4}} \left(\dfrac{\partial \bar{h}^*}{\partial \bar{x}} - \dfrac{f^*}{4} \right) \psi_n^R + \dfrac{\bar{\rho}\bar{Q}^{*2}}{\bar{h}^{*3}} \dfrac{\partial \psi_n^R}{\partial \bar{x}} \end{array} \right) d\bar{x} ,$$

$$+\omega_m \left[\int \psi_m^I \right]_{\bar{x}_L} \zeta_{in} \bar{\rho} \bar{Q}^* \left(\bar{Q}^* \left[\frac{\psi_n^R}{\bar{h}^{*3}} \right]_{\bar{x}_L} - \omega_n \left[\frac{\int \psi_n^I}{\bar{h}^{*2}} \right]_{\bar{x}_L} + \frac{\zeta_{in} \bar{b}^2 C_d^2 \bar{Q}^*}{2} \left[\frac{\psi_n^R}{\bar{h}^{*5}} \right]_{\bar{x}_L} \right)$$

$$+\omega_m \left[\int \psi_m^I \right]_{\bar{x}_R} \zeta_{ex} \bar{\rho} \bar{Q}^* \left(\bar{Q}^* \left[\frac{\psi_n^R}{\bar{h}^{*3}} \right]_{\bar{x}_R} - \omega_n \left[\frac{\int \psi_n^I}{\bar{h}^{*2}} \right]_{\bar{x}_R} + \frac{\zeta_{in} \bar{b}^2 C_d^2 \bar{Q}^*}{2 \left[\bar{h}^{*2} \right]_{\bar{x}_R}} \left[\frac{\psi_n^R}{\bar{h}^{*3}} \right]_{\bar{x}_L} \right)$$

$$\mathbf{D}_{mn}^{RI} =$$

$$\omega_m \int_{\bar{x}_L}^{\bar{x}_R} \int \psi_m^I \left(\begin{array}{l} \omega_n \dfrac{\varsigma_L \bar{\rho} \bar{b}^2 C_d^2 \bar{Q}^*}{2\bar{h}^*} \left[\dfrac{\psi_n^R}{\bar{h}^{*3}} \right]_{\bar{x}_L} \\ -\dfrac{2\bar{\rho}\bar{Q}^*}{\bar{h}^{*3}} \left(\dfrac{\partial \bar{h}^*}{\partial \bar{x}} - \dfrac{f^*}{8} \left(2 + \dfrac{\bar{Q}^*}{f^*} \dfrac{\partial f^*}{\partial \bar{Q}^*} \right) \right) \left(\omega_n \int \psi_n^R + \dfrac{\varsigma_L \bar{b}^2 C_d^2 \bar{Q}^*}{2} \left[\dfrac{\psi_n^I}{\bar{h}^{*3}} \right]_{\bar{x}_L} \right) \\ +\dfrac{2\bar{\rho}\bar{Q}^*}{\bar{h}^{*2}} \omega_n \psi_n^R - \dfrac{3\bar{\rho}\bar{Q}^{*2}}{\bar{h}^{*4}} \left(\dfrac{\partial \bar{h}^*}{\partial \bar{x}} - \dfrac{f^*}{4} \right) \psi_n^I + \dfrac{\bar{\rho}\bar{Q}^{*2}}{\bar{h}^{*3}} \dfrac{\partial \psi_n^I}{\partial \bar{x}} \end{array} \right) d\bar{x} ,$$

$$+\omega_m \left[\int \psi_m^I \right]_{\bar{x}_L} \zeta_{in} \bar{\rho} \bar{Q}^* \left(\bar{Q}^* \left[\frac{\psi_n^I}{\bar{h}^{*3}} \right]_{\bar{x}_L} + \omega_n \left[\frac{\int \psi_n^R}{\bar{h}^{*2}} \right]_{\bar{x}_L} + \frac{\zeta_{in} \bar{b}^2 C_d^2 \bar{Q}^*}{2} \left[\frac{\psi_n^I}{\bar{h}^{*5}} \right]_{\bar{x}_L} \right)$$

$$+\omega_m \left[\int \psi_m^I \right]_{\bar{x}_R} \zeta_{ex} \bar{\rho} \bar{Q}^* \left(\bar{Q}^* \left[\frac{\psi_n^I}{\bar{h}^{*3}} \right]_{\bar{x}_R} + \omega_n \left[\frac{\int \psi_n^R}{\bar{h}^{*2}} \right]_{\bar{x}_R} + \frac{\zeta_{in} \bar{b}^2 C_d^2 \bar{Q}^*}{2 \left[\bar{h}^{*2} \right]_{\bar{x}_R}} \left[\frac{\psi_n^I}{\bar{h}^{*3}} \right]_{\bar{x}_L} \right)$$

$$\mathbf{D}_{mn}^{IR} =$$

$$-\omega_m \int_{\bar{x}_L}^{\bar{x}_R} \int \psi_m^R \begin{pmatrix} -\omega_n \dfrac{\zeta_{in}\bar{\rho}\bar{b}^2 C_d^2 \bar{Q}^*}{2\bar{h}^*} \left[\dfrac{\psi_n^I}{\bar{h}^{*3}}\right]_{\bar{x}_L} \\ -\dfrac{2\bar{\rho}\bar{Q}^*}{\bar{h}^{*3}}\left(\dfrac{\partial \bar{h}^*}{\partial \bar{x}} - \dfrac{f^*}{8}\left(2 + \dfrac{\bar{Q}^*}{f^*}\dfrac{\partial f^*}{\partial \bar{Q}^*}\right)\right)\left(-\omega_n \int \psi_n^I + \dfrac{\varsigma_L \bar{b}^2 C_d^2 \bar{Q}^*}{2}\left[\dfrac{\psi_n^R}{\bar{h}^{*3}}\right]_{\bar{x}_L}\right) \\ -\dfrac{2\bar{\rho}\bar{Q}^*}{\bar{h}^{*2}}\omega_n \psi_n^I - \dfrac{3\bar{\rho}\bar{Q}^{*2}}{\bar{h}^{*4}}\left(\dfrac{\partial \bar{h}^*}{\partial \bar{x}} - \dfrac{f^*}{4}\right)\psi_n^R + \dfrac{\bar{\rho}\bar{Q}^{*2}}{\bar{h}^{*3}}\dfrac{\partial \psi_n^R}{\partial \bar{x}} \end{pmatrix} d\bar{x} ,$$

$$-\omega_m \left[\int \psi_m^R\right]_{\bar{x}_L} \zeta_{in}\bar{\rho}\bar{Q}^* \left(\bar{Q}^* \left[\frac{\psi_n^R}{\bar{h}^{*3}}\right]_{\bar{x}_L} - \omega_n \left[\frac{\int \psi_n^I}{\bar{h}^{*2}}\right]_{\bar{x}_L} + \frac{\zeta_{in}\bar{b}^2 C_d^2 \bar{Q}^*}{2}\left[\frac{\psi_n^R}{\bar{h}^{*5}}\right]_{\bar{x}_L} \right)$$

$$-\omega_m \left[\int \psi_m^R\right]_{\bar{x}_R} \zeta_{ex}\bar{\rho}\bar{Q}^* \left(\bar{Q}^* \left[\frac{\psi_n^R}{\bar{h}^{*3}}\right]_{\bar{x}_R} - \omega_n \left[\frac{\int \psi_n^I}{\bar{h}^{*2}}\right]_{\bar{x}_R} + \frac{\zeta_{in}\bar{b}^2 C_d^2 \bar{Q}^*}{2\left[\bar{h}^{*2}\right]_{\bar{x}_R}}\left[\frac{\psi_n^R}{\bar{h}^{*3}}\right]_{\bar{x}_L} \right)$$

$$\mathbf{D}_{mn}^{II} =$$

$$-\omega_m \int_{\bar{x}_L}^{\bar{x}_R} \int \psi_m^R \begin{pmatrix} \omega_n \dfrac{\zeta_{in}\bar{\rho}\bar{b}^2 C_d^2 \bar{Q}^*}{2\bar{h}^*} \left[\dfrac{\psi_n^R}{\bar{h}^{*3}}\right]_{\bar{x}_L} \\ -\dfrac{2\bar{\rho}\bar{Q}^*}{\bar{h}^{*3}}\left(\dfrac{\partial \bar{h}^*}{\partial \bar{x}} - \dfrac{f^*}{8}\left(2 + \dfrac{\bar{Q}^*}{f^*}\dfrac{\partial f^*}{\partial \bar{Q}^*}\right)\right)\left(\omega_n \int \psi_n^R + \dfrac{\varsigma_L \bar{b}^2 C_d^2 \bar{Q}^*}{2}\left[\dfrac{\psi_n^I}{\bar{h}^{*3}}\right]_{\bar{x}_L}\right) \\ +\dfrac{2\bar{\rho}\bar{Q}^*}{\bar{h}^{*2}}\omega_n \psi_n^R - \dfrac{3\bar{\rho}\bar{Q}^{*2}}{\bar{h}^{*4}}\left(\dfrac{\partial \bar{h}^*}{\partial \bar{x}} - \dfrac{f^*}{4}\right)\psi_n^I + \dfrac{\bar{\rho}\bar{Q}^{*2}}{\bar{h}^{*3}}\dfrac{\partial \psi_n^I}{\partial \bar{x}} \end{pmatrix} d\bar{x}$$

$$-\omega_m \left[\int \psi_m^R\right]_{\bar{x}_L} \zeta_{in}\bar{\rho}\bar{Q}^* \left(\bar{Q}^* \left[\frac{\psi_n^I}{\bar{h}^{*3}}\right]_{\bar{x}_L} + \omega_n \left[\frac{\int \psi_n^R}{\bar{h}^{*2}}\right]_{\bar{x}_L} + \frac{\zeta_{in}\bar{b}^2 C_d^2 \bar{Q}^*}{2}\left[\frac{\psi_n^I}{\bar{h}^{*5}}\right]_{\bar{x}_L} \right)$$

$$-\omega_m \left[\int \psi_m^R\right]_{\bar{x}_R} \zeta_{ex}\bar{\rho}\bar{Q}^* \left(\bar{Q}^* \left[\frac{\psi_n^I}{\bar{h}^{*3}}\right]_{\bar{x}_R} + \omega_n \left[\frac{\int \psi_n^R}{\bar{h}^{*2}}\right]_{\bar{x}_R} + \frac{\zeta_{in}\bar{b}^2 C_d^2 \bar{Q}^*}{2\left[\bar{h}^{*2}\right]_{\bar{x}_R}}\left[\frac{\psi_n^I}{\bar{h}^{*3}}\right]_{\bar{x}_L} \right)$$

with dimension $N \times N$. Elements of these matrices are in terms of the equilibrium web displacement, air pressure, and expansion functions. Therefore, the equilibrium solutions are useful to obtain unsteady motions.

Substitution of the solution

$$\mathbf{q} = \mathbf{q}_0 e^{\lambda t} \tag{3.5.52}$$

leads to the asymmetric eigenvalue problem such that

$$\lambda \mathbf{C}\mathbf{q}_0 = \mathbf{D}\mathbf{q}_0 \tag{3.5.53}$$

where λ is the eigenvalue, and $\mathbf{q}_0$ is the eigenvector. Eigensolutions occur in complex conjugate pairs such that $\mathrm{Re}(\lambda)$ represents temporal variation of its amplitude in which positive values imply instability, and negative values imply dissipation, and $\mathrm{Im}(\lambda)$ represents dimensionless modal frequency of the web. The dimensionless frequency is related to the dimensional circular one (radian), Ω by

$$\mathrm{Im}(\lambda) = \Omega \frac{t}{\bar{t}} = \Omega L \sqrt{\frac{m}{T}} . \tag{3.5.54}$$

In particular, if $\mathrm{Re}(\lambda) > 0$, and $\mathrm{Im}(\lambda) \neq 0$, a flutter (dynamic instability) occurs in the system, and if $\mathrm{Re}(\lambda) > 0$, and $\mathrm{Im}(\lambda) = 0$, a divergence (static instability) occurs.

Substituion of the eigenvectors $\mathbf{q}_0$ into the mode shapes of the web displacement (3.5.32) provides the responses of the air-web system. The first four mode shapes of the web over the air bar located at $\bar{x} = 0.25$ is superposed at nine time instants during one period of vibration as plotted in Figure 16. It seems that the node exists around the exit region of the air-bar head ($\bar{x} = 0.4$). The strong static pressure is developed at the cushion region from $\bar{x}_L = 0.1$ to $\bar{x}_R = 0.4$, and it decays at the ambient (from $\bar{x} = 0.4$ to $\bar{x} = 1$).

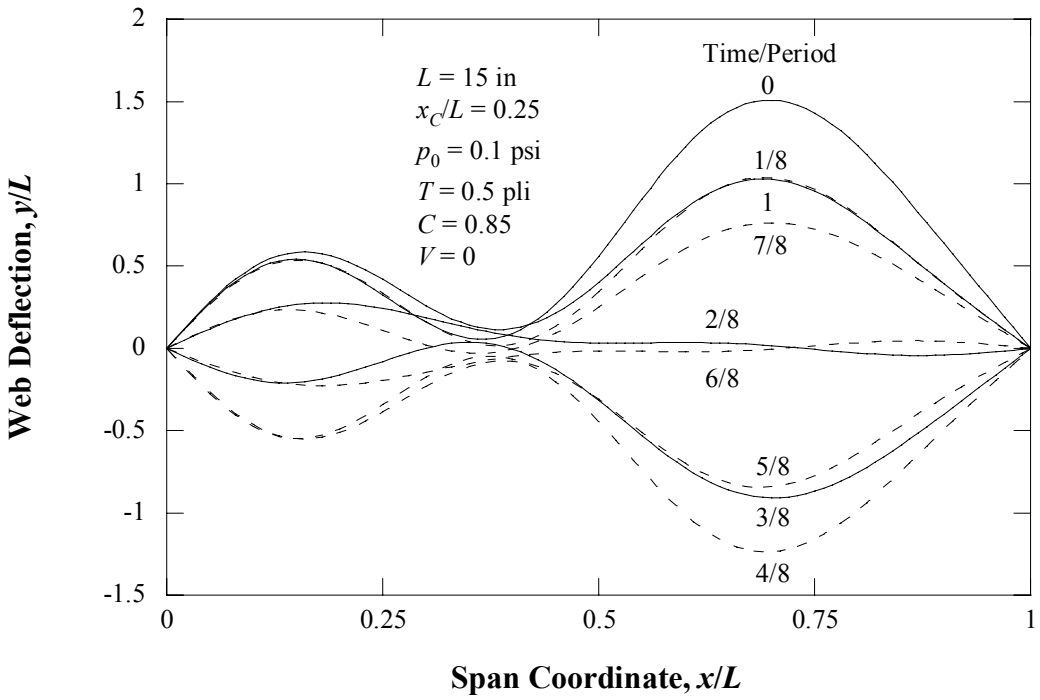

Figure 16 Superposed First Four Modes

CHAPTER IV

EXPERIMENTS

4.1 Test Setup

Experiments were performed in order to verify the presented theory. A schematic of the test setup is shown in Figure 17. The characteristics of the plastic web and pressure-pad air bar are such that

Web:

Mass (per-unit-area)	9.8×10^{-5} lb/in^2
Thickness	0.002 inches
Width	12 inches
Young's modulus	8.7×10^{5} psi

Air Bar:

Nozzle width	0.13 inches
Distance between two nozzles	4.5 inches.

Longitudinal pressure distributions on the pressure-pad air bar can be obtained from 19 pressure taps which are installed in a row on its top surface, and connected to a Scanivalve system. The Scanivalve system is controlled by a data-acquisition program so that it can scan and measure each static pressure from the 19 taps.

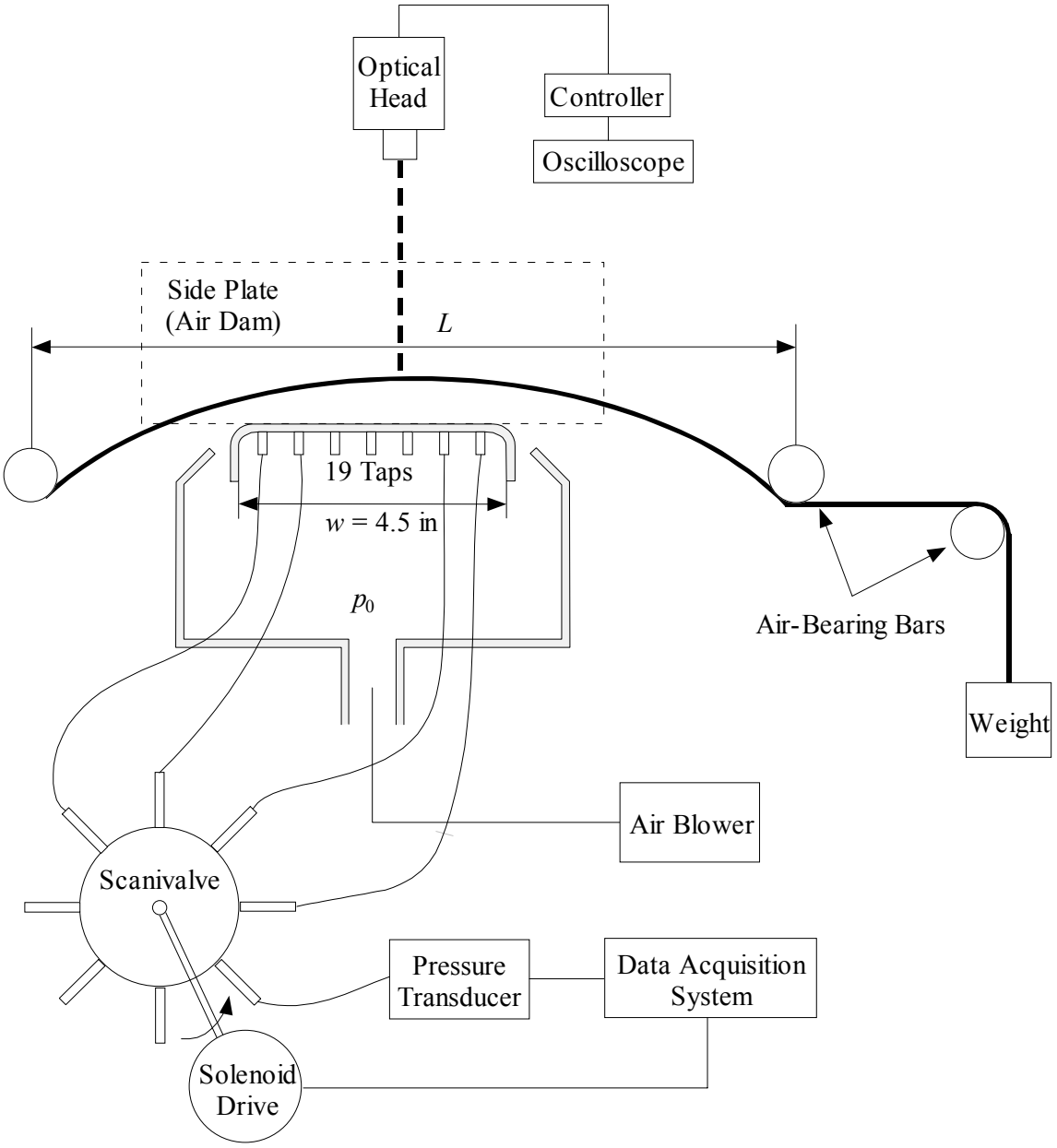

Figure 17 Schematic of Experimental Setup

The air dams are installed along both free edges of the web to block air leakage, and maintain two-dimensional air flows. Aluminum air-bearing bars restrain vertical motions at the both ends of the web while reducing frictions between the web and bars so that the web can slide easily. Tension (pound per linear inch, pli) is applied by a weight,

and can be changed with various weights. A blower with curved blades provides the supply pressure to the pressure-pad air bar. A variable-frequency inverter (AC drive) controls the speed of the blower to change supply pressures.

A laser-Doppler vibrometer is used for non-contact measurement of web flutter. The signal from the laser-Doppler vibrometer is sent to an oscilloscope, and dominant frequencies are identified through the FFT analysis.

Due to equipment limitations, the tests were performed for stationary webs floating over air bars. The test variables are the tension, supply pressure, web length, and vertical and longitudinal location of the pressure-pad air bar.

4.2 Test Results

It was observed that as the pressure supplied to the air bar was increased, the flexible web was deflected from its initial configuration. Steady deflection starts with pressure developed by the air jet flowing under the web; it bulges upward. If the supply pressure is increased further, then the displacement is also increased.

Figure 18 shows that cushion pressure distributions are nearly constant when the pressure-pad air bar is located at the mid-point of the web span, that is, for symmetric web profiles. Pressures are shown to increase with tension (because it reduces flotation heights), which agrees with the ground-effect theory mentioned in Chapter 2. The effect of supply pressure on the static pressure is shown in Figure 19. The prediction curves show good agreement with the experiments.

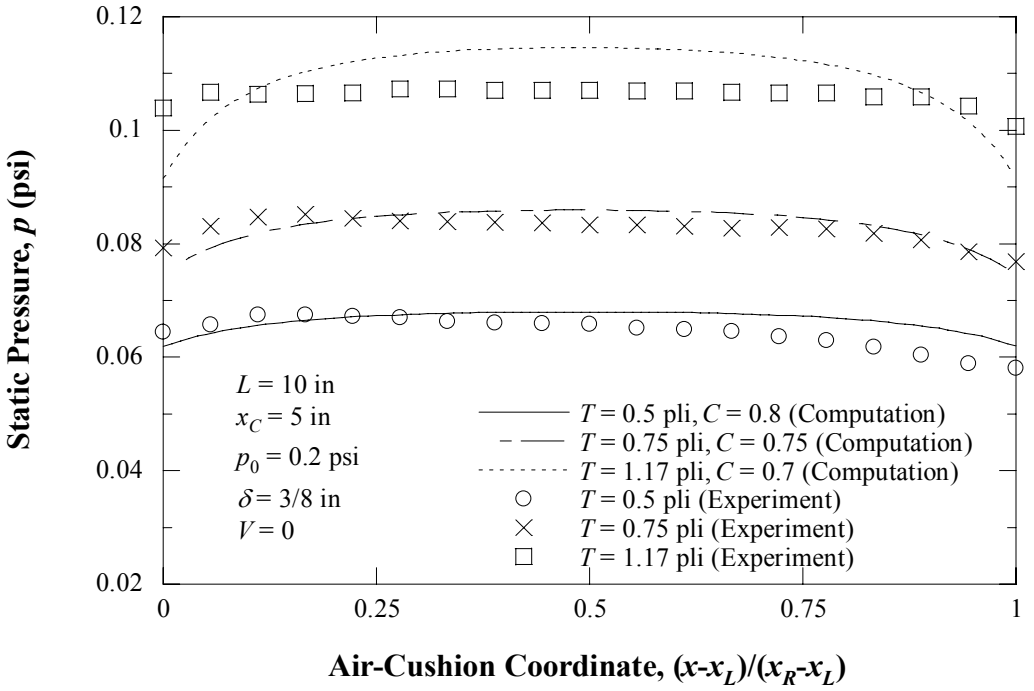

Figure 18 Effect of Tension on Pressure at $\overline{x}_C = 0.5$

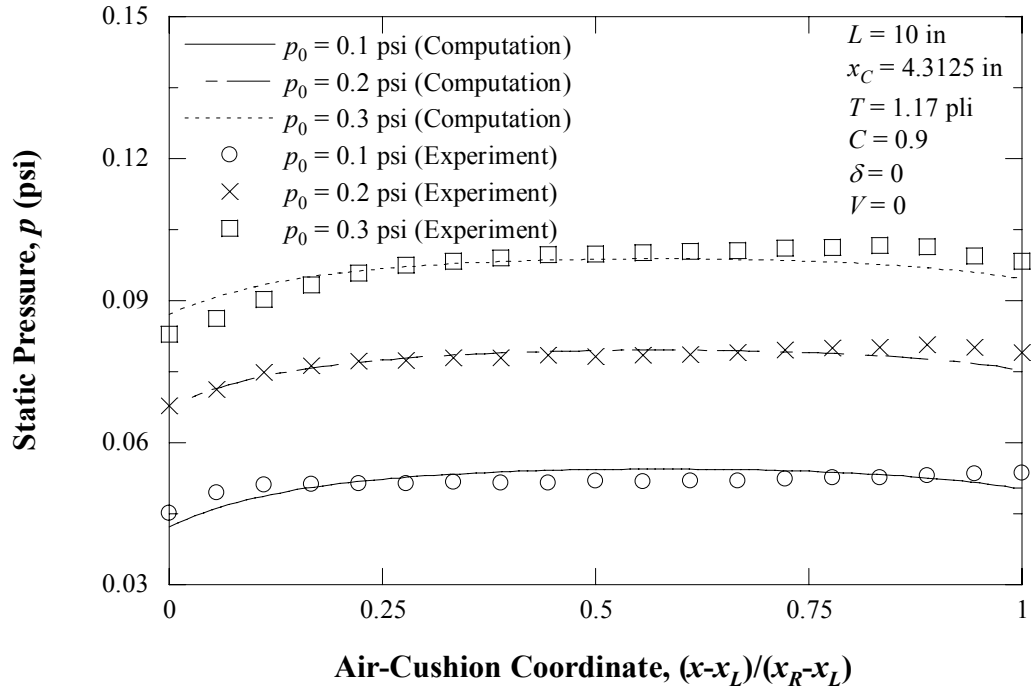

Figure 19 Effect of Supply Pressure on Pressure at $\overline{x}_C = 0.43125$

The effect of tension on the static pressure is presented Figures 20 and 21. The pressure distributions change along the machine direction x as the air bar moves from the middle of the web span to the origin. As x_c is smaller, pressure drops around x_L become more significant, as shown in Figure 22. It is shown that, at the region after the left-hand nozzle, the escaping air jet flows through the region with higher velocity than at the other region because the region has a smaller air gap (flotation height) than the other region. The air gaps are shown in Figure 23.

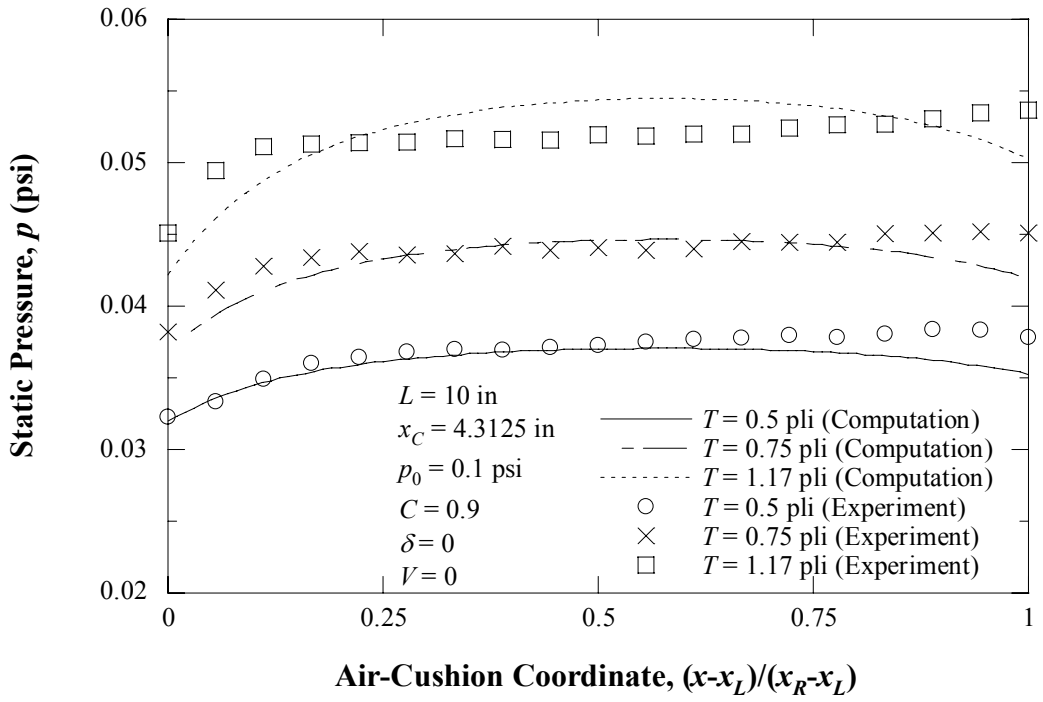

Figure 20 Effect of Tension on Pressure at $\overline{x}_C = 0.43125$

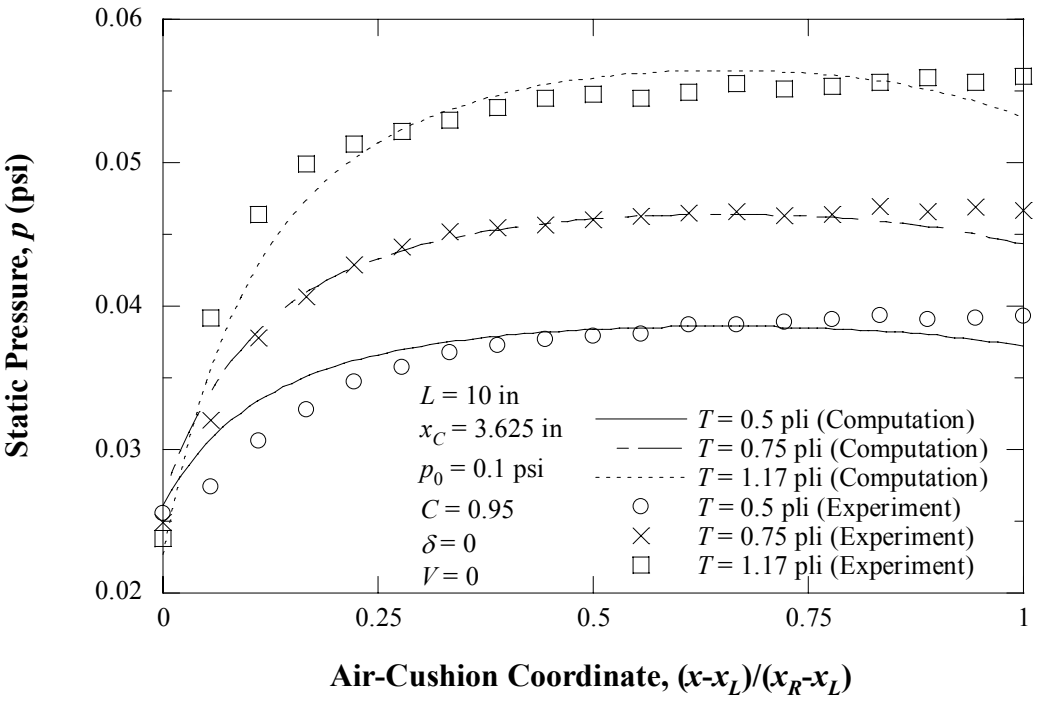

Figure 21 Effect of Tension on Pressure at $\bar{x}_C = 0.3625$

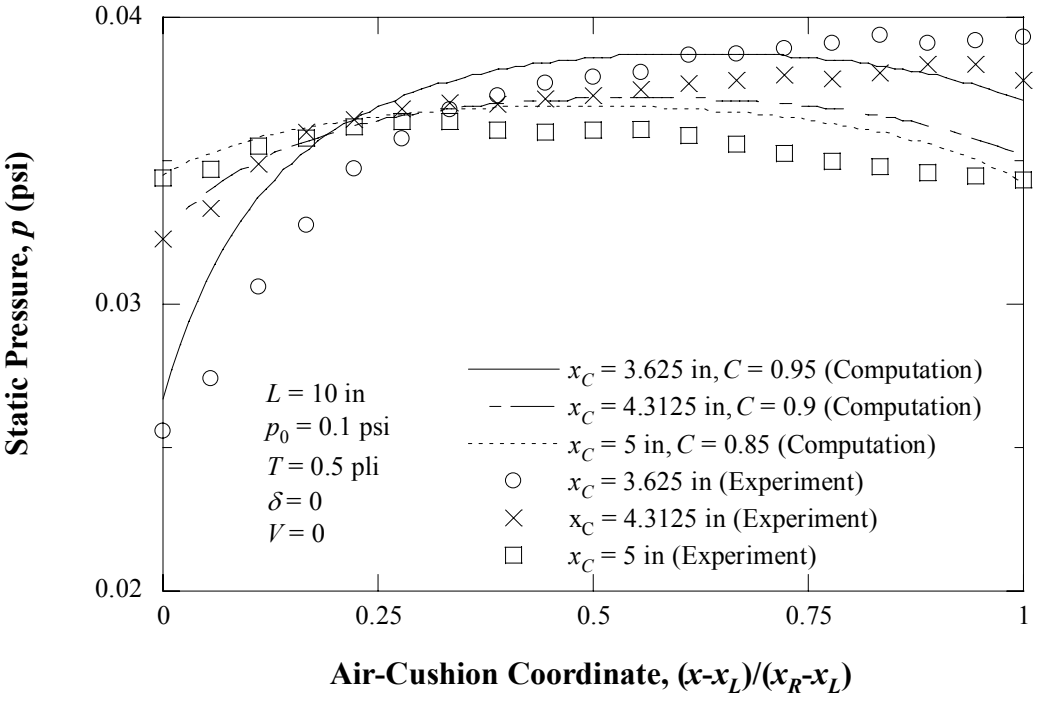

Figure 22 Effect of Horizontal Location of Air-Bar Center on Pressure

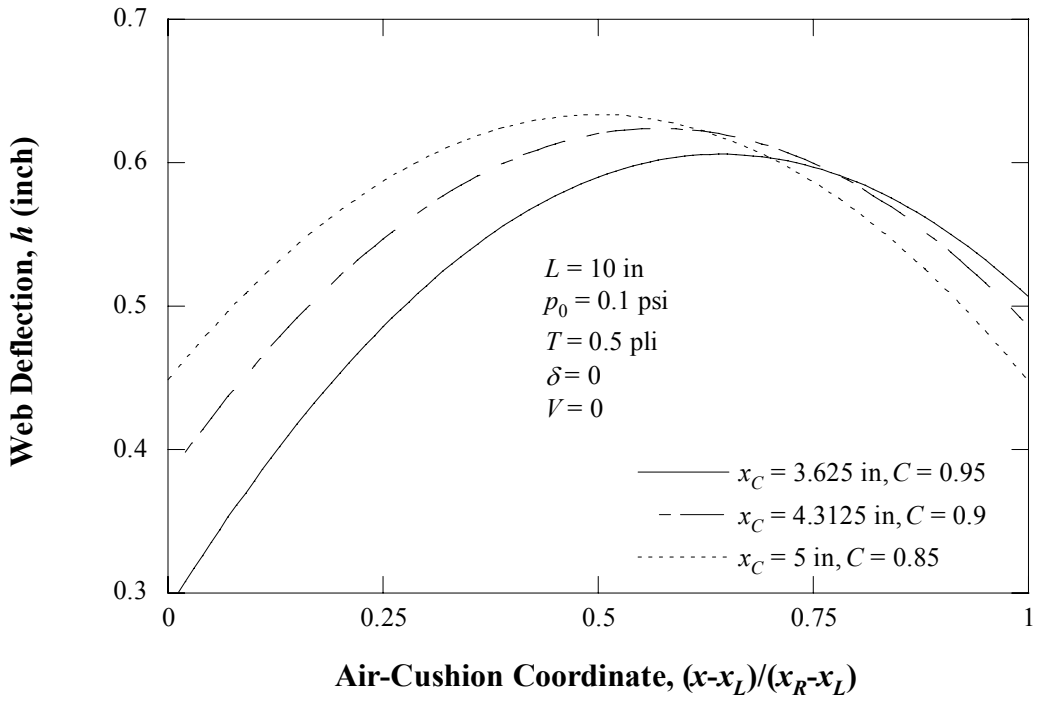

Figure 23 Effect of Horizontal Location of Air-Bar Center on Web Deflection

For equilibrium solutions, the theoretical results show good agreement with the experimental results. Asymmetric web profiles about the pressure-pad air bar cause the cushion pressure to change in the longitudinal direction while it is nearly uniform under symmetric web profiles. It is observed that the pressure variations, especially at the entrance region of the air-bar head, are strongly related to the web deflection, while the pressures become almost uniform as the air jet flows to the exit region.

At flow speed higher than a divergence speed, a flutter occurs. The oscillation amplitude and frequency grow with the supply pressure into a violent flutter, so that the boundaries between static and dynamic instability can be found. In some cases, a static deflection is suddenly changed to a flutter by a small increase in the supply pressure. Due

to the sudden transition, the critical supply pressure can be determined accurately. We use $\zeta_{in} = \zeta_{ex} = 0.96$ for analytical calculations.

Figure 24 shows the effect of tension on the stability boundary of flutter. The flutter pressure increases linearly as the web tension becomes higher. The experimental results are higher that the prediction curves, but they show the same tendency. It is shown that increasing tension is a factor to suppress the web flutter. It seems that the flutter frequency also increases with increase in tension and $\overline{x}_C$ as plotted Figure 25. However, the effect of $\overline{x}_C$ on the flutter frequency is insignificant as $\overline{x}_C$ becomes higher than 0.35.

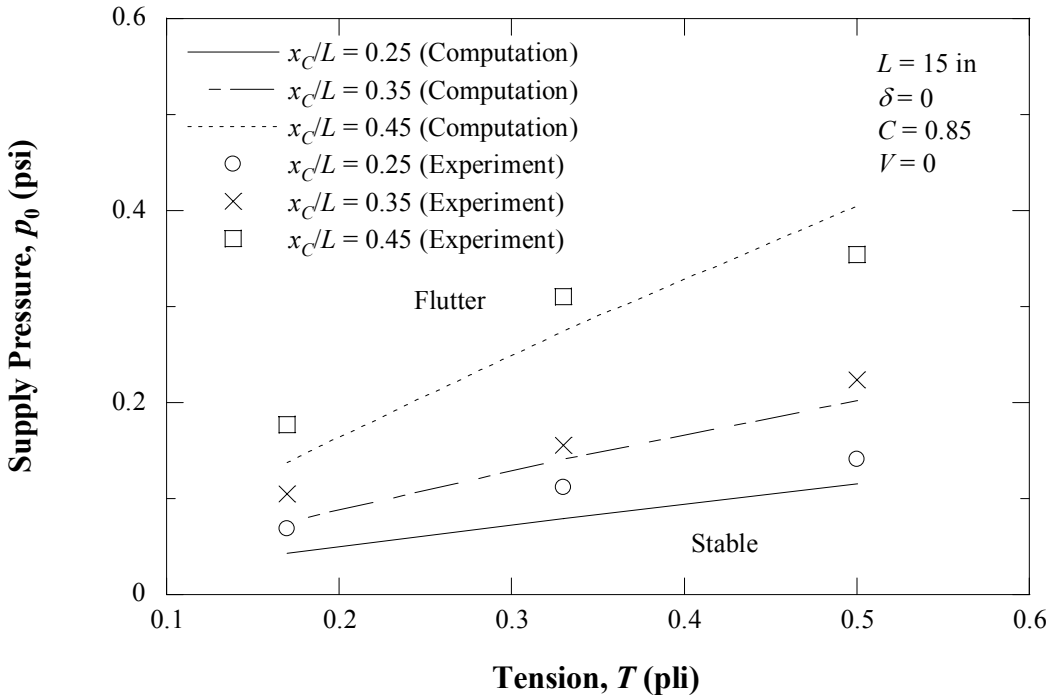

Figure 24 Effect of Tension on Flutter Pressure

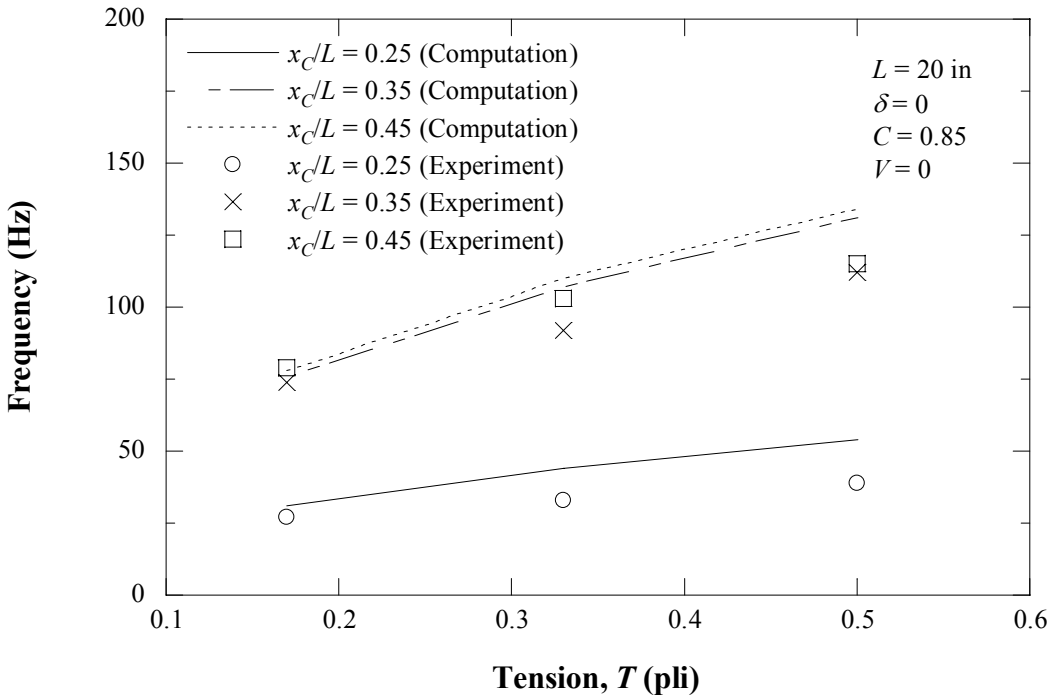

Figure 25 Effect of Tension on Flutter Frequency

As the air bar moves away from the middle of the span along the x axis, the flutter pressure becomes reduced as shown in Figure 26; this asymmetry makes the cushion pressure unstable, and the web is vulnerable to fluttering. It is notable that, physically, it is impossible to always keep the deflection profile of a web symmetric over pressure-pad air bars in the air flotation oven.

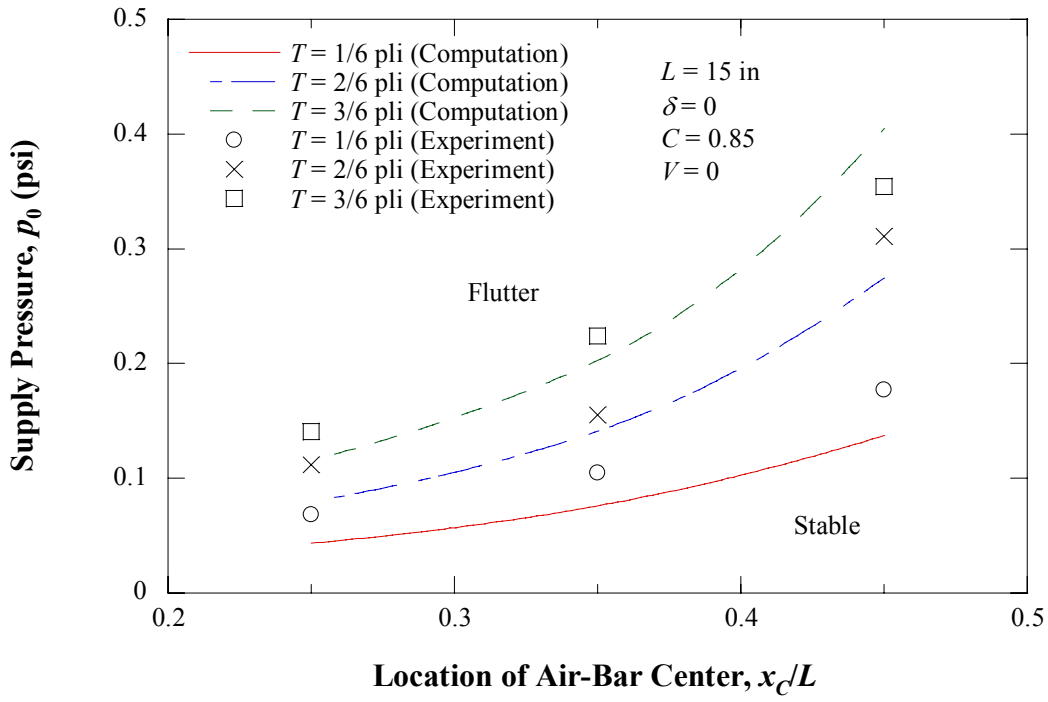

Figure 26 Effect of Horizontal Location of Air-Bar Center on Flutter Pressure

The effect of web length on the stability boundaries is shown in Figure 27. As expected, the longer web tends to be more unstable than the shorter one. Flutter frequency is sensitive not only to tension but also web length, as shown in Figure 28. It seems that a longer web has a lower frequency.

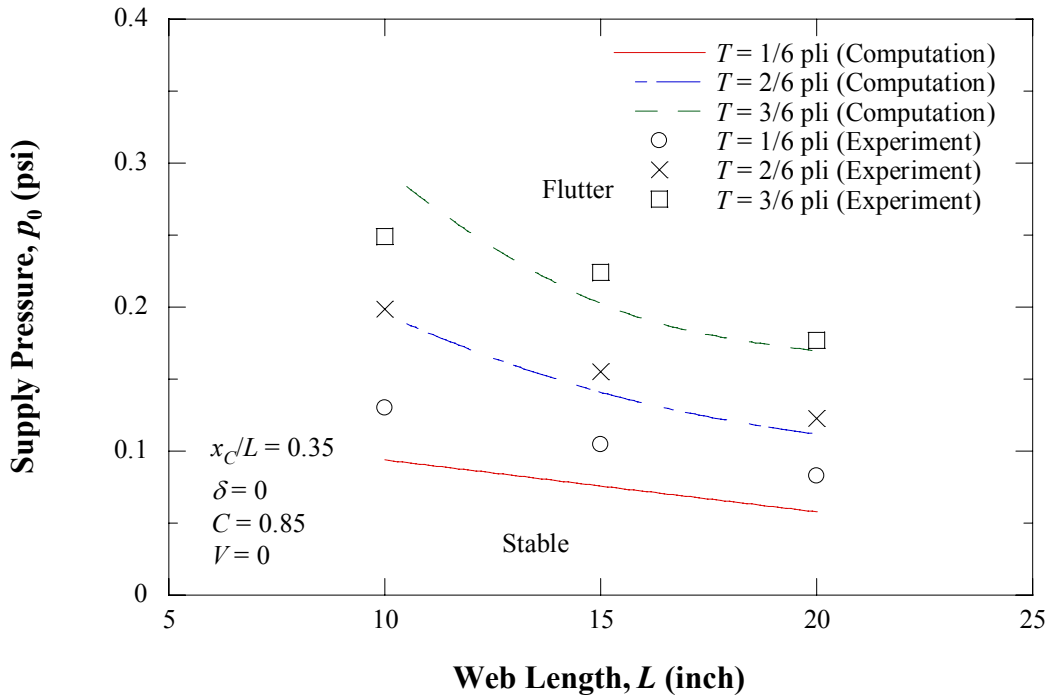

Figure 27 Effect of Web Length on Flutter Pressure

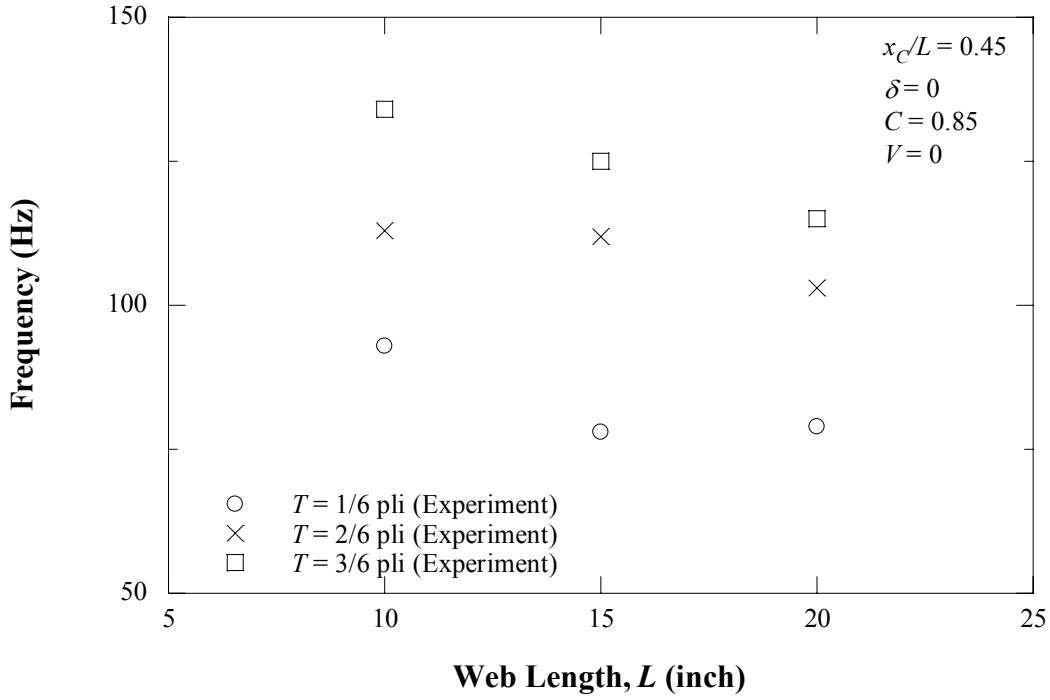

Figure 28 Effect of Web Length on Flutter Frequency

Figures 29 and 30 show the effect of vertical location of the air-bar head on the web flutter. It seems that δ has no appreciable effect on the flutter pressure and frequency under the same tension.

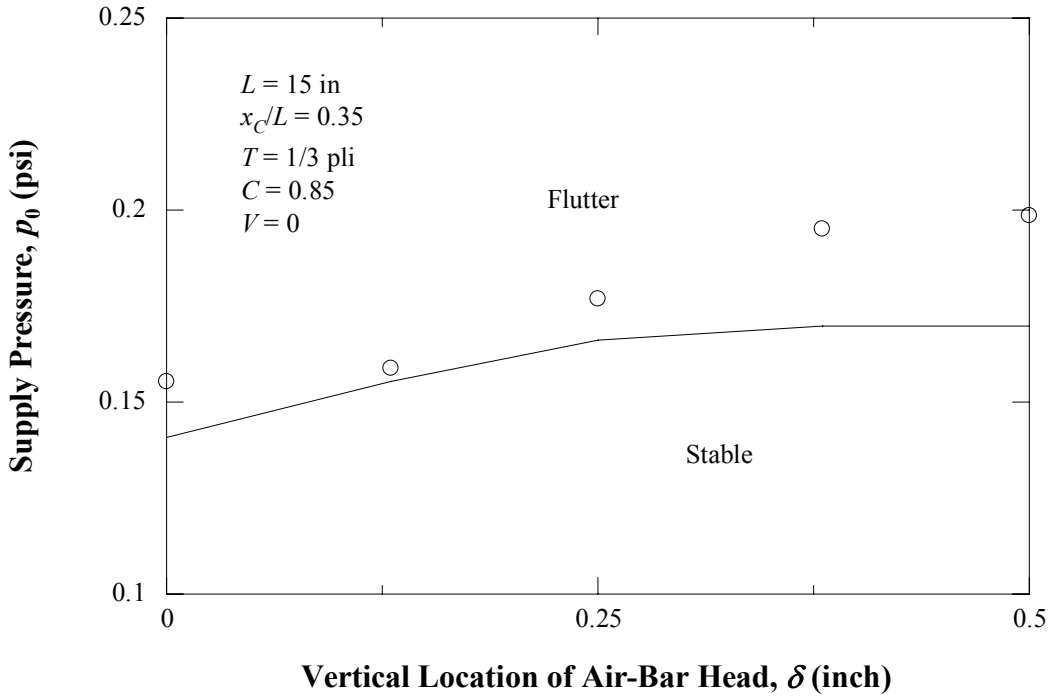

Figure 29 Effect of Vertical Location of Air-Bar Head on Flutter Pressure

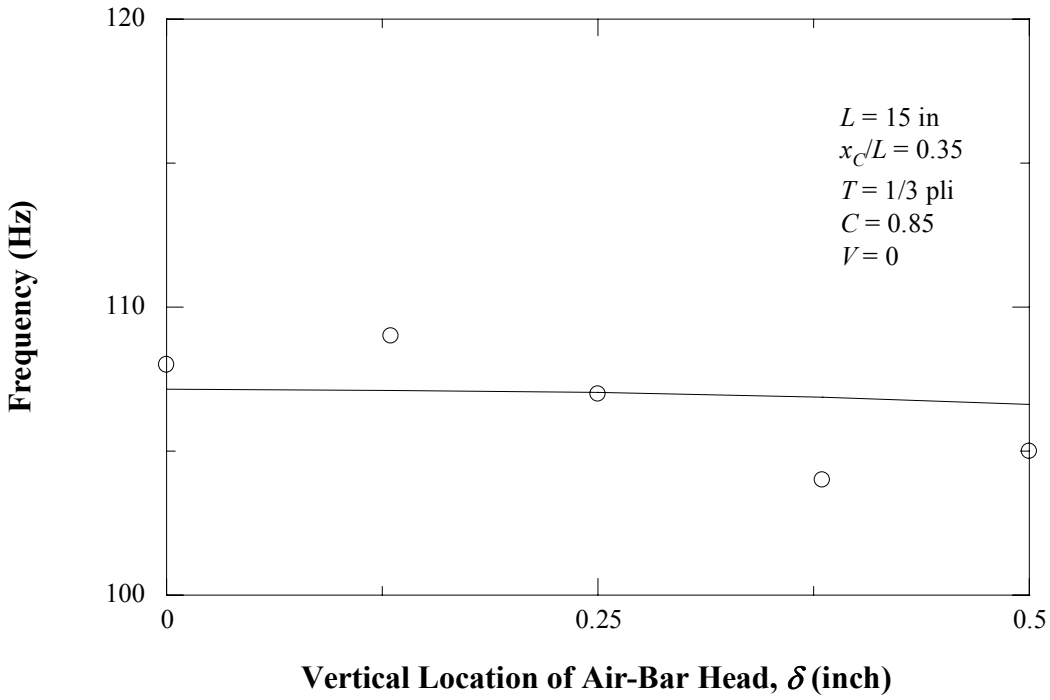

Figure 30 Effect of Vertical Location of Air-Bar Head on Flutter Frequency

CHAPTER V

CONCLUSIONS

The flow-induced vibration of a web floating over a pressure-pad air bar was studied analytically and experimentally. The equations of motion for the web and air flows were solved at equilibrium through the Green's function, and the linearized discrete model was obtained through the Galerkin's method. The equilibrium solutions of web deflection and air pressure provide good agreement with experimental results, and explain the relations between the deflection, cushion pressure, tension, and location of the air bar, which follows the results of ground-effect theories. The equilibrium solution is embedded into the discrete model for finding flutter criteria. The theoretical model was solved through numerical implementation for a number of cases.

Experiments were performed to verify the presented theory. It is found that divergence-type instability (unsymmetrical static deflection) and flutter-type instability (vibration) both occur in the web due to the air-jet flow. Computed stability criteria were compared with experiments. The experimental results for both static deflection and flutter have the same trends as the theory. Primary theoretical variables are supply pressure, tension, web span, and location of the pressure-pad-air bar. It is shown that the variables significantly affect the dynamic characteristics of the web, and flutter depends strongly on flow speed and web deflection. Flutter can be controlled by increasing tension, shortening the span, and (for a single span) centering the air-bar location. Except for

small discrepancies, it is shown that the developed theory is useful to predict equilibrium and dynamic solutions for a web floating over a pressure-pad air bar.

Both the computational and the experimental studies show a substantially lower flutter threshold for unsymmetrical web paths. Since asymmetry is empirically observed in air-flotation ovens, this has important application to drying, where flutter is detrimental to wet coatings or ink.

The theory used to develop the computations was well supported by the experimental results, and may be used to determine acceptable air pressure after the amount of asymmetry has been estimated. Furthermore, the same theoretical and computational approach could be used for multi-bar analysis.

REFERENCES

Bezella, G. L., 1976, "Application of Floater Dryers to the Paper Industry," *Tappi Journal*, Vol. 59, No. 4, pp. 92-96.

Blevins, R. D., 1990, *Flow-Induced Vibration*, Second ed., Van Nostrand Reinhold Co.

Blevins, R. D., 1992, *Applied Fluid Dynamics Handbook*, Reprint ed., Krieger Publishing Company.

Cancelli, C. and Pedley, T. J., 1985, "A Separated-Flow Model for Collapsible-Tube Oscillations," *Journal of Fluid Mechanics*, Vol. 157, pp. 375-404.

Chang, Y. B., 1990, "An Experimental and Analytical Study of Web Flutter," Ph.D. Dissertation, Oklahoma State University, Stillwater, OK.

Chang, Y. B., Swanson, R. P., and Moretti, P.M., 1999 "Resiliency of an Air-Floated Web," *Proceedings of the Fifth International Conference on Web Handling*, Stillwater, OK.

Chang, Y. B. and Moretti, P.M., 2000 "Aerodynamic Characteristics of Pressure-pad Air Bars," ASME *Journal of Applied Mechanics*, Vol. 67, No. 1, pp. 177-182.

Cho, H., 1999, "An Analytical and Computational Study of the Asymmetry of Webs Passing over Pressure-Pad Air Bars," M.S. Thesis, Oklahoma State University, Stillwater, OK.

Constantinescu, V. N., 1969, *Gas Lubrication* (English translation from Romanian), ASME Publications.

Constantinescu, V. N., 1970, "On the Influence of Inertia Forces in Turbulent and Laminar Self-Acting Films," ASME *Journal of Lubrication Technology*, Vol. 92, pp. 473-481.

Crewe, P. R. and Eggington, W. J., 1960, "The Hovercraft - A New Concept in Maritime Transport," *Transactions of the Royal Institution of Naval Architects*, Vol. 102, pp. 315-356.

Davies, M. J. and Wood, D. H., 1983, "The Basic Aerodynamics of Flotation," ASME *Journal of Fluids Engineering*, Vol. 105, No. 3, pp. 323-328.

Elsley, G. H. and Devereux, A. J., 1968, *Hovercraft Design and Construction*, Cornell Maritime Press.

Fujita, K., Shintani, A., and Yoshino, T., 2000, "Vibrational Behavior of a Rigid Body Supported by a Damper-Spring System in a Narrow Passage with Fluid," *Proceedings of the 7th International Conference on Flow-Induced Vibration*, pp. 829-836.

Gerhart, P. M. and Gross, R. J., 1985, *Fundamentals of Fluid Mechanics*, Reprint ed., Addison-Wesley Publishing Company.

Graff, K. F., 1975, *Wave Motion in Elastic Solids*, Ohio State University Press.

Hayashi, S., Hayase, T., Miura, Y., and Iimura, I., 1999, "Dynamic Characteristics of Collapsible Tube Flow," JSME *International Journal*, Series C, Vol. 42, No. 3, pp. 689-696.

Inada, F. and Hayama, S., 1990, "A Study on Leakage-Flow-Induced Vibrations. Part 1: Fluid-Dynamic Forces and Moments Acting on the Walls of a Narrow Tapered Passage," *Journal of Fluids and Structures*, Vol. 4, pp. 395-412.

Inada, F. and Hayama, S., 1990, "A Study on Leakage-Flow-Induced Vibrations. Part 2: Stability Analysis and Experiments for Two-Degree-of-Freedom Systems Combining Translational and Rotational Motions," *Journal of Fluids and Structures*, Vol. 4, pp. 413-428.

Jaumotte, A. and Kiedrzynski, A., 1965, "Theory and Experiments on Air Cushion Vehicles at Zero Speed," *Hovering Craft and Hydrofoils*, Vol. 4, pp. 4-25.

Jones, O. C., 1976, "An Improvement in the Calculation of Turbulent Friction in Rectangular Ducts," ASME *Journal of Fluids Engineering*, Vol. 98, pp. 173-181.

Krizek, F., 1986, "Impinging Jet Systems to Support and Dry Paper," *Drying Technology*, Vol. 4, No. 2, pp. 271-294

Mair, W. A., 1964, "The Physical Principles of Hovercraft," *Hovering Craft and Hydrofoil*, Vol. 4, No. 3, pp. 5-13.

Meirovitch, L., 1974, "A New Method of Solution of the Eigenvalue Problem for Gyroscopic Systems," *AIAA Journal*, Vol. 12, No. 10, pp. 1337-1342.

Meirovitch, L., 1975, "A Modal Analysis for the Response of Linear Gyroscopic Systems," ASME *Journal of Applied Mechanics*, Vol. 42, No. 2, pp. 446-450.

Moretti, P. M. and Chang, Y. B., 1998, "Lateral Deflection of Air-Supported Web Spans: Continuum PDE Approximation for an Air-flotation Oven", WHRC Project 9192-2, Tab 2.

Muftu, S., Lewis, T. S., Cole, K. A., and Benson, R. C., 1998, "A Two-Dimensional Model of the Fluid Dynamics of an Air Reverser," ASME *Journal of Applied Mechanics*, Vol. 65, No. 1, pp. 171-177.

Murdoch, D. C., 1970, *Linear Algebra*, John Wiley & Sons, Inc.

Nagakura, H. and Kaneko, S., 1991, "The Stability of a Cantilever Beam Subjected to One-Dimensional Leakage Flow," *Transactions of the 11th International Conference on Structural mechanics in Reactor Technology*, pp. 135-140.

Nisankararao, K., 1994, "An Experimental Study of Aerodynamic Forces of Air Bars," M.S. Thesis, Oklahoma State University, Stillwater, OK.

Obrzut, J. J., 1976, "Coil Coaters Float Strip through Ovens," *Iron Age*, Nov. 29, pp. 31-33.

Paidoussis, M. P., 1998, *Fluid-Structure Interactions*; *Slender Structures and Axial Flow*, Vol. 1, Academic Press.

Perdue, D. M., 1993, "Lateral Stability Investigation of Air Bar and Web Interaction for Use in Flotation Ovens," M.S. Thesis, Oklahoma State University, Stillwater, OK.

Pinnamaraju, R., 1992, "Measurements on Air Bar/Web Interaction for the Determination of Lateral Stability of a Web in Flotation Ovens," M.S. Report, Oklahoma State University, Stillwater, OK.

Pramila, A., 1986, "Sheet Flutter and the interaction between Sheet and Air," *Tappi Journal*, Vol. 69, No. 7, pp. 70-74.

Roach, G. F., 1970, *Green's Functions: Introductory Theory with Applications*, Van Nostrand Reinhold Company.

Samin, A., 1999, "Flutter of Flexible Tubes in Sub and Supercritical Flows," M.S. Thesis, University of Toronto, Toronto, Canada.

Stakgold, I., 1998, *Green's Functions and Boundary Value Problems*, 2nd ed., John Wiley & Sons.

Ulsoy, A. G., Mote, C. D., and Szymani, R., 1978, "Principal Developments in Band Saw Vibration and Stability Research," *Holz als Roh- und Werkstoff*, Vol. 36, pp. 273-280.

Watanabe, M. and Kobayashi, N, 2001, "Flow-Induced Vibrations of Axially Moving Web Subjected to Shear Fluid Flow," *Advances in Fluid Mechanics*, Vol. 30, pp. 109-118.

Wickert, J. A. and Mote, C. D., 1988, "Current Research on the Vibration and Stability of Axially Moving Materials," *Shock and Vibration Digest*, Vol. 20, No. 5, pp. 3-13.

Wickert, J. A. and Mote, C. D., 1990, "Classical Vibration Analysis of Axially Moving Continua," ASME *Journal of Applied Mechanics*, Vol. 57, pp. 738-744.

Wickert, J. A., 1993, "Free Linear Vibration of Self-Pressurized Foil Bearings," ASME *Journal of Vibration and Acoustics*, Vol. 115, pp. 145-151.

Wu, X. and Kaneko, S., 2003, "Nonlinear Analysis of Sheet Flutter Subjected to a Leakage Flow Based on Multibody Dynamics," JSME *International Journal*, Series C, Vol. 46, No. 2, pp. 500-507.

APPENDIX A

DERIVATION OF FRICTION FACTORS

Approximate methods to provide a better equivalent circular pipe dimension have been developed to evaluate friction factors for laminar and tubulent flows in noncircular ducts. The most general and simple methods are to compute equivalent diameters, i.e., hydraulic diameter (Gerhart and Gross, 1985; Blevins, 1992) and effective diameter (Jones, 1976; Gerhart and Gross, 1985; Blevins, 1992) for ducts to apply the friction factor f formula for circular pipes using equivalent diameters instead of the pipe diameters.

For laminar flow ($\mathrm{Re}_d < 2000$) in pipes where d is the pipe diameter, each definition for the friction factors of the hydraulic diameter D_h and the effective diameter D_e can be given by, respectively,

$$f = \frac{k}{\mathrm{Re}_h} \tag{A.1}$$

and

$$f = \frac{64}{\mathrm{Re}_e} \tag{A.2}$$

where k is the friction coefficient which can be found exactly by solving the Poisson (elliptic) equation over the cross section. The friction coefficient is dependent only on the shapes of the cross section. Re_h and Re_e are the Reynolds numbers for D_h and D_e, respectively, defined by

$$\mathrm{Re}_h = \frac{D_h u_{ave}}{\nu} \tag{A.3}$$

and

$$\mathrm{Re}_e = \frac{D_e u_{ave}}{\nu}. \tag{A.4}$$

The hydraulic diameter D_h and the effective diameter D_e are defined by, respectively,

$$D_h = \frac{4A}{P} \tag{A.5}$$

and

$$D_e = \frac{64}{k} D_h \tag{A.6}$$

where A is the flow area of cross section, and P is the wetted perimeter of cross section.

For a high aspect ratio rectangle (very wide channel), it is given that $k = 96$ and $D_h = 2h$ where *h* is the height of the channel. Both the hydraulic diameter method (using Eqs. (A.1), (A.3), and (A.5)) and the hydraulic diameter method (using Eqs. (A.2), (A.4), and (A.6)) give the same friction factor

$$f = \frac{48}{\mathrm{Re}} \tag{A.7}$$

where

$$\mathrm{Re} = \frac{h u_{ave}}{\nu} = \frac{Q}{\nu}. \tag{A.8}$$

For turbulent flow ($4000 < \mathrm{Re}_d < 10^5$), f in smooth pipes was approximated by H. Blasius

$$f \approx \frac{0.316}{\mathrm{Re}_h^{0.25}} \quad \text{or} \quad f \approx \frac{0.316}{\mathrm{Re}_e^{0.25}}. \tag{A.9}$$

Using the hydraulic diameter to evaluate the friction factor gives

$$f = \frac{0.266}{\mathrm{Re}^{0.25}}, \tag{A.10}$$

and, for the effective diameter, we have

$$f = \frac{0.294}{\mathrm{Re}^{0.25}} \tag{A.11}$$

where $k = 96$ and $D_h = 2h$ are used to evaluate f. As shown, each method leads to the different f but the discrepancy between them is relatively small. Taking an average of the two friction factors gives (Wu and Kaneko, 2003)

$$f = \frac{0.280}{\mathrm{Re}^{0.25}} \tag{A.12}$$

APPENDIX B

CONSTRUCTION OF THE GREEN'S FUNCTION

Green's function for the elastic equation (3.2.1) is constructed by solving the equation

$$\frac{\partial^4 G}{\partial \bar{x}^4} - \alpha^2 \frac{\partial^2 G}{\partial \bar{x}^2} = \frac{1}{D^2}\delta\left(\bar{x} - \xi\right), \tag{B.1}$$

which has the concentrated load at $\bar{x}_L \le \bar{x} = \xi \le \bar{x}_R$, where $\alpha = \sqrt{1 - V^2}\big/D$. Because of the Dirac delta function, we have two solutions to Eq. (B.1) as follows:

$$\begin{aligned} G_1\left(\bar{x}\right) &= A_1 + B_1\bar{x} + C_1 e^{\alpha\bar{x}} + D_1 e^{-\alpha\bar{x}}, \qquad \left(\bar{x} < \xi\right) \\ G_2\left(\bar{x}\right) &= A_2 + B_2\bar{x} + C_2 e^{\alpha\bar{x}} + D_2 e^{-\alpha\bar{x}}, \qquad \left(\bar{x} > \xi\right) \end{aligned} \tag{B.2}$$

which are subject to the conditions as discussed in Sec. 3.2

$$\begin{aligned} G_1\left(0\right) &= G_1''\left(0\right) = 0 \\ G_2\left(1\right) &= G_2''\left(1\right) = 0 \end{aligned} \tag{B.3}$$

$$\begin{aligned} G_1\left(\xi - \varepsilon\right) &= G_2\left(\xi + \varepsilon\right) \\ G_1'\left(\xi - \varepsilon\right) &= G_2'\left(\xi + \varepsilon\right) \\ G_1''\left(\xi - \varepsilon\right) &= G_2''\left(\xi + \varepsilon\right) \end{aligned} \tag{B.4}$$

$$G_2'''\left(\xi\right) - G_1'''\left(\xi\right) = \frac{1}{D^2}\,. \tag{B.5}$$

For convenience, derivatives with respect to x of Eq. (B.2) are presented as follows:

$$\begin{aligned} G_1'\left(\bar{x}\right) &= B_1 + \alpha C_1 e^{\alpha\bar{x}} - \alpha D_1 e^{-\alpha\bar{x}} \\ G_2'\left(\bar{x}\right) &= B_2 + \alpha C_2 e^{\alpha\bar{x}} - \alpha D_2 e^{-\alpha\bar{x}} \end{aligned} \tag{B.6}$$

$$G_1''(\bar{x}) = \alpha^2 C_1 e^{\alpha\bar{x}} + \alpha^2 D_1 e^{-\alpha\bar{x}}$$
$$G_2''(\bar{x}) = \alpha^2 C_2 e^{\alpha\bar{x}} + \alpha^2 D_2 e^{-\alpha\bar{x}} \tag{B.7}$$

$$G_1'''(\bar{x}) = \alpha^3 C_1 e^{\alpha\bar{x}} - \alpha^3 D_1 e^{-\alpha\bar{x}}$$
$$G_2'''(\bar{x}) = \alpha^3 C_2 e^{\alpha\bar{x}} - \alpha^3 D_2 e^{-\alpha\bar{x}} . \tag{B.8}$$

Applying the conditions (B.3) into Eqs. (B.2) and (B.7) yields

$$G_1(0) = A_1 + C_1 + D_1 = 0$$
$$G_1''(0) = \alpha^2 C_1 + \alpha^2 D_1 = 0 \tag{B.9}$$

$$G_2(1) = A_2 + B_2 + e^{\alpha} C_2 + e^{-\alpha} D_2 = 0$$
$$G_2''(1) = \alpha^2 e^{\alpha} C_2 + \alpha^2 e^{-\alpha} D_2 = 0 \tag{B.10}$$

so that, from Eqs. (B.9) and (B.10), we have, respectively,

$$A_1 = 0$$
$$D_1 = -C_1 \tag{B.11}$$

and

$$B_2 = -A_2$$
$$D_2 = -e^{2\alpha} C_2 . \tag{B.12}$$

By virtue of Eqs. (B.11) and (B.12), applying the conditions (B.4) into Eqs. (B.2), (B.6), and (B.7) gives

$$G_1(\xi) = \xi B_1 + \left(e^{\alpha\xi} - e^{-\alpha\xi}\right) C_1 = (1-\xi) A_2 + \left(e^{\alpha\xi} - e^{2\alpha} e^{-\alpha\xi}\right) C_2 = G_2(\xi) \tag{B.13}$$

$$G_1'(\xi) = B_1 + \alpha\left(e^{\alpha\xi} + e^{-\alpha\xi}\right) C_1 = -A_2 + \alpha\left(e^{\alpha\xi} + e^{2\alpha} e^{-\alpha\xi}\right) C_2 = G_2'(\xi) \tag{B.14}$$

$$G_1''(\xi) = \alpha^2\left(e^{\alpha\xi} - e^{-\alpha\xi}\right) C_1 = \alpha^2\left(e^{\alpha\xi} - e^{2\alpha} e^{-\alpha\xi}\right) C_2 = G_2''(\xi) \tag{B.15}$$

so that, from Eq. (B.15), we have

$$C_2 = -\frac{e^{-\alpha}\sinh\alpha\xi}{\sinh\alpha(1-\xi)} C_1 . \tag{B.16}$$

In order to eliminate A_2, mutiplying Eq. (B.14) by $1-\xi$, adding the resultant equation and Eq. (B.13), and substitutng Eq. (B.16) yield B_1 in terms of C_1

$$B_1 = -2\alpha(1-\xi)\frac{\sinh\alpha}{\sinh\alpha(1-\xi)}C_1 \tag{B.17}$$

so that A_2 is expressed also in terms of C_1 by substituting Eqs. (B.16) and (B.17) into Eq. (B.14)

$$A_2 = -2\alpha\xi\frac{\sinh\alpha}{\sinh\alpha(1-\xi)}C_1. \tag{B.18}$$

Now all coefficients are expressed in terms of C_1 so that C_1 needs to be evaluated. Applying the condition (B.5) into Eq. (B.8) gives

$$\alpha^3 e^{\alpha\xi}C_2 - \alpha^3 e^{-\alpha\xi}D_2 - \alpha^3 e^{\alpha\xi}C_1 + \alpha^3 e^{-\alpha\xi}D_1 = \frac{1}{D^2} \tag{B.19}$$

so that, using Eqs. (B.11), (B.12), and (B.16), Eq. (B.19) is solved

$$C_1 = -\frac{1}{2\alpha^3 D^2}\frac{\sinh\alpha(1-\xi)}{\sinh\alpha}. \tag{B.20}$$

For convenience, all evaluated coefficients are presented as follows:

$$\begin{aligned} A_1 &= 0 & A_2 &= \frac{\xi}{\alpha^2 D^2} \\ B_1 &= \frac{1-\xi}{\alpha^2 D^2} & B_2 &= -\frac{\xi}{\alpha^2 D^2} \\ C_1 &= -\frac{1}{2\alpha^3 D^2}\frac{\sinh\alpha(1-\xi)}{\sinh\alpha} \quad \text{and} & C_2 &= \frac{e^{-\alpha}}{2\alpha^3 D^2}\frac{\sinh\alpha\xi}{\sinh\alpha} \\ D_1 &= \frac{1}{2\alpha^3 D^2}\frac{\sinh\alpha(1-\xi)}{\sinh\alpha} & D_2 &= -\frac{e^{\alpha}}{2\alpha^3 D^2}\frac{\sinh\alpha\xi}{\sinh\alpha} \end{aligned} \tag{B.21}$$

Substitution of all coefficients (B.21) into Eq. (B.2) provides the Green's function

$$G_1(\bar{x}) = \frac{1}{1-V^2}\left((1-\xi)\bar{x} - \frac{\sinh\alpha(1-\xi)}{\alpha\sinh\alpha}\sinh\alpha\bar{x}\right)$$
$$= \frac{1}{1-V^2}\left((1-\xi)\bar{x} - \frac{1}{2\alpha}\frac{e^{\alpha(1-\xi)} - e^{-\alpha(1-\xi)}}{e^{\alpha} - e^{-\alpha}}\left(e^{\alpha\bar{x}} - e^{-\alpha\bar{x}}\right)\right), \quad (\bar{x} < \xi) \tag{B.22}$$

and

$$G_2(\bar{x}) = \frac{1}{1-V^2}\left((1-\bar{x})\xi - \frac{\sinh\alpha\xi}{\alpha\sinh\alpha}\sinh\alpha(1-\bar{x})\right)$$
$$= \frac{1}{1-V^2}\left((1-\bar{x})\xi - \frac{1}{2\alpha}\frac{e^{\alpha\xi} - e^{-\alpha\xi}}{e^{\alpha} - e^{-\alpha}}\left(e^{\alpha(1-\bar{x})} - e^{-\alpha(1-\bar{x})}\right)\right), \quad (\bar{x} > \xi) \tag{B.23}$$

or, using the Heaviside function,

$$G(\bar{x},\xi) = \frac{1}{1-V^2}\left((1-\xi)\bar{x} - \frac{\sinh\alpha(1-\xi)\sinh\alpha\bar{x}}{\alpha\sinh\alpha}\right)\mathrm{H}(\xi-\bar{x})$$
$$+ \frac{1}{1-V^2}\left((1-\bar{x})\xi - \frac{\sinh\alpha\xi\sinh\alpha(1-\bar{x})}{\alpha\sinh\alpha}\right)\mathrm{H}(\bar{x}-\xi). \tag{B.24}$$

For a certain large value of α, computers cannot manage to evaluate hyperbolic functions because they have exponential functions. To avoid this difficulty, it is necessary for Eq. (B.24) to be modified to make exponential terms' exponents be negative

$$G(\bar{x}) = \frac{1}{1-V^2}\left((1-\xi)\bar{x} - \frac{\sinh\left(\alpha(1-\xi)\right)}{\alpha\left(1-e^{-2\alpha}\right)}\left(e^{-\alpha(1-\bar{x})} - e^{-\alpha(1+\bar{x})}\right)\right)\mathrm{H}(\xi-\bar{x})$$
$$+ \frac{1}{1-V^2}\left((1-\bar{x})\xi - \frac{e^{-\alpha(1-\xi)} - e^{-\alpha(1+\xi)}}{\alpha\left(1-e^{-2\alpha}\right)}\sinh\left(\alpha(1-\bar{x})\right)\right)\mathrm{H}(\bar{x}-\xi). \tag{B.25}$$

Also, its derivative with respect to $\bar{x}$ is given by

$$\frac{\partial G(\bar{x},\xi)}{\partial\bar{x}} = \frac{1}{1-V^2}\left(1-\xi - \frac{\sinh\left(\alpha(1-\xi)\right)}{1-e^{-2\alpha}}\left(e^{-\alpha(1-\bar{x})} + e^{-\alpha(1+\bar{x})}\right)\right)\mathrm{H}(\xi-\bar{x})$$
$$+ \frac{1}{1-V^2}\left(-\xi + \frac{e^{-\alpha(1-\xi)} - e^{-\alpha(1+\xi)}}{1-e^{-2\alpha}}\cosh\left(\alpha(1-\bar{x})\right)\right)\mathrm{H}(\bar{x}-\xi). \tag{B.26}$$

APPENDIX C

NUMERICAL ANALYSIS FOR EQUILIBRIUM SOLUTIONS

At the spatial nodes $n = 1, 2, \ldots, N$,

$$\overline{x}_n = \overline{x}_L + \frac{\overline{x}_R - \overline{x}_L}{N-1}(n-1) = \overline{x}_L + \Delta\overline{x}(n-1), \tag{C.1}$$

Eqs. (3.2.22) and (3.2.24) can be discretized with the forward-difference method and trapezoidal rule as follows:

for $n = 1, 2, \ldots, N\text{-}1$,

$$\frac{\overline{p}^*_{n+1} - \overline{p}^*_n}{\overline{x}_{n+1} - \overline{x}_n} = \frac{2\overline{b}^2 C_d^2 \left(\overline{p}_0 - 0.5\overline{p}^*_1\right)}{\overline{h}^{*3}_n}\left(\overline{h}^{*\prime}_n - \frac{f^*}{4}\right), \tag{C.2}$$

and for $n = N$,

$$\frac{\overline{p}^*_n}{\overline{p}_0} = 1 - e^{-\frac{2\overline{b}C_d^2}{\overline{h}^*_n}} \tag{C.3}$$

where

$$\overline{h}^*_n = \sum_{m=1}^{N-1} \frac{\overline{x}_{m+1} - \overline{x}_m}{2}\left(G\left(\overline{x}_n, \overline{x}_{m+1}\right)\overline{p}^*_{m+1} + G\left(\overline{x}_n, \overline{x}_m\right)\overline{p}^*_m\right) - \overline{\delta} \tag{C.4}$$

$$\overline{h}^{*\prime}_n = \sum_{m=1}^{N-1} \frac{\overline{x}_{m+1} - \overline{x}_m}{2}\left(G'\left(\overline{x}_n, \overline{x}_{m+1}\right)\overline{p}^*_{m+1} + G'\left(\overline{x}_n, \overline{x}_m\right)\overline{p}^*_m\right) \tag{C.5}$$

$$f^* = \begin{cases} 48\left(\dfrac{\bar{b}C_d}{\bar{\nu}}\sqrt{\dfrac{2\left(\bar{p}_0 - 0.5\bar{p}_1^*\right)}{\bar{\rho}}}\right)^{-1}, & \text{for laminar flow} \\ 0.28\left(\dfrac{\bar{b}C_d}{\bar{\nu}}\sqrt{\dfrac{2\left(\bar{p}_0 - 0.5\bar{p}_1^*\right)}{\bar{\rho}}}\right)^{-0.25}, & \text{for turbulent flow} \end{cases} . \tag{C.6}$$

Therefore, $N-1$ nonlinear algebraic equations in $\bar{p}_n^*$ are provided for the points $n = 1, 2, \ldots, N\text{-}1$, and one boundary condition for $n = N$.

The equilibrium solution can be found numerically by the Newton-Raphson method whose calculation scheme is given by

$$\bar{\mathbf{p}}_{\text{new}}^* = \bar{\mathbf{p}}_{\text{old}}^* - \left(\nabla\mathbf{f}\left(\bar{\mathbf{p}}_{\text{old}}^*\right)\right)^{-1}\mathbf{f}\left(\bar{\mathbf{p}}_{\text{old}}^*\right) \tag{C.7}$$

where $\mathbf{f}\left(\bar{p}_1^*, \bar{p}_2^*, ..., \bar{p}_N^*\right)$ is the set of nonlinear equations such that

$$\mathbf{f}_n = \begin{cases} \bar{p}_{n+1}^* - \bar{p}_n^* - 2\bar{b}^2 C_d^2\left(\bar{x}_{n+1} - \bar{x}_n\right)\left(\bar{p}_0 - 0.5\bar{p}_1^*\right)\bar{h}_n^{*-3}\left(\bar{h}_n^{*\prime} - 0.25f^*\right), & \text{for } n = 1, 2, \ldots, N\text{-}1 \\ \bar{p}_n^* - \bar{p}_0\left(1 - e^{-2\bar{b}C_d^2\bar{h}_n^{*-1}}\right), & \text{for } n = N \end{cases}, \tag{C.8}$$

and ∇ is the Jacobian operator so that

$$\nabla\mathbf{f} = \begin{bmatrix} -1 + A_1^1 + B_1 & 1 + 2A_1^2 & 2A_1^3 & \cdot & \cdot & \cdot & \cdot & 2A_1^{N-1} & A_1^N \\ A_2^1 + B_2 & -1 + 2A_2^2 & 1 + 2A_2^3 & 2A_2^4 & \cdot & \cdot & \cdot & 2A_2^{N-1} & A_2^N \\ \cdot & \cdot & \cdot & \cdot & \cdot & \cdot & \cdot & \cdot & \cdot \\ \cdot & \cdot & \cdot & \cdot & \cdot & \cdot & \cdot & \cdot & \cdot \\ \cdot & \cdot & \cdot & \cdot & \cdot & \cdot & \cdot & \cdot & \cdot \\ \cdot & \cdot & \cdot & \cdot & \cdot & \cdot & \cdot & \cdot & \cdot \\ A_{N-2}^1 + B_{N-2} & 2A_{N-2}^2 & \cdot & \cdot & \cdot & 2A_{N-2}^{N-3} & -1 + 2A_{N-2}^{N-2} & 1 + 2A_{N-2}^{N-1} & A_{N-2}^N \\ A_{N-1}^1 + B_{N-1} & 2A_{N-1}^2 & \cdot & \cdot & \cdot & \cdot & 2A_{N-1}^{N-2} & -1 + 2A_{N-1}^{N-1} & 1 + A_{N-1}^N \\ C_N^1 & 2C_N^2 & \cdot & \cdot & \cdot & \cdot & \cdot & 2C_N^{N-1} & 1 + C_N^N \end{bmatrix} \tag{C.9}$$

where

$$A_n^m = \bar{b}^2 C_d^2 \Delta\bar{x}^2 \left(\bar{p}_0 - 0.5\bar{p}_1^*\right) \bar{h}_n^{*-4} \left(\left(3\bar{h}_n^{*\prime} - 0.75 f^*\right) G\left(\bar{x}_n, \bar{x}_m\right) - \bar{h}_n^* G'\left(\bar{x}_n, \bar{x}_m\right)\right) \quad \text{(C.10)}$$

$$B_n = \begin{cases} \bar{b}^2 C_d^2 \Delta\bar{x} \bar{h}_n^{*-3} \left(\bar{h}_n^{*\prime} - 0.125 f^*\right), & \text{for laminar flow} \\ \bar{b}^2 C_d^2 \Delta\bar{x} \bar{h}_n^{*-3} \left(\bar{h}_n^{*\prime} - 0.21875 f^*\right), & \text{for turbulent flow} \end{cases} \quad \text{(C.11)}$$

$$C_N^m = \bar{b} C_d^2 \bar{p}_0 \Delta\bar{x} \bar{h}_N^{*-2} e^{-2\bar{b}C_d^2 \bar{h}_N^{*-1}} G\left(\bar{x}_N, \bar{x}_m\right). \quad \text{(C.12)}$$

The calculation starts with initial guess values of pressure, and then it continues iterating until the error $\sqrt{\sum \left|\bar{\mathbf{p}}_{\text{new}}^* - \bar{\mathbf{p}}_{\text{old}}^*\right|^2}$ approaches within the tolerance 10^{-15}.

APPENDIX D

COMPUTER CODE

The code is written in MATLAB. This provides equilibrium solutions (web deflection and air pressure), and solves the eigenvalue problem for the air-web system.

```
clear all;
format compact;
format short;

% Number of node and mode

n = 101;                        % node points
N = 4;                          % mode number

% Web properties

L = 15*0.0254;                  % variable length [m]
t = 0.002*0.0254;               % thickness [m]
w = 12*0.0254;                  % width [m]
M = 0.0689;                     % web mass-per-unit-area [Kg/m^2]
v = 0;                          % velocity [m/s]
W = 2;                          % variable weight [lb]
T = 4.448222*W/w;               % tension-per-unit-width [N/m]
E = 6*10^9;                     % Young's modulus [Pa]
EI = E*t^3/(12*(1-0.4^2));      % flexural rigidity-per-unit-width [N*m]

% Air-bar properties

b = 0.13*0.0254;                % nozzle thickness [m]
aw = 4.5*0.0254;                % air-bar width [m]
p0 = 6894.757*0.1;              % variable supply pressure [Pa]
rho = 1.21;                     % air density [kg/m^3]
nu = 1.514*10^(-5);             % kinematic viscosity [m^2/s]

% Dimensionless parameters


B = b/L;                        % nondimensional nozzle thickness
delta = 0/l;                    % nondimensional delta
D = sqrt(EI/(T*L^2));           % nondimensional flexural rigidity
V = v*sqrt(M/T);                % nondimensional web velocity
```

```
P0 = p0*L/T;                    % nondimensional supply pressure
a = sqrt(1-V^2)/D;              % nondimensional parameter
Rho = rho*L/M;                  % nondimensional air density
Nu = nu*sqrt(M/(T*L^2));        % nondimensional kinematic viscosity
C = 0.85;                       % nozzle discharge coefficient
etaL = 0.96;                    % pressure loss coefficient at the inlet
etaR = 0.96;                    % pressure loss coefficient at the outlet
mu = 1.0;                       % acceleration factor for convergence

% Air-bar location

xc = 0.35;
xs = (L*xc-aw/2)/L;
xe = (L*xc+aw/2)/L;

% Building nodes

pt = 1:n;
x = xs+(xe-xs)*(pt-1)./(n-1);
dx = (xe-xs)/(n-1);

% Building the Green's function

G = zeros(n,n);
Gx = zeros(n,n);

for i = 1:n
  for j = 1:n
    if i <= j
      G(i,j) = 1/(1-V^2)*((1-x(j))*x(i)-sinh(a*(1-x(j)))*(exp(-a*(1-x(i)))-exp(-a*(1+x(i))))
               /(a*(1-exp(-2*a))));
      Gx(i,j) = 1/(1-V^2)*(1-x(j)-sinh(a*(1-x(j)))*(exp(-a*(1-x(i)))+exp(-a*(1+x(i))))/(1-exp(-2*a)));
    else
      G(i,j) = 1/(1-V^2)*(x(j)*(1-x(i))-(exp(-a*(1-x(j)))-exp(-a*(1+x(j))))
               *sinh(a*(1-x(i)))/(a*(1-exp(-2*a))));
      Gx(i,j) = 1/(1-V^2)*(-x(j)+(exp(-a*(1-x(j)))-exp(-a*(1+x(j))))*cosh(a*(1-x(i)))/(1-exp(-2*a)));
    end
  end
end

% Calculating equilibrium solutions (web displacement and air pressure)

F = zeros(n,1);
P = ones(n,1);

error = 1;
it = 0;
while ((10e-15<error) & (it < 10))
   it = it + 1

   Y = zeros(n,1);
   Yx = zeros(n,1);

   for i = 1:n
     for j = 1:n-1
       temp1 = (x(j+1)-x(j))/2*(G(i,j+1)*P(j+1)+G(i,j)*P(j));
```

```
        Y(i) = Y(i)+temp1;

        temp2 = (x(j+1)-x(j))/2*(Gx(i,j+1)*P(j+1)+Gx(i,j)*P(j));
        Yx(i) = Yx(i)+temp2;
      end
    end

    H(1:n) = Y(1:n) - delta;
    U = C^2*sqrt(2*(P0-0.5*P(1))/Rho);
    Q = B*U;
    f = 0.28./(Q/Nu).^0.25;

    C1(1:n-1) = B^2*C^2*dx*(Y(1:n-1)-delta).^(-3).*(P0-0.5*P(1)).*(Yx(1:n-1)-0.25*f);
    C2(1:n-1) = B^2*C^2*dx^2*(Y(1:n-1)-delta).^(-4).*(P0-0.5*P(1));
    C3(1:n-1) = 3*Yx(1:n-1)-0.75*f;
    C4(1:n-1) = B^2*C^2*dx*(Y(1:n-1)-delta).^(-3).*(Yx(1:n-1)-0.21875*f);
    C5(n) = B*C^2*P0*dx*(Y(n)-delta).^(-2)*exp(-2*B*C^2*(Y(n)-delta).^(-1));

    F(1:n-1) = P(2:n)-P(1:n-1)-2*C1(1:n-1)';
    F(n) = P(n)-P0*(1-exp(-2*B*C^2*(Y(n)-delta).^(-1)));

    dF = zeros(n,n);
    for i = 1:n-1
      dF(i,1) = C2(i)*(C3(i)*G(i,1)-Y(i)*Gx(i,1))+C4(i);
      dF(i,2:n-1) = 2*C2(i)*(C3(i)*G(i,2:n-1)-Y(i)*Gx(i,2:n-1));
      dF(i,n) = C2(i)*(C3(i)*G(i,n)-Y(i)*Gx(i,n));
    end

      dF(n,1) = C5(n)*G(n,1);
      dF(n,2:n-1) = 2*C5(n)*G(n,2:n-1);
      dF(n,n) = 1+C5(n)*G(n,n);

    dF = dF+sparse(1:n-1,1:n-1,-1,n,n)+sparse(1:n-1,2:n,1,n,n);
    dP = inv(dF)*(0-F);
    P = P + mu*dP;
    error = norm(dP)
end

% Building eigenfunctions

psir = zeros(n,N);
psirx = zeros(n,N);
psii = zeros(n,N);
psiix = zeros(n,N);

for i = 1:n
    for j = 1:N
        psir(i,j) = 1/(j*pi)*sqrt(2/(1-V^2))*sin(j*pi*x(i))*cos(j*pi*V*x(i));
        psirx(i,j) = sqrt(2/(1-V^2))*(cos(j*pi*x(i))*cos(j*pi*V*x(i))-V*sin(j*pi*x(i))*sin(j*pi*V*x(i)));
        psirI(i,j) = -1/(j*pi)^2*sqrt(2/(1- V^2)^3)*(cos(j*pi*x(i))*cos(j*pi*V*x(i))
                    +V*sin(j*pi*x(i))*sin(j*pi*V*x(i)));

        psii(i,j) = 1/(j*pi)*sqrt(2/(1-V^2))*sin(j*pi*x(i))*sin(j*pi*V*x(i));
        psiix(i,j) = sqrt(2/(1-V^2))*(cos(j*pi*x(i))*sin(j*pi*V*x(i))+V*sin(j*pi*x(i))*cos(j*pi*V*x(i)));
        psiiI(i,j) = -1/(j*pi)^2*sqrt(2/(1-V^2)^3)*(cos(j*pi*x(i))*sin(j*pi*V*x(i))
                    -V*sin(j*pi*x(i))*cos(j*pi*V*x(i)));
```

```
   end
end

% Building the eigenvalue problem

Crr = zeros(N,N);
Cri = zeros(N,N);
Cir = zeros(N,N);
Cii = zeros(N,N);
Drr = zeros(N,N);
Dri = zeros(N,N);
Dir = zeros(N,N);
Dii = zeros(N,N);

for i = 1:N
   for j = 1:N
      for k = 1:n-1
         temp3 = (x(k+1)-x(k))/2*i*pi*(1-V^2)*j*pi*(1-V^2)*(psiiI(k+1,i)*Rho/H(k+1) *psiiI(k+1,j)
                  +psiiI(k,i)*Rho/H(k)*psiiI(k,j));
         Crr(i,j) = Crr(i,j)+temp3;

         temp4 = -(x(k+1)-x(k))/2*i*pi*(1-V^2)*j*pi*(1-V^2)*(psiiI(k+1,i)*Rho/H(k+1)*psirI(k+1,j)
                  +psiiI(k,i)*Rho/H(k)*psirI(k,j));
         Cri(i,j) = Cri(i,j)+temp4;

          temp5 = -(x(k+1)-x(k))/2*i*pi*(1-V^2)*j*pi*(1-V^2)*(psirI(k+1,i)*Rho/H(k+1)*psiiI(k+1,j)
                  +psirI(k,i)*Rho/H(k)*psiiI(k,j));
         Cir(i,j) = Cir(i,j)+temp5;

         temp6 = (x(k+1)-x(k))/2*i*pi*(1-V^2)*j*pi*(1-V^2)*(psirI(k+1,i)*Rho/H(k+1)*psirI(k+1,j)
                  +psirI(k,i)*Rho/H(k)*psirI(k,j));
         Cii(i,j) = Cii(i,j)+temp6;

         temp7 = (x(k+1)-x(k))/2*i*pi*(1-V^2)*(psiiI(k+1,i)*(-j*pi*(1-V^2) *etaL*Rho*(B*C)^2*Q
                  *psii(1,j)/(2*H(k+1)*H(1)^3) -2*Rho*Q/H(k+1)^3*(Yx(k+1)-f/8*1.75) *(-j*pi*(1-V^2)
                  *psiiI(k+1,j)+etaL*(B*C)^2*Q*psir(1,j)/(2*H(1)^3))-2*Rho*Q/H(k+1)^2*j*pi*(1-V^2)
                  *psii(k+1,j)-3*Rho*Q^2/H(k+1)^4*(Yx(k+1)- f/4)*psir(k+1,j)+Rho*Q^2/H(k+1)^3
                  *psirx(k+1,j))+psiiI(k,i)*(-j*pi*(1-V^2)*etaL*Rho*(B*C)^2*Q*psii(1,j)/(2*H(k)*H(1)^3)
                   -2*Rho*Q/H(k)^3*(Yx(k)-f/8*1.75)*(-j*pi*(1- V^2)*psiiI(k,j) +etaL*(B*C)^2*Q*psir(1,j)
                  /(2*H(1)^3))- 2*Rho*Q/H(k)^2*j*pi*(1-V^2)*psii(k,j)-3*Rho*Q^2/H(k)^4*(Yx(k)-f/4)
                  *psir(k,j)+Rho*Q^2/H(k)^3*psirx(k,j)));
         Drr(i,j) = Drr(i,j)+temp7;

         temp8 = (x(k+1)-x(k))/2*i*pi*(1-V^2)*(psiiI(k+1,i)*(j*pi*(1-V^2)*etaL*Rho*(B*C)^2*Q
                  *psir(1,j)/(2*H(k+1)*H(1)^3)-2*Rho*Q/H(k+1)^3*(Yx(k+1)-f/8*1.75)*(j*pi*(1-V^2)
                  *psirI(k+1,j)+etaL*(B*C)^2*Q*psii(1,j)/(2*H(1)^3))+2*Rho*Q/H(k+1)^2*j*pi*(1-V^2)
                  *psir(k+1,j)-3*Rho*Q^2/H(k+1)^4*(Yx(k+1)-f/4)*psii(k+1,j)+Rho*Q^2/H(k+1)^3
                  *psiix(k+1,j))+psiiI(k,i)*(j*pi*(1-V^2)*etaL*Rho*(B*C)^2*Q*psir(1,j)/(2*H(k)*H(1)^3)
                   -2*Rho*Q/H(k)^3*(Yx(k)-f/8*1.75)*(j*pi*(1-V^2)*psirI(k,j)+etaL*(B*C)^2*Q*psii(1,j)
                  /(2*H(1)^3))+2*Rho*Q/H(k)^2*j*pi*(1-V^2)*psir(k,j)-3*Rho*Q^2/H(k)^4*(Yx(k)-f/4)
                  *psii(k,j)+Rho*Q^2/H(k)^3*psiix(k,j)));
         Dri(i,j) = Dri(i,j)+temp8;

         temp9 = -(x(k+1)-x(k))/2*i*pi*(1-V^2)*(psirI(k+1,i)*(-j*pi*(1-V^2)*etaL*Rho*(B*C)^2*Q
                  *psii(1,j)/(2*H(k+1)*H(1)^3)-2*Rho*Q/H(k+1)^3*(Yx(k+1)-f/8*1.75)*(-j*pi*(1-V^2)
                  *psiiI(k+1,j)+etaL*(B*C)^2*Q*psir(1,j)/(2*H(1)^3))-2*Rho*Q/H(k+1)^2*j*pi*(1-V^2)
```

```
                *psii(k+1,j)-3*Rho*Q^2/H(k+1)^4*(Yx(k+1)-f/4)*psir(k+1,j)+Rho*Q^2/H(k+1)^3
                *psirx(k+1,j))+psirI(k,i)*(-j*pi*(1-V^2)*etaL*Rho*(B*C)^2*Q*psii(1,j)/(2*H(k)*H(1)^3)
                 -2*Rho*Q/H(k)^3*(Yx(k)-f/8*1.75)*(-j*pi*(1-V^2)*psiiI(k,j)+etaL*(B*C)^2*Q*psir(1,j)
                 /(2*H(1)^3))-2*Rho*Q/H(k)^2*j*pi*(1-V^2)*psii(k,j)-3*Rho*Q^2/H(k)^4*(Yx(k)-f/4)
                *psir(k,j)+Rho*Q^2/H(k)^3*psirx(k,j)));
        Dir(i,j) = Dir(i,j)+temp9;

        temp10 = -(x(k+1)-x(k))/2*i*pi*(1-V^2)*(psirI(k+1,i)*(j*pi*(1-V^2)*etaL*Rho*(B*C)^2*Q
                  *psir(1,j)/(2*H(k+1)*H(1)^3)-2*Rho*Q/H(k+1)^3*(Yx(k+1)-f/8*1.75)*(j*pi*(1-V^2)
                  *psirI(k+1,j)+etaL*(B*C)^2*Q*psii(1,j)/(2*H(1)^3))+2*Rho*Q/H(k+1)^2*j*pi*(1-V^2)
                  *psir(k+1,j)-3*Rho*Q^2/H(k+1)^4*(Yx(k+1)-f/4)*psii(k+1,j)+Rho*Q^2/H(k+1)^3
                  *psiix(k+1,j))+psirI(k,i)*(j*pi*(1-V^2)*etaL*Rho*(B*C)^2*Q*psir(1,j)/(2*H(k)* H(1)^3)
                  -2*Rho*Q/H(k)^3*(Yx(k)-f/8*1.75)*(j*pi*(1-V^2)*psirI(k,j)+etaL*(B*C)^2*Q*psii(1,j)
                  /(2*H(1)^3))+2*Rho*Q/H(k)^2*j*pi*(1-V^2)*psir(k,j)-3*Rho*Q^2/H(k)^4*(Yx(k)-f/4)
                  *psii(k,j)+Rho*Q^2/H(k)^3*psiix(k,j)));
        Dii(i,j) = Dii(i,j)+temp10;
      end
   end
end

for i = 1:N
   for j = 1:N
      Drr1(i,j) = i*pi*(1-V^2)*Rho*Q*(psiiI(1,i)*etaL*(Q*psir(1,j)/H(1)^3-j*pi*(1-V^2)*psiiI(1,j)/H(1)^2
                  +etaL*(B*C)^2*Q*psir(1,j)/(2*H(1)^5))+psiiI(n,i)*etaR*(Q*psir(n,j)/H(n)^3-j*pi*(1-V^2)
                  *psiiI(n,j)/H(n)^2+etaL*(B*C)^2*Q*psir(1,j)/(2*H(n)^2*H(1)^3)));
      Dri1(i,j) = i*pi*(1-V^2)*Rho*Q*(psiiI(1,i)*etaL*(Q*psii(1,j)/H(1)^3+j*pi*(1-V^2)*psirI(1,j)/H(1)^2
                  +etaL*(B*C)^2*Q*psii(1,j)/(2*H(1)^5))+psiiI(n,i)*etaR*(Q*psii(n,j)/H(n)^3+j*pi*(1-V^2)
                  *psirI(n,j)/H(n)^2+etaL*(B*C)^2*Q*psii(1,j)/(2*H(n)^2*H(1)^3)));
      Dir1(i,j) = -i*pi*(1-V^2)*Rho*Q*(psirI(1,i)*etaL*(Q*psir(1,j)/H(1)^3-j*pi*(1-V^2)*psiiI(1,j)/H(1)^2
                  +etaL*(B*C)^2*Q*psir(1,j)/(2*H(1)^5))+psirI(n,i)*etaR*(Q*psir(n,j)/H(n)^3-j*pi*(1-V^2)
                  *psiiI(n,j)/H(n)^2+etaL*(B*C)^2*Q*psir(1,j)/(2*H(n)^2*H(1)^3)));
      Dii1(i,j) = -i*pi*(1-V^2)*Rho*Q*(psirI(1,i)*etaL*(Q*psii(1,j)/H(1)^3+j*pi*(1-V^2)*psirI(1,j)/H(1)^2
                 +etaL*(B*C)^2*Q*psii(1,j)/(2*H(1)^5))+psirI(n,i)*etaR*(Q*psii(n,j)/H(n)^3+j*pi*(1-V^2)
                 *psirI(n,j)/H(n)^2+etaL*(B*C)^2*Q*psii(1,j)/(2*H(n)^2*H(1)^3)));
   end
end

Drr2 = Drr + Drr1;
Dri2 = Dri + Dri1;
Dir2 = Dir + Dir1;
Dii2 = Dii + Dii1;

MC = zeros(2*N,2*N);
MD = zeros(2*N,2*N);

for i = 1:N
   MC(i,1:N) = Crr(i,1:N);
   MC(i,N+1:2*N) = Cri(i,1:N);
   MC(N+i,1:N) = Cir(i,1:N);
   MC(N+i,N+1:2*N) = Cii(i,1:N);
   MD(i,1:N) = Drr2(i,1:N);
   MD(i,N+1:2*N) = Dri2(i,1:N);
   MD(N+i,1:N) = Dir2(i,1:N);
   MD(N+i,N+1:2*N) = Dii2(i,1:N);
end
```

```
MC = MC+sparse(1:2*N,1:2*N,1,2*N,2*N);
MD = MD+sparse(1:N,N+1:2*N,(1:N)*pi*(1-V^2),2*N,2*N)
        +sparse(N+1:2*N,1:N,-(1:N)*pi*(1-V^2),2*N,2*N);

% Solving the eigenvalue problem

[Ve,Va]=eig(MD,MC,'qz');

[y,I]=sort(diag(Va))
plot(diag(real(Va)),diag(imag(Va)),'o')
```

VITA

Hyun-Ki Cho

Candidate for the Degree of

Doctor of Philosophy

Dissertation: FLOW-INDUCED VIBRATION OF A WEB FLOATING OVER A PRESSURE-PAD AIR BAR

Major Field: Mechanical Engineering

Biographical:

Personal Data: Born in Seoul, Korea, On November 21, 1971, the son of Mr. Kyu-Su Cho and Mrs. Soon-Kum La.

Education: Received the Bachelor of Science degree in Mechanical Design and Production Engineering from Konkuk University, Seoul, South Korea in February 1997; Received the Master of Science degree in Mechanical Engineering from Oklahoma State University, Stillwater, Oklahoma in May 1999; Completed the requirements for the Doctor of Philosophy degree with a major in Mechanical Engineering at Oklahoma State University in July 2005.

Professional Experience: Graduate Research Assistant, Web Handling Research Center (WHRC), Oklahoma State University, 1998 to 2005.

Name: Hyun-Ki Cho Date of Degree: July, 2005

Institution: Oklahoma State University Location: Stillwater, Oklahoma

Title of Study: FLOW-INDUCED VIBRATION OF A WEB FLOATING OVER A PRESSURE-PAD AIR BAR

Pages in Study: 96 Candidate for the Degree of Doctor of Philosophy

Major Field: Mechanical Engineering

Scope and Method of Study: The aeroelastic (air/web) model is developed by theories of elasticity and fluid dynamics. The flexible web is modeled as a traveling Euler-Bernoulli beam under tension which is exposed to high-speed air flows underneath it, and the aerodynamic pressure is developed from continuity and Navier-Stokes equations. The web is assumed to be a threadline traveling between two rollers over one air bar; there is no variation across the width. To keep a valid threadline model, two-dimensional flow is obtained by two air dams installed along both free edges of the web, to block air escaping in the cross-machine direction. Experiments are limited to a non-traveling web exposed to air-jet flows. The present study is focused on effects of high-speed air flows on the flexible tensioned web; the velocity of the web is neglected because the velocity of the air jet is much higher than the translational velocity in practical applications.

Findings and Conclusions: It is observed that divergence-type instability (static deflection) and flutter-type instability (vibration) both occur in the web due to the air-jet flow. The theory used to develop the computations is well supported by the experimental results. Stability criteria are provided and compared with analytical calculations and experiments. Flutter depends strongly on flow speed, and can be controlled by increasing tension, shortening the web span, and (for a single span) centering the air-bar position. The developed theoretical and computational approach could be used for multi-bar analysis.

ADVISER'S APPROVAL: Dr. Peter M. Moretti